NASA CONTRACTOR REPORT

NASA CR-2020

# INVESTIGATION OF THE PERFORMANCE CHARACTERISTICS OF A DOPPLER RADAR TECHNIQUE FOR AIRCRAFT COLLISION HAZARD WARNING

## PHASE III

*Prepared by*
RESEARCH TRIANGLE INSTITUTE
Research Triangle Park, N.C. 27709
*for Langley Research Center*



NATIONAL AERONAUTICS AND SPACE ADMINISTRATION • WASHINGTON, D. C. • MARCH 1972

| 1. Report No. | 2. Government Accession No. | 3. Recipient's Catalog No: |
|---|---|---|
| NASA CR-2020 | | |

| 4. Title and Subtitle | 5. Report Date |
|---|---|
| INVESTIGATION OF THE PERFORMANCE CHARACTERISTICS OF A DOPPLER RADAR TECHNIQUE FOR AIRCRAFT COLLISION HAZARD WARNING - PHASE III | March 1972 |
| | 6. Performing Organization Code |
| 7. Author(s) | 8. Performing Organization Report No. None |
| | 10. Work Unit No. |
| 9. Performing Organization Name and Address<br>RESEARCH TRIANGLE INSTITUTE<br>RESEARCH TRIANGLE PARK<br>NORTH CAROLINA 27709 | 11. Contract or Grant No. NAS1-7537 |
| | 13. Type of Report and Period Covered Contractor Report |
| 12. Sponsoring Agency Name and Address<br>National Aeronautical & Space Administration<br>Washington, DC 20546 | 14. Sponsoring Agency Code |

15. Supplementary Notes

16. Abstract

System studies, equipment simulation, hardware development and flight tests which have been conducted during the development of an Aircraft Collision Hazard Warning System are discussed. The system uses a cooperative, continuous wave Doppler radar principle with pseudo-random frequency modulation. The report present a description of the system operation and deals at length with the use of pseudo-random coding techniques. In addition, the use of mathematical modeling and computer simulation to determine the alarm statistics and system saturation characteristics in terminal area traffic of variable density is discussed.

17. Key Words (Suggested by Author(s))
Collision Avoidance
Pseudo-random frequency modulation
Computer Simulation
Cooperative Doppler radar

18. Distribution Statement
Unclassified-Unlimited

| 19. Security Classif. (of this report) | 20. Security Classif. (of this page) | 21. No. of Pages | 22. Price* |
|---|---|---|---|
| Unclassified | Unclassified | 151 | $3.00 |

*For sale by the National Technical Information Service, Springfield, Virginia 22151

## FOREWORD

This report was prepared by the Research Triangle Institute, Research Triangle Park, North Carolina, under Contract NAS1-7537. The work is being administered by the Communications Research Section, Telecommunications Research Branch, Flight Instrumentation Division, Langley Research Center. Mr. Richard H. Couch is the Langley technical representative for the Contract.

This report presents the results of Phase III of a three-phase program which began on July 6, 1967. Phase I and Phase II results were presented in Reference [2]. RTI staff members participating in the study were as follows: C. L. Britt, Jr., Project Leader; E. G. Baxa, Jr., Systems Engineer; E. L. Sheppard, Systems Engineer; R. C. Haws, Systems Analyst; Mrs. C. M. Davis, Programmer; and Mrs. J. L. Gatz, Research Assistant.

TABLE OF CONTENTS

TABLE OF CONTENTS, Continued

## LIST OF ILLUSTRATIONS

LIST OF ILLUSTRATIONS (Continued)

LIST OF ILLUSTRATIONS (Continued)

LIST OF ILLUSTRATIONS (Continued)

LIST OF ILLUSTRATIONS (Continued)

LIST OF ILLUSTRATIONS (Continued)

LIST OF TABLES

# INVESTIGATION OF THE PERFORMANCE CHARACTERISTICS OF A DOPPLER RADAR TECHNIQUE FOR AIRCRAFT COLLISION HAZARD WARNING

## PHASE III

## I. SUMMARY AND CONCLUSIONS

A program of system studies, equipment simulations, hardware development, and flight tests has been conducted with the objective of the development of a low-cost device to warn the pilot of an impending mid-air collision hazard. The program has resulted in the development of a cooperative CW Doppler radar system which has the capability of providing a minimum warning time of 15 to 35 seconds (adjustable) and which has the potential of low user cost. In this report, the Pilot Warning Indicator (PWI) system operation is described and various systems analyses are discussed which were conducted to predict and evaluate the system performance.

In order to realistically evaluate the system under multiple aircraft conditions, a computer simulation approach was chosen. Actual aircraft traffic data obtained by the FAA from the radar system at the Atlanta airport were used as a major input to the simulations. A mathematical model of the warning system was developed and simulated using both the Atlanta traffic data and extended data based on statistics derived from the Atlanta traffic data.

The Atlanta traffic data consisted of the three-dimensional position coordinates of each aircraft on the radar track in the terminal area taken at four-second intervals. Twelve one-hour samples of data were taken at peak hours over a five-day period. Using these data, it was possible to determine the system performance as if each aircraft had been equipped with a PWI system during the period covered by the data base. Particular attention was given to determining the alarm statistics and the probabilities of system saturation under multiple aircraft conditions.

General studies were conducted to compare the alarm performance of various ideal systems using different warning criteria. These general studies are documented in NASA Contractor Report CR-1470. It was concluded from the general studies that, as a minimum, the required measurements for a PWI system were measurements of relative range,

closing velocity, and altitude difference to the most hazardous target. Using these measurements, it is possible to provide a minimum warning time of 25 seconds of an impending hazard while maintaining the probability of an alarm while in the terminal area to a value less than .003 under conditions similar to those in the Atlanta data base.

Previous studies have also indicated that the probability of observing two hazardous targets simultaneously (for warning times on the order of 25 seconds) is negligible. Thus, the data indicate that the equipment does not require a capability of providing for multiple target alarms if means are provided for selecting the most hazardous target. By equipment design that effectively filters out aircraft that are less hazardous, considerable equipment simplification can and has been achieved.

It is possible for the following two types of erroneous indications to occur in the system: (1) an alarm occurs when a collision hazard does not exist, and (2) an alarm is missed when a collision hazard does exist. The first type of alarm occurs even in ideal systems because the alarm criteria selected fail to provide sufficient discrimination between hazards and nonhazards. The probability of this type of alarm can be reduced to any degree desired by reducing the warning time (see NASA CR-1470). Thus, a tradeoff is involved between warning time and pilot workload allocated to responding to alarms. It is believed desirable to provide an adjustable threshold such that the pilot sets the warning time on the basis of the existing flight conditions. For example, it may be desirable to accept a shorter warning time in the terminal area than in en route sectors.

The second type of false indication may occur because of the particular techniques used in generating and decoding the recognition code for the radar. It is possible for codes from different transmitters to be in synchronism and if this situation occurs, a loss of communications will exist and result in a failure in the indication of an alarm in either aircraft. The probability of total communication loss during a period when an alarm should be given due to this effect is called the probability of a missed alarm.

The probability of a missed alarm has been calculated for various recognition codes and other system parameters. For the coding technique and parameters selected, a calculation indicates that the probability of a missed alarm (defined as a communications loss of 10 seconds or greater) is less than $1 \times 10^{-6}$ (see Section V-E). This probability could be reduced to an even smaller value by using different recognition codes for different transmitters or by increasing system bandwidths.

Another factor which can result in a failure in the indication of an alarm in one of the two aircraft involved in an encounter is the intentionally restricted antenna coverage. The transceiver antenna pattern is shaped to provide uniform coverage in the forward half plane over an angle of $\pm 100°$ horizontally and $\pm 15°$ vertically. The transponder antenna pattern is uniform over 360° horizontally and $\pm 15°$ vertically. Thus, alarms due to aircraft approaching from behind the protected aircraft or from above or below with a large vertical velocity may not be indicated until the range between the aircraft becomes very small.

In order to determine the severity of the saturation and interference problems for the PWI system, a simulated system has been "flown" on all aircraft represented in the radar traffic data from the Atlanta airport. Statistics have been derived which indicate the probabilities of system saturation and interference.

Figure 41, page 61, shows the saturation performance of the transponder. The vertical scale indicates the average percent of time that the power level from the transponder was greater than the level given along the horizontal axis. Several curves are plotted; one (dotted) represents the saturation performance obtained when using the Atlanta radar data, while the others represent results obtained from a simulation with traffic densities up to three times as great as the Atlanta radar traffic density. Note that for all cases the power output of the transponder did not exceed one watt (or 30 dbm), and for a large percent of the time the transponder is operating at power levels considerably less than this value. Thus, the transponder is not prone to saturation under traffic densities considerably in excess of the Atlanta density. The

total transponder output power exceeded 0.3 watt only 0.7 percent of the time for the Atlanta density.

At the receiver, the most important saturation-indicating parameter is the signal-to-interference ratio during periods in which a hazard should be indicated. Figure 43, page 62, indicates the percent of alarm time that the signal-to-interference ratio is greater than a value given along the horizontal axis, with a warning time of 25 seconds used. Again, curves are shown for results taken from the Atlanta traffic data and also from the simulation using traffic densities up to three times that of the Atlanta data. As may be seen, the signal-to-interference ratio during alarm situations exceeded 35 (15.5 db) in the case of the Atlanta traffic density and exceeded 12 (11 db) for the 40 A/C simulated-density case during at least 90 percent of the alarm time.

It may be concluded that considerable progress has been made towards the development of a PWI system suitable for all classes of aircraft including general aviation. The system requirements and technical approach are now well defined and the major problem areas, such as differentiation between hazards and nonhazards and development of the capability for handling a large number of aircraft without saturation, have been solved with relatively simple equipment. The studies indicate that the operation of the system will be satisfactory in a multiple-aircraft environment. Finally, the system concept has the potential of being made available at a moderate to low user cost.

## II. INTRODUCTION

Since 1967, research has been conducted at NASA - Langley Research Center on the problem of providing a low-cost instrument to warn the pilot of an impending mid-air collision hazard. This research has consisted of a program of system studies, equipment simulations, hardware development, and flight tests. A first-generation warning system has been constructed and two engineering models have been successfully flight tested. Based on this development and the flight tests, a second-generation system has been developed which provides more accurate measurements and has a potentially lower cost.

This report documents the Phase III effort of supporting system studies to the NASA - Langley Research Center program. The objectives of the Phase III efforts have been to: 1) assist in the development of specifications for the second-generation collision warning system, 2) develop mathematical models and conduct computer simulations of the system to evaluate the system performance, 3) investigate and develop mathematical modeling techniques for the simulation of terminal area traffic with variable density and 4) investigate techniques for the real-time simulation of intruding aircraft flying within the terminal area traffic.

In Phase I of this contract, the feasibility of a dynamic computer simulation of the aircraft collision hazard warning system developed by NASA-Langley personnel was investigated. The simulation was found to be feasible and well within the capabilities of the available digital computers.

One of the major objectives of the Phase I effort was to obtain data defining aircraft motions in a typical airport terminal area. Through the FAA, twelve one-hour samples of digitized radar data, controller-aircraft voice communications tapes, and controller log sheets were collected at the Atlanta, Georgia terminal. These data were taken during morning, afternoon, and evening peak traffic periods over a five day interval during the month of August 1967. The data were edited by

FAA personnel at National Aviation Facilities Experimental Center (NAFEC) and made available to RTI in the form of digital magnetic tape. The edited data contain, for the majority of the aircraft within a 35-mile radius of the Atlanta airport, (1) position data in xyz coordinates for all aircraft under track at four-second intervals (approximately 700 aircraft tracks with a total flight time of approximately 119 hours), (2) coordinate rates at four-second intervals for all aircraft under track, and (3) supplementary data such as identification of aircraft and time of day. The data base is described in detail in the Phase II Interim Report on this contract, Ref. [1].

In Phase II of the contract, general studies of PWI and CAS alarm statistics were made using the Atlanta traffic data and various analytical studies were conducted to evaluate the performance of the first-generation system. The Phase II effort has been reported upon in various contract reports and publications, Refs. [2] to [4].

In the following, the Phase III studies are described in detail. These studies were primarily concerned with analyses of the range and Doppler measurement techniques and with analysis of the performance of the system under multiple aircraft conditions with particular attention given to the possibility of system saturation in high density traffic situations.

## III. SYSTEM DESCRIPTION

### A. General Operation

The hardware under development at LRC is shown pictorially in Fig. 1. It consists of a transceiver and display unit on-board the protected aircraft and a linear transponder on-board the intruding aircraft. The protected aircraft should also carry the transponder. The display might consist of an alarm indication coupled variously with indications of relative intruder position, altitude separation, and time-to-collision.

A functional block diagram of the system is shown in Fig. 2. Fig. 3 indicates the type of signal processing used to accomplish the functions given in Fig. 2. The system is basically a continuous wave (CW) cooperative Doppler radar. It operates at a transmitter power of approximately one watt to ensure a low probability of system saturation. The carrier frequency of 5.20 GHz is frequency modulated by a recognition code generated on each aircraft by a pseudo-noise (PN) process. The purpose of this recognition code is to allow all aircraft to operate simultaneously in the same frequency allocation without significant interference, and also to provide for measurement of relative range.

The transponder on-board the intruding aircraft is simply a linear repeater which receives, amplifies, shifts frequency and retransmits all interrogations from other aircraft transmitters. The recognition code on each received signal is preserved at the transponder output. In addition, a coded message is applied to all transponder reply signals which conveys the intruding aircraft altitude. The maximum transponder output power is one watt, and the nominal output frequency is 5.1 GHz.

At the receiver, the signal strength varies inversely as the fourth power of the range between aircraft. The received frequency differs from the transmitted frequency by an amount equal to the offset introduced in the transponder plus the Doppler shift associated with the closing velocity between the two aircraft. The received frequency also has associated with it modulation components which are the result of

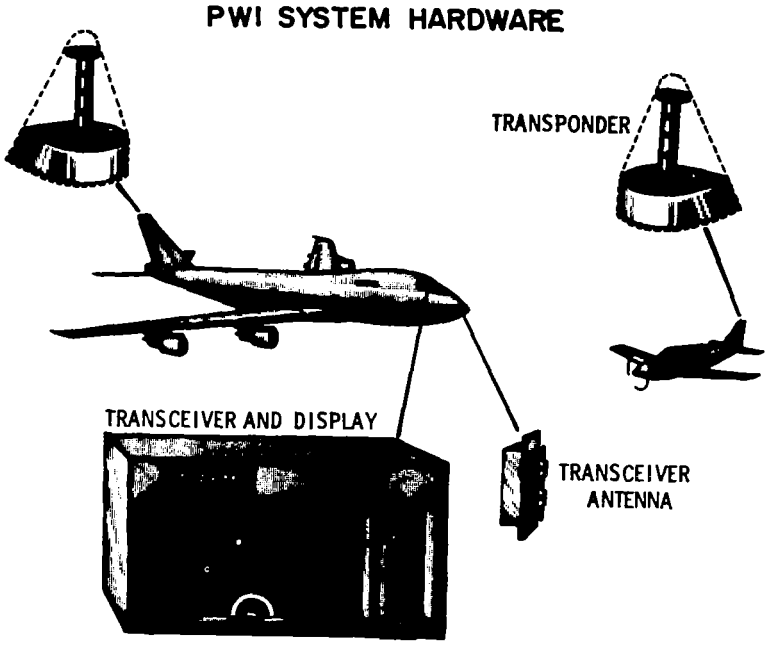


Fig. 1. Pictorial Diagram of the System.

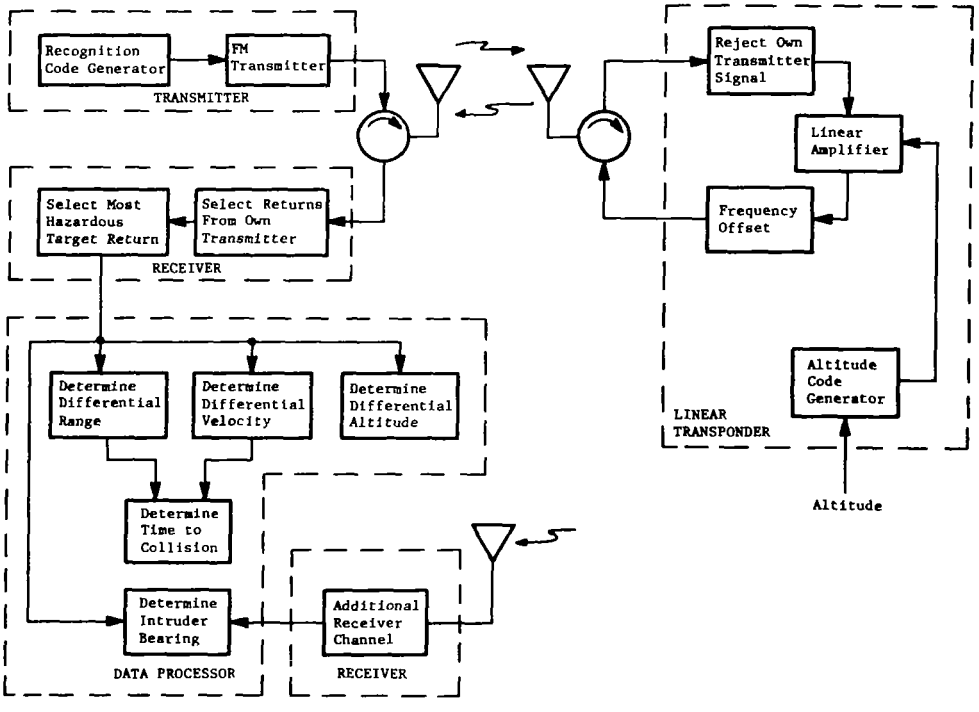


Fig. 2. Functional Block Diagram of the PWI System.

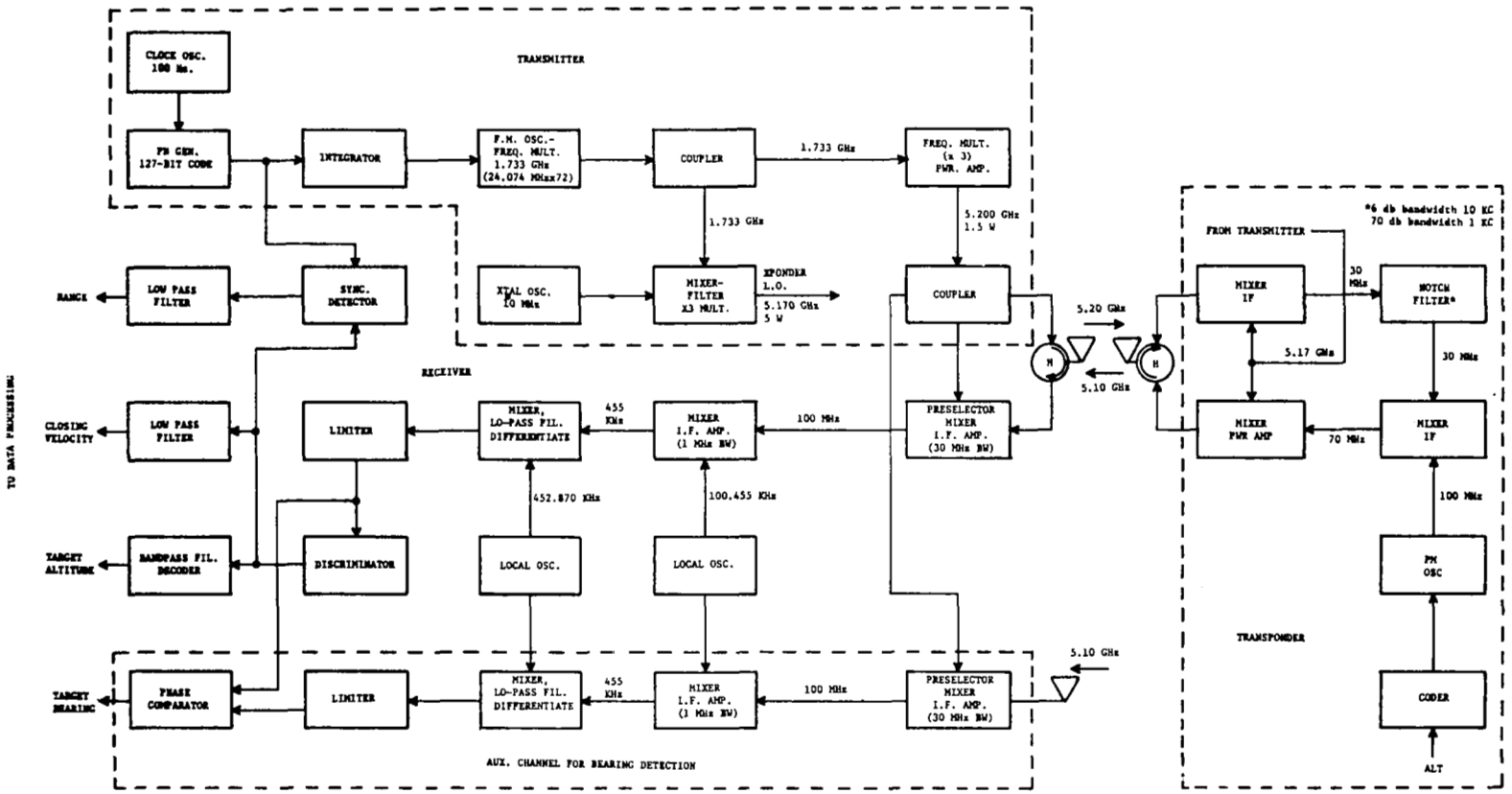


Fig. 3. Block Diagram Indicating Signal Processing Techniques.

the recognition code and the altitude coded message.

In practice there will be many reply signals present at the receiver input simultaneously. Some of these replies will be the result of interrogations of a number of transponders by the ownship transmitter (desired). Others will be replies to transmitters other than the ownship transmitter (interfering). One function of the receiver is to distinguish between the desired replies and the interfering replies. This is accomplished in the receiver front end by a correlation process which suppresses interfering replies and amplifies desired replies.

The overall receiver gain-versus-frequency characteristic is chosen such that the signal from the intruding aircraft which has the most hazardous combination of range and closing velocity produces the largest magnitude signal at the receiver output. Thus, the signal with the shortest apparent time-to-collision appears largest at the receiver output. The above statement implies that degree of hazard is measured in the receiver by observing a combination of signal strength and Doppler shift.

After the signal from the most hazardous aircraft has been selected, it is further acted upon by the data processor to measure closing velocity, range, and altitude difference. The closing velocity is measured by observing the average Doppler shift of the received signal. The range is measured by observing the time delay between the time of transmission and the time of arrival of the recognition code. The altitude difference is measured by comparing the decoded altitude message from the intruding aircraft with the ownship altitude. Approximate time-to-closest approach is determined by calculating the ratio of measured range to measured closing velocity.

Other measurements that may be made by the system include intruder bearing, which is measured by the incorporation of an additional receiver channel, and projected miss distance, which is obtained by additional data processing. The desirability and feasibility of the miss distance measurement has not yet been determined.

The warning criteria used and the measurement techniques are discussed in more detail in the following sections.

## B. Warning Criteria

Various warning criteria have been investigated in previous studies (Ref. [1]). The modified tau criterion developed by Holt (Ref. [5]) was selected as the criterion that provided the best tradeoff of protection versus discrimination against non-hazardous targets.

The modified tau criterion is based on the following philosophy: one considers any intruder a hazard if it is possible for the aircraft involved to collide within a designated time, $\tau_{mk}$, if each aircraft makes the worst possible maneuver. Since aircraft maneuvers have definite acceleration limits, an acceleration constraint can be used to define a set of possible maneuvers.

The set of all aircraft that can reach a protected craft's position in a time less than a given time $\tau_{mk}$, using a relative acceleration no greater than a given acceleration (U), have values of relative range (R), closing velocity ($\dot{R}$), and normal velocity ($V_n$), which satisfy the equation

$$(R - \dot{R}t)^2 + V_n^2 t^2 = \frac{U^2 t^4}{4} \tag{1}$$

for some t between 0 and $\tau_{mk}$.

The region in R, $\dot{R}$, $V_n$ space defined by equation (1) will also be contained in a region defined by

$$R - \dot{R}\tau_{mk} < \frac{U\tau_{mk}^2}{2} \tag{2}$$

or

$$\tau_{mk} < \frac{R - \left(\frac{U\tau_{mk}^2}{2}\right)}{\dot{R}}$$

which uses range (R) and closing velocity ($\dot{R}$) only. Note that the terms $U\tau_{mk}^2/2$ and $\tau_{mk}$ are selected constants defining the alarm threshold

and relative acceleration allowed*. The criterion given by equation (2) thus provides an approximation to the region defined by equation (1) and leads to a warning criterion designated as the "modified tau" criterion, with an encounter defined by $\tau_m < \tau_{mk}$ where

$$\tau_m = \frac{-\dot{R} + (\dot{R}^2 + 2UR)^{1/2}}{U} \quad . \tag{3}$$

The region in the R, $\dot{R}$ plane for the modified tau criterion is shown in Fig. 4 for a modified tau value of 25 seconds. Notice that this criterion provides a proximity warning even if the closing velocity is zero and that it takes into account the possibility of curved (accelerating) relative trajectories.

Previous studies have also indicated the desirability of the inclusion of relative altitude measurements to provide discrimination against false alarms. That is, it is desirable to suppress the alarm for aircraft separated more than approximately 1,000 feet in altitude even though the modified tau measurement indicates a potential hazard.

To provide for calculation of the warning criterion, then, the basic measurements made by the system are measurements of relative range, closing velocity, and altitude difference. As mentioned previously, it is also desirable to measure the bearing to the hazard in order to assist in visual acquisition. The following section discusses the techniques used to obtain these basic measurements.

### C. Measurement Techniques

1. Range and closing velocity measurements.— The technique for measuring range and closing velocity is illustrated in Fig. 5. Fig. 5a shows a portion of the PN code as generated by a shift register. This PN code is then integrated to provide a wave shape as shown in Fig. 5b. The integrated PN code is then used to modulate the FM transmitter and represents the transmitted frequency.

The transmitted waveform is returned by a linear transponder, received at

*$U = 16.6$ fps$^2$ and $\tau_{mk} \approx 15$ to 35 secs. are representative values.

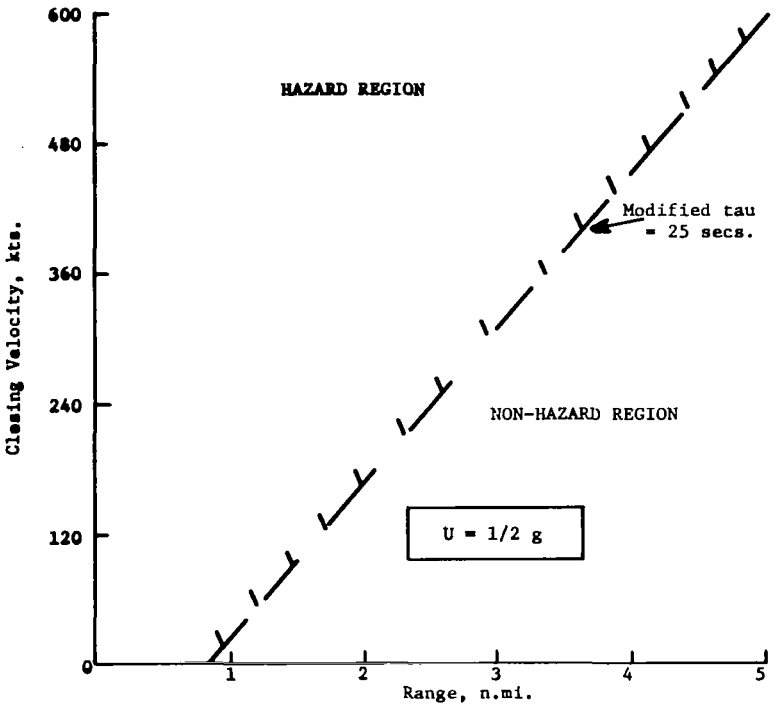


Fig. 4. Hazard region in the range, closing velocity plane for a modified tau criterion of 25 seconds.

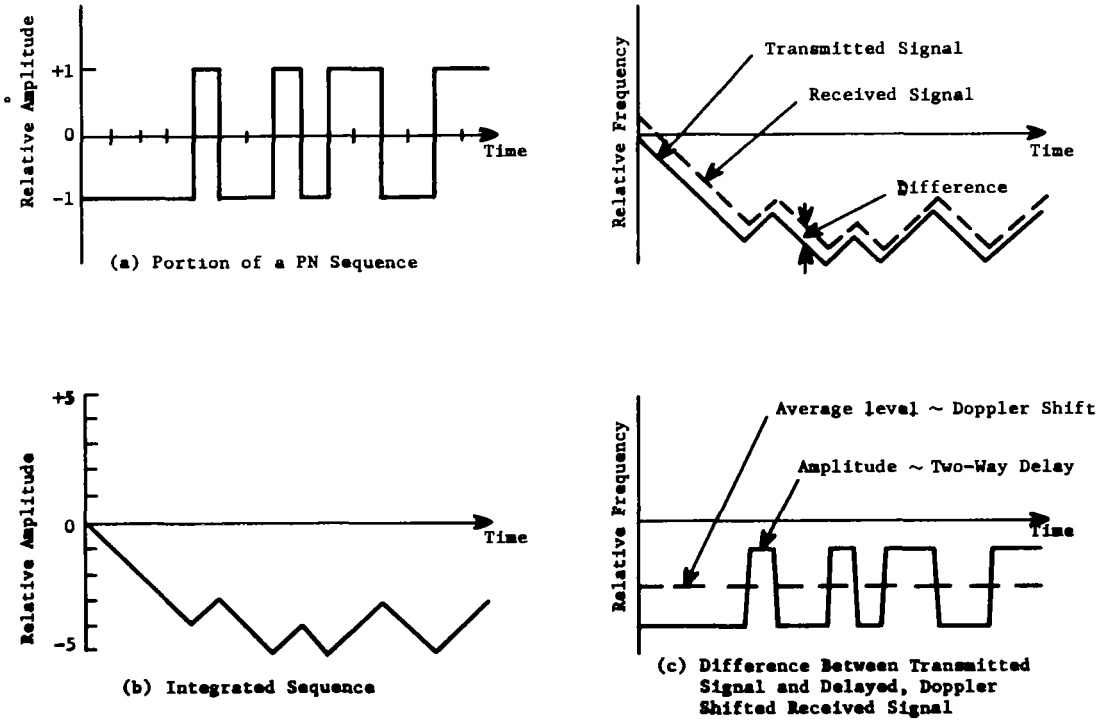


Fig. 5. Technique for measurement of range and closing velocity.

the protected aircraft receiver, and mixed with a frequency-shifted version of the outgoing signal. The mixing operation effectively subtracts the frequencies of the returned signal and the transmitted signal to provide a waveform as shown in Fig. 5c. This waveform has an amplitude proportional to the range to the target and an average value proportional to the Doppler shift or closing velocity of the target. Further processing to derive the amplitude and average frequency of the waveform provides voltages proportional to relative range and closing velocity.

2. Relative altitude difference measurements.— It is anticipated that altitude will be measured using barometric pressure sensors on board the protected and cooperating aircraft. These sensors will produce a voltage proportional to absolute altitude, which will be used to drive identical voltage-controlled RC oscillators in both the receiver on the protected aircraft and the transponder on cooperating aircraft.

As indicated in the block diagram of Fig. 3, the altitude tones are phase-modulated onto the interrogating signals present in the transponder. At the receiver, the altitude tones are separated from the PN and Doppler modulation, demodulated, and the frequency difference is compared and converted into altitude difference in the data processing unit.

3. Target bearing measurements.— Intruder bearing is obtained by measuring the phase difference between a pair of dipoles on the 5.10 GHz transceiver antenna. These dipoles are separated approximately 1/2 wavelength (2.9 cm.) such that there is an unambiguous $\pm 180°$ phase difference range in the forward half-horizontal plane.

Each dipole signal is amplified in a separate receiver channel, and the phase difference measurement is made at an IF frequency. A voltage is derived which is analogous to the target bearing and used to drive a range-bearing display of the type shown in Fig. 1.

The performance of the bearing-indicating system will be evaluated experimentally upon completion of the laboratory prototype system.

### D. Technique for Selection of the Most Hazardous Target

The most hazardous target is selected by shaping the receiver pass band such that the target return with the largest value of modified tau captures

the receiver. The receiver is designed so that the signal power level into the limiter-discriminator varies with range and closing velocity approximately as illustrated in Fig. 6.

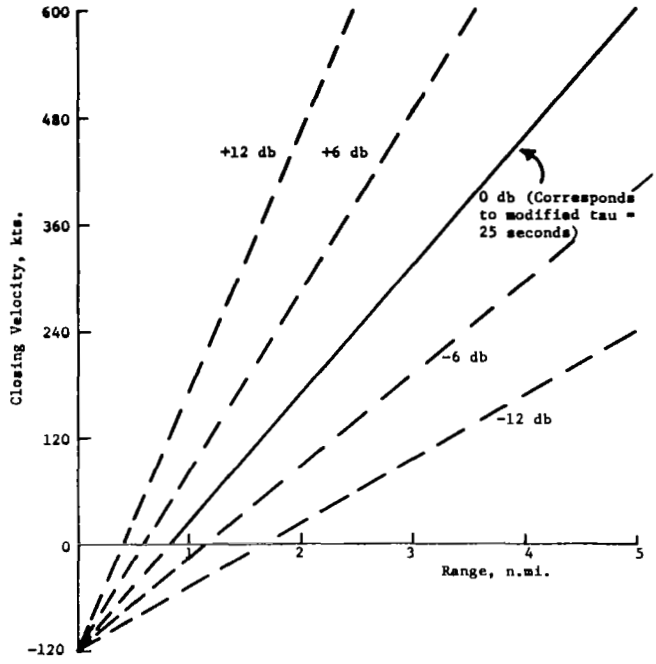


Fig. 6. Signal levels relative to alarm thresholds (0 db) as a function of range and closing velocity. The closing velocity intercept is held fixed to prevent undue complexity in the system.

The signal from the second receiver mixer is offset slightly and differentiated twice to provide a signal whose amplitude is approximately inversely proportional to the square of modified tau. The technique may be further illustrated by considering the operations performed on the Doppler signal. Consider a single sideband Doppler signal given by (where the modulation terms have been neglected for simplicity)

$$e_1 = -A \sin \omega_d t \tag{4}$$

where A is signal amplitude and $\omega_d$ is the Doppler frequency shift. Offsetting the Doppler signal by an amount $\omega_o$ and differentiating twice gives a signal which may be represented as

$$e_2 = +A(\omega_d + \omega_o)^2 \sin(\omega_d + \omega_o)t. \tag{5}$$

Since the amplitude of the signal is inversely proportional to range squared and the Doppler shift is proportional to closing velocity, the signal may be re-written as

$$e_2 = K\left(\frac{\dot{R} + C}{R}\right)^2 \sin\,(\omega_d + \omega_o)t \qquad (6)$$

where K and C are constants. Thus, the amplitude of the signal processed in this manner can be seen to be inversely proportional to range squared and directly proportional to closing velocity squared. By proper adjustment of system parameters, targets having values of $\dot{R}$ and R nearest the hazard region defined by the modified tau criterion will have the largest amplitude or power level after processing. This situation is shown in Fig. 6, where the power level of the received signal is indicated as a function of range and closing velocity. The 0 db line corresponds to a value of modified tau of 25 seconds (compare with Fig. 4). The other power level lines represent approximations to various values of modified tau since the closing velocity intercept (determined by the IF offset frequency) is held constant in the system to prevent undue complexity.

In practice, the double differentiation operation and sideband filtering can be accomplished at the IF frequency using an equivalently shaped IF filter characteristic. This pass-band shaping technique is planned for use in the present laboratory prototype model of the system.

## E. Rejection of Unwanted Signals

1. Types of undesired signals.— Because of the large population of transmitters and receivers, there are numerous undesired signals in the frequency band which must be discriminated against. These undesired signals may be listed as follows:

(1) Signals from the ownship transmitter to the ownship transponder,

(2) Signals from the ownship transponder to the ownship receiver,

(3) Signals at the receiver which are due to interrogations other than those from the ownship transmitter.

The techniques for rejecting each class of undesired signal is explained in the following.

2. Rejection of ownship transmitter signals at the ownship transponder.— The notch filter in the transponder (see block diagram of Fig. 3) is used to provide the rejection of the ownship-transmitted signal from the ownship transponder. The first mixer in the transponder uses an oscillator signal which is varying in accordance with the integrated pseudo-noise modulation. Since the ownship transmitter signal is varying in the same manner, the ownship transmitter signal will appear stationary in frequency at the output of the transponder first mixer. Thus the signal will be in the rejection band of the notch filter and will suffer on the order of 60 db attenuation.

Signals from other aircraft transmitters interrogating the transponder will be sweeping over a band determined by the deviation of the FM transmitter. When mixed with the ownship transmitter signal, the FM deviation will be increased to approximately twice that of the transmitter alone. Thus, desired interrogating signals periodically sweep through the notch filter, but due to the sweeping effect do not lose significant energy when passing through the notch filter.

At the final mixer in the transponder, the modulation introduced by the ownship transmitter is removed so that the signal transmitted from the transponder is an amplified and frequency-shifted replica of the interrogating signal.

This situation is shown pictorially in Fig. 7, where the initial transmitted spectrum is assumed to be approximately rectangular. It should be noted that the notch filter attenuation is supplemented by the attenuation obtained by physical separation of the transponder antenna and the transmitter/receiver antenna.

3. Rejection of ownship transponder signals from ownship receiver.— The rejection of this type of undesired signal depends upon the physical separation of the transponder and receiver antenna, and on the fact that the transponder signals are spread over a band corresponding to the deviation of the FM transmitters. These signals are noncoherent with the oscillator signal used at the first mixer in the receiver (the local oscillator used in the first mixer is a sample of the transmitted signal). Thus, the energy from the ownship transponder is filtered out in the IF state of the receiver by the narrow-band side-band filter.

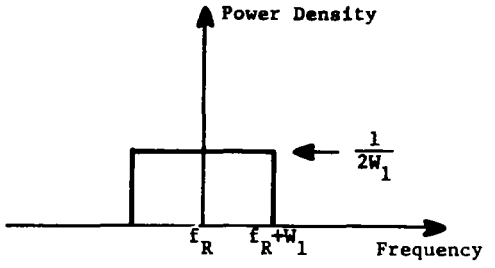


Normalized spectral density at transponder input (approximately rectangular). $W_1$ is the peak deviation.

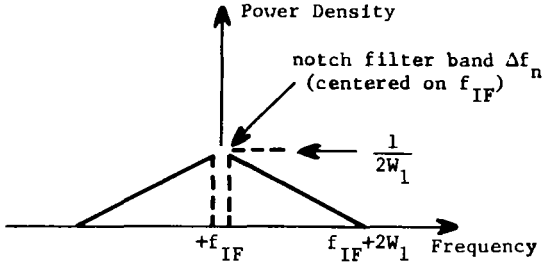


Normalized spectral density at transponder IF freq.

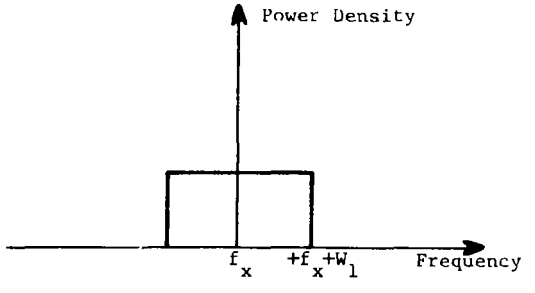


Spectral density at transponder output

Fig. 7. Modulation spectra at the transponder showing technique for rejection of ownship transmitter signal.

4. Rejection of undesired returns.— These signals are rejected in the same manner as those from the ownship transmitter. That is, signals received from a target transponder which are due to interrogations from a third aircraft are noncoherent at the output of the ownship receiver first mixer. The signals are spread over a band corresponding to twice the deviation of the FM transmitters and are filtered out by the receiver narrow-band IF system.

## F. System Parameters

The system parameters selected to date are only tentative, since the development program is still in progress. Parameters for the laboratory prototype have been selected to provide a system with maximum range coverage of 6.5 nautical miles and a closing velocity range of 500 knots.

Table 1 lists the tentative parameters for the laboratory prototype systems.

Table 1. System Parameters

Max. Range 6.5 n.mi. Velocity Coverage 500 KTS

| PARAMETER | NOMINAL VALUE |
|---|---|
| **Transmitter** | |
| Transmitted Power | 30 dbm |
| Transmitted Frequency | 5200 MHz |
| FM Waveform Slope ($\beta$) | 16.6 MHz/sec |
| Peak Deviation of FM Transmitter (one sided) | 1.08 MHz |
| PN Code Length | 127 bits |
| PN Code Bit Period | 10 m sec |
| Transmitter Ant. Peak Gain | 0 db* |
| **Transponder** | |
| Transponder Gain Constant | 112 db |
| Transponder Noise Bandwidth | 4 MHz |
| Transponder Noise Figure | 10 db |
| Notch Filter 6 db Bandwidth | 10 KHz |
| Notch Filter 70 db Bandwidth | 1 KHz |
| Transponder Output Saturation Level | 30 dbm |
| Transponder Receiver Ant. Peak Gain | 0 db* |
| Transponder-Transmitter Ant. Peak Gain | 0 db* |
| Transmitter-Transponder Isolation | -150 db* |

*Assumed value, actual value to be experimentally determined.

System Parameters, Continued

| PARAMETER | NOMINAL VALUE |
|---|---|
| **Receiver** | |
| Received Frequency | 5100 MHz |
| Receiver Noise Figure | 10 db |
| Receiver 1st IF Noise Bandwidth | 1 MHz |
| SSB Filter Equivalent Noise Bandwidth | 6.9 KHz* |
| Receiver Ant. Peak Gain | 0 db** |
| Receiver Gain to Limiter (at 500 Kts closing velocity) | 86 db |
| Alarm Threshold (Modified Tau) | 15-35 secs (adjustable) |
| Alarm Threshold (Range) | 1 n.mi. |
| Alarm Threshold (Altitude) | ±1000 ft. |
| Velocity Offset (Discriminator) | 118 Kts |
| Acceleration Constant U in Modified Tau Criterion | .5 g units |

*See Section IV-C.

**Assumed value, actual value to be experimentally determined.

It should be noted that higher performance aircraft will require greater range and closing velocity coverage. The range coverage is increased by increasing the transmitted power and the closing velocity coverage is increased by changing the receiver Doppler bandwidth characteristics.

## IV. APPLICATION OF PSEUDO-NOISE CODING TECHNIQUES

### A. Characteristics of PN Sequences

1. Definition of a PN sequence.— The class of binary sequences that have certain randomness properties are termed PN (pseudo-noise) sequences. For ranging purposes, the most important property the sequence satisfies is the "correlation property." This property states that if a period of the sequence is compared, term-by-term, with any cyclic shift of itself, the number of agreements differs from the number of disagreements by at most unity [7].

Thus, the autocorrelation function of a PN sequence of period p appears as shown in Fig. 8. From the autocorrelation, the power spectrum is obtained as

$$\phi(\omega) = \frac{p+1}{p^2}\left[\frac{\sin(\omega t_o/2)}{\omega t_o/2}\right]^2 \sum_{\substack{n=-\infty \\ n\neq 0}}^{n=\infty} \delta\left(\omega - \frac{2\pi n}{p t_o}\right) + \frac{1}{p^2}\,\delta(\omega), \qquad (7)$$

where $t_o$ is the period of one digit. A plot of the spectrum is shown in Fig. 9.

There are, of course, a large number of sequences of a given period which have autocorrelation properties that are not quite as ideal as that of Fig. 8. The investigation of these sequences is usually accomplished on a trial-and-error basis since no general theory is available to generate a code with a specified non-ideal autocorrelation.

In the following, the emphasis will be on PN codes with autocorrelation as given in Fig. 8.

2. Generation of PN sequences.— All maximum length linear shift register sequences have PN properties, and are periodic with period $2^n - 1$ (where n is the number of stages in the shift register). Non-maximal linear shift register sequences may also have PN properties; however, it can be shown that such a non-maximal PN code can also be generated from a shift register with fewer stages. Thus, there appears to be no advantage in the use of a non-maximal sequence.

A seven-stage shift register with feedback connections for the generation of a PN code of length 127 bits is shown in Fig. 10. The recursive relations

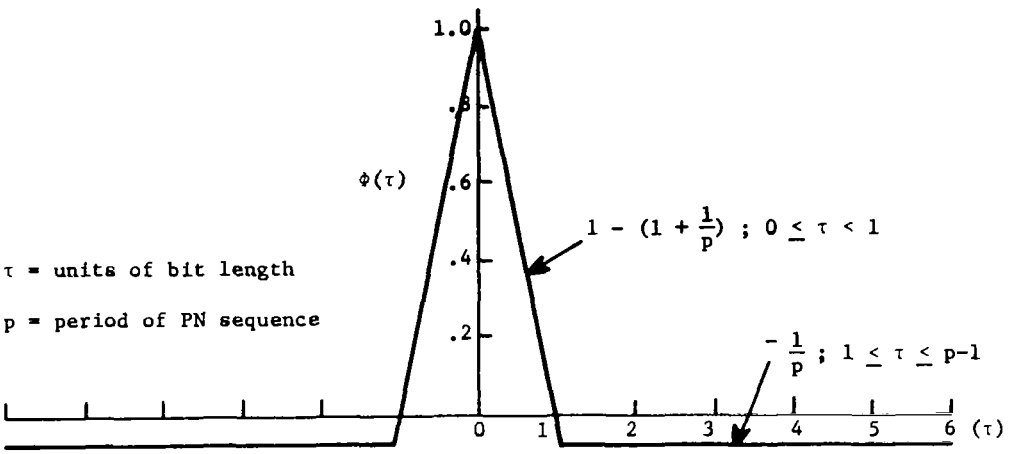


Fig. 8. Autocorrelation function of PN sequence of period p (from Ref. [6]).

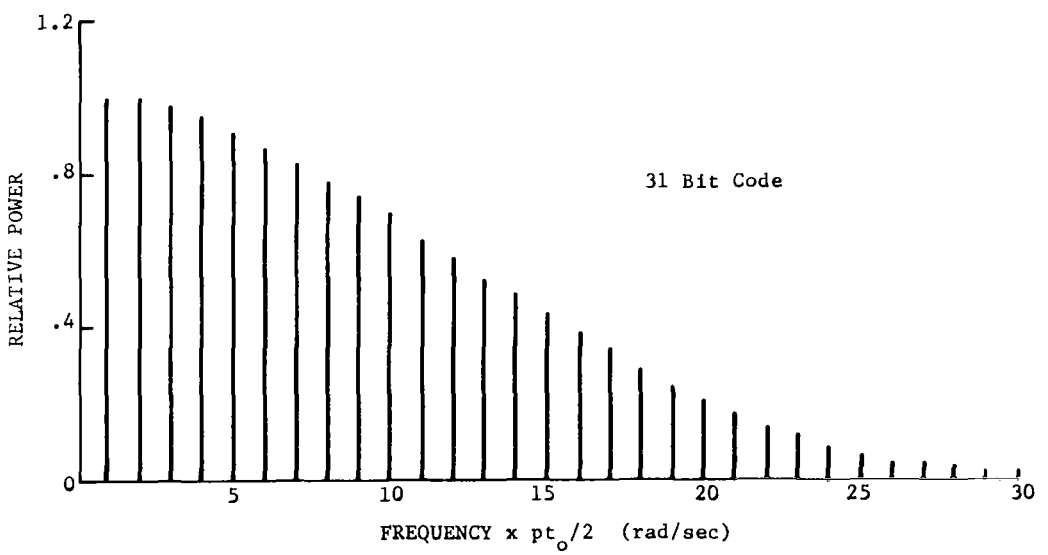


Fig. 9. Power spectrum of PN waveform.

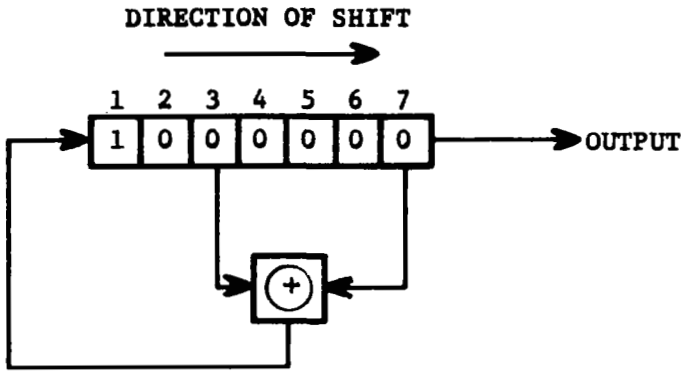


SEQUENCE GENERATED:

| | | | | |
|---|---|---|---|---|
| 00000 | 01001 | 00110 | 10011 | 11011 |
| 10000 | 11111 | 11000 | 11101 | 10001 |
| 01001 | 01111 | 10101 | 01000 | 01011 |
| 01111 | 00111 | 00101 | 01100 | 11000 |
| 00110 | 11010 | 11101 | 00011 | 00100 |
| 01 | | | | |

Fig. 10. Seven stage shift register with (7,3) feedback taps.

for this particular code (i.e. the feedback connections) are designated as (7,3) for convenience in notation.

The number of maximal sequences possible for a given n stage register up to n = 255 is shown in Table 2. Note that one-half of the sequences generated with a given shift register are reversed versions of the other sequences.

It is also possible to generate so-called non-linear sequences. These non-linear sequences can be generated by non-linear logic in the feedback circuits (such as adding the outputs of a given stage to an "and" combination of two other stage outputs). One advantage of a non-linear shift register sequence is that many more maximum sequences are possible for a given shift register. For example, there are $2^{(2^{n-1}-n)}$ maximum sequences of length $2^n$ possible from an n stage non-linear generator. The difficulty with non-linear sequences is that no theory is available to determine the correlation characteristics of the generated codes.

3. Integration of the sequences and effective modulation bandwidth.— If it is assumed that the DC line is removed (see equation (7)), then the spectrum of an integrated version of the PN code is given by

Table 2. Generation of Maximal Length Sequences

| No. of Stages | Sequence Length | No. of Max. Length Codes | Feedback Taps | |
|---|---|---|---|---|
| 2 | 3 | 1 | (2,1) | |
| 3 | 7 | 2 | (3,2) | (3,1) |
| 4 | 15 | 2 | (4,1) | (4,3) |
| 5 | 31 | 6 | (5,3) | (5,2) |
| | | | (5,3,2,1) | (5,4,3,2) |
| | | | (5,4,2,1) | (5,4,3,1) |
| 6 | 63 | 6 | (6,1) | (6,5) |
| | | | (6,5,2,1) | (6,5,4,1) |
| | | | (6,4,3,1) | (6,5,3,2) |
| 7 | 127 | 18 | (7,3) | (7,4) |
| | | | (7,3,2,1) | (7,6,5,4) |
| | | | (7,4,3,2) | (7,5,4,3) |
| | | | (7,6,5,4,2,1) | (7,6,5,3,2,1) |
| | | | (7,5,4,3,2,1) | (7,6,5,4,3,2) |
| | | | (7,6,4,2) | (7,5,3,1) |
| | | | (7,1) | (7,6) |
| | | | (7,6,3,1) | (7,6,4,1) |
| | | | (7,6,5,2) | (7,5,2,1) |
| 8 | 255 | 16 | (8,4,3,2) | (8,6,5,4) |
| | | | (8,6,5,3) | (8,5,3,2) |
| | | | (8,7,6,5,2,1) | (8,7,6,3,2,1) |
| | | | (8,5,3,1) | (8,7,5,3) |
| | | | (8,6,5,2) | (8,6,3,2) |
| | | | (8,6,5,1) | (8,7,3,2) |
| | | | (8,6,4,3,2,1) | (8,7,6,5,4,2) |
| | | | (8,7,6,1) | (8,7,2,1) |

$$\phi_i(\omega) = \left(\frac{2\pi}{pt_o\omega}\right)^2 \frac{p+1}{p^2}\left[\frac{\sin(\omega t_o/2)}{\omega t_o/2}\right]^2 \sum_{\substack{n=-\infty \\ n\neq 0}}^{\infty} \delta\left(\omega - \frac{2\pi n}{pt_o}\right) \qquad (8)$$

where the spectrum has been normalized such that the first line in the spectrum has the same value for the integrated function as for the original function. The integrated spectrum is plotted in Fig. 11. Note that the lines in the integrated spectrum are reduced in accordance with the sequence

$$1, \frac{1}{4}, \frac{1}{9}, \frac{1}{16}, \frac{1}{25}, \ldots$$

This sequence sums to approximately 1.64 or $(\pi^2/6)$; thus, 61% of the power is in the first line, 76% in the first two lines, 83% in the first three lines, and 87% in the first four lines. It is, however, the higher frequency lines that are of importance for reproduction of the linear-slope segments of the function. The effective bandwidth occupancy of the integrated code may be assumed to be twice the frequency at which the sin X/X term first goes to zero, or $1/t_o$ in Hz, where $t_o$ is the digit width in seconds.

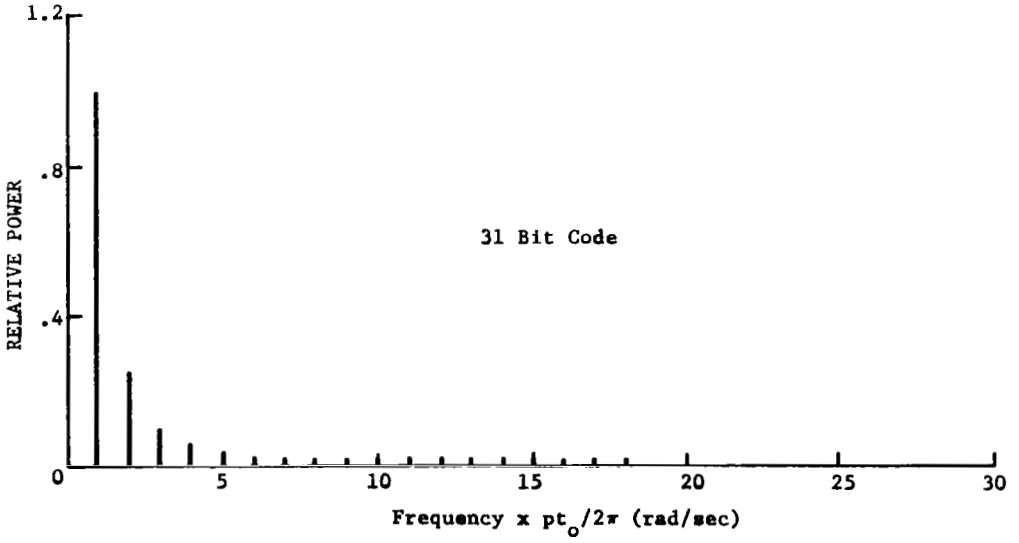


**Fig. 11. Power spectrum of integrated PN code.**

A sketch of a 127-bit integrated waveform is shown in Fig. 12. Note that the waveform has a value of one bit unit at the end of one period. In the system, the code generator is AC coupled to the FM modulator to maintain a constant center frequency over several code periods. Thus, in practice, the final value of the code is approximately the same as the initial value (i.e., the DC component is removed).

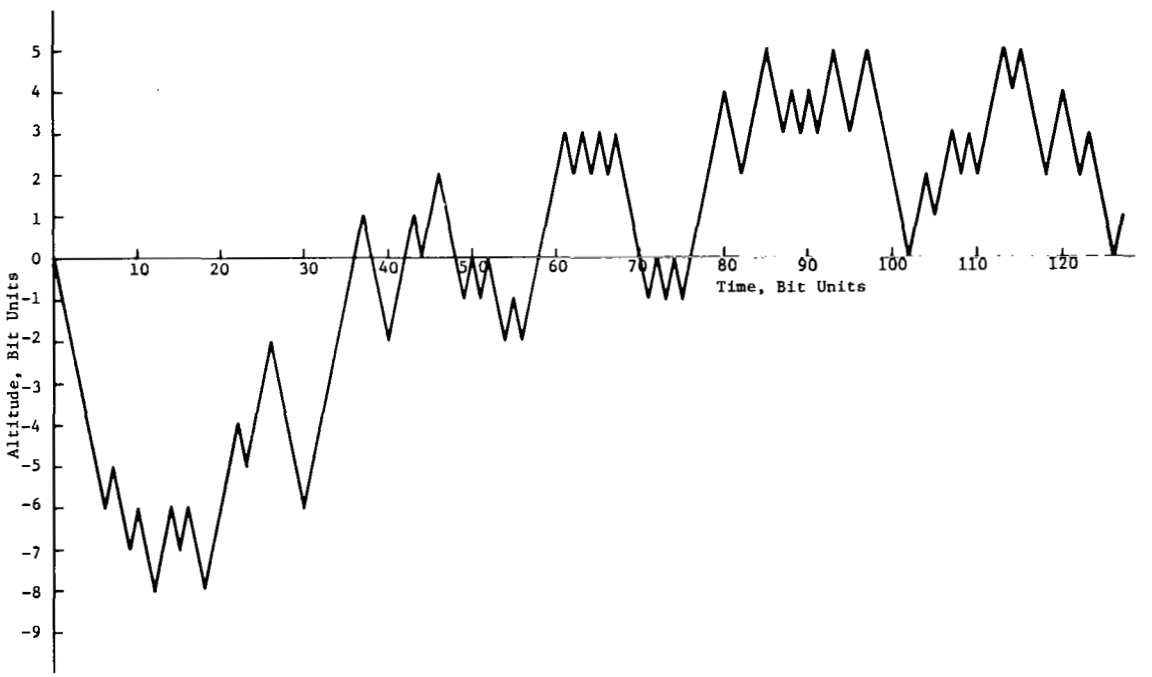


Fig. 12. Integrated PN sequence, 127 bit code, feedback taps (7,3).

B. Application to Range and Closing Velocity Measurements

1. General Discussion.— In Appendix A, several types of integrated pseudo-noise codes are investigated to determine the parameters of importance in system design. These parameters include the bandwidth occupancy of the code, the energy distribution over the bandwidth, and the actual code generated by given shift register feedback connections.

Since the pseudo-noise sequence is used to provide a recognition code as well as for making the range and closing velocity measurements, it is desirable, from this standpoint, to use a long sequence. However, there is a trade-off involved between the length of the sequence and

the accuracy obtainable in the closing velocity measurements (i.e., the closing velocity is measured by averaging the waveform, hence it is desirable to average over more than one full period of the sequence). In addition, of course, the longer codes require longer shift registers, hence more complexity than shorter codes.

A PN sequence is defined by its correlation function. That is, only sequences which have a correlation function as shown in Fig. 8 are designated as PN sequences. From the aurocorrelation function, we see that a PN sequence has the capability of making an unambiguous range measurement of a two-way range such that the round trip propagation time is less than the time corresponding to one bit period. Thus, the minimum basic bit period usable is determined by the maximum range designed into the system. Other factors, such as shift register size and the trade-off of velocity measurement accuracy with code length, more strongly determine the actual basic bit period used.

As previously discussed, the result of the signal processing (neglecting the effect of the notch filter and the altitude coding technique) provides an output at the limiter-discriminator as shown in Fig. 13a. The average value of this waveform is proportional to the closing velocity, whereas the rms value is proportional to range. To detect the rms value, the DC component is blocked and the discriminator output is synchronously detected to provide a waveform as shown in Fig. 13b. The waveforms of Figs. 13a and 13b are then low-pass filtered to provide DC outputs proportional to range and closing velocity.

In order to evaluate the trade-off of measurement accuracy versus measurement time, it is necessary to investigate the characteristics of the output waveform at the discriminator. The following sections derive the power spectrum of the discriminator output voltage and use the spectrum characteristics to estimate the filtering time constants necessary to reduce the AC ripple on the velocity and range measurements to acceptable values.

2. Velocity measurement accuracy versus integration time.— In order to determine the integration or smoothing time necessary to achieve a given accuracy in the velocity measurement, it is necessary to determine

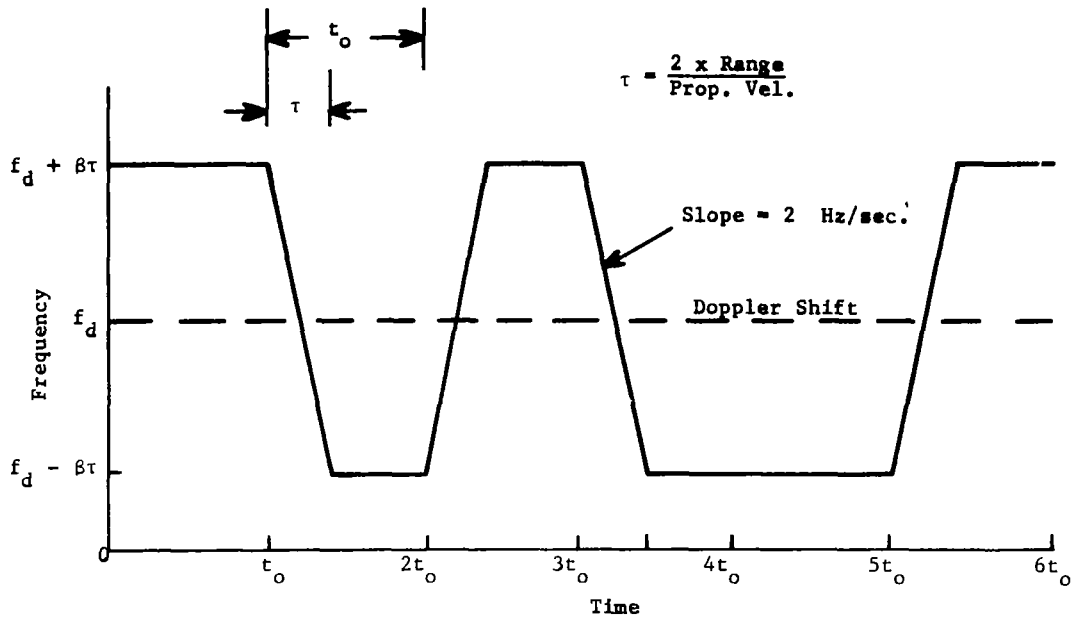


Fig. 13a. Frequency of waveform into discriminator ($t_o$ = bit period; $f_d$ = two-way Doppler shift; $\tau$ = two-way propagation delay).

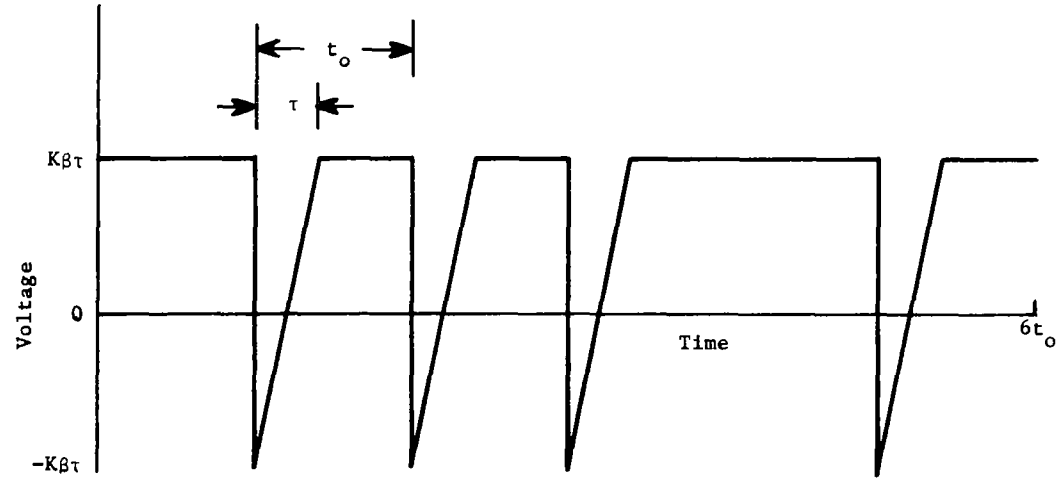


Fig. 13b. Output of discriminator after synchronous detection (range voltage). K is a conversion constant.

the spectral characteristics of the base-band signal from the discriminator. For simplicity, we will use frequency units (e.g., amplitude in Hz and power in $Hz^2$).

The power spectrum of the base-band signal from the discriminator, prior to filtering, is derived by noting that the signal is proportional to the difference between the frequency of the outgoing and incoming signal, or

$$f_o(t) = f_i(t) - f_i(t - \tau) \tag{9}$$

where $\tau$ is the two-way delay. The autocorrelation ($R_o(x)$) of $f_o(t)$ is then

$$R_o(x) = 2R(x) - R(x + \tau) - R(x - \tau) \tag{10}$$

and taking the Fourier transform gives

$$\Phi_o(\omega) = 2\Phi_i(\omega)[1 - \cos \omega\tau] \tag{11}$$

or

$$\Phi_o(\omega) = 4\Phi_i(\omega) \sin^2 \omega\tau/2 \tag{12}$$

where $\Phi_i(\omega)$ is the spectrum given in equation (8). Note that the DC component introduced by the Doppler shift is not included in the above spectrum because we assumed a constant delay $\tau$ in the derivation of equation (12).

Substitution of equation (8) into equation (12) gives

$$\Phi_o(\omega) = \left(\frac{2\pi\tau}{pt_o}\right)^2 \frac{p+1}{p^2} \sum_{\substack{n=-\infty \\ n\neq 0}}^{n=\infty} \left(\frac{\sin \pi n/p}{\pi n/p}\right)^2 \left(\frac{\sin \pi n\tau/pt_o}{\pi n\tau/pt_o}\right)^2 \delta\left(\omega - \frac{2\pi n}{pt_o}\right). \tag{13}$$

This spectrum is similar in form to equation (7) except for the added $\text{sinc}^2 \pi n\tau/pt_o$ term. This term is approximately unity over the lines of

interest for small ratios of delay/bit period. Since the total power in the waveform of Figure 12 is approximately $\beta^2\tau^2$ (where $\beta$ is slope of the integrated waveform), the spectrum of equation (13) can be re-normalized such that

$$\int_{-\infty}^{\infty} \Phi_{on}(\omega)\, d\omega \approx \beta^2\tau^2 \quad Hz^2 \tag{14}$$

by rewriting equation (13) as

$$\Phi_{on}(\omega) = \beta^2\tau^2\left(\frac{1}{p-1}\right) \sum_{\substack{n=-\infty \\ n\neq 0}}^{n=\infty} \left(\frac{\sin \pi n/p}{\pi n/p}\right)^2 \left(\frac{\sin \pi n\tau/pt_o}{\pi n\tau/pt_o}\right)^2 \delta\left(\omega - \frac{2\pi n}{pt_o}\right) . \tag{15}$$

If we assume that the voltage from the discriminator (Fig. 12) is passed through a unity gain low-pass filter with transfer function

$$H(j\omega) = \frac{\gamma}{j\omega + \gamma} , \tag{16}$$

then the spectrum of the filter output is

$$\Phi_v(\omega) = |H(j\omega)|^2\, \Phi_{on}(\omega) \tag{17}$$

and the total AC output power is

$$P_o = \int_{-\infty}^{\infty} \Phi_v(\omega)\, d\omega \qquad Hz^2.$$

This integral is difficult to evaluate exactly; however, it is possible to show that the output AC power will satisfy the inequalities

$$\begin{aligned} &(1) \quad \text{For } \gamma >> \frac{2\pi}{pt_o} ; \quad \frac{P_o}{P_{in}} < \frac{1}{p-1}\left(\frac{\gamma pt_o}{2} + 1\right) \\ &(2) \quad \text{For } \gamma << \frac{2\pi}{pt_o} ; \quad \frac{P_o}{P_{in}} < \frac{1}{p-1}\left(\frac{\gamma pt_o}{\pi}\right)^2 \approx p\left(\frac{\gamma t_o}{\pi}\right)^2 \end{aligned} \tag{18}$$

In the above, $t_o$ is the basic pulse period, $\gamma$ is the break frequency of the low-pass filter in rad/sec., and p is the number of bits in the code. Thus, for $\gamma << 2\pi/pt_o$, the AC rms output ripple is approximately

$$\text{AC rms} \approx \frac{1}{\pi} \beta\tau\gamma t_o \sqrt{p} \quad \text{Hz}, \tag{19}$$

since the input power is $\approx \beta^2\tau^2$ $\text{Hz}^2$.

The magnitude of the ripple is given in Table 3 for various conditions in Hz and in knots using the Doppler conversion factor of 1 Kt = 17.7 Hz.

Table 3. Approximate RMS ripple on Closing Velocity Measurement for 127-bit PN codes with FM slope ($\beta$) of 16.6 MHz/sec and a bit period ($t_o$) of 10 ms for various values of low-pass filter break frequency.

| RANGE (n. mi.) | Low-Pass Filter Break Frequency (rad/sec) | | | |
|---|---|---|---|---|
| | .5 | 1 | 2 | 4 |
| 1 | 3.7 Hz (.2 Kts) | 7.4 Hz (.4 Kts) | 14.8 Hz (.8 Kts) | 29.6 Hz (1.6 Kts) |
| 2 | 7.4 Hz (.4 Kts) | 14.8 Hz (.8 Kts) | 29.6 Hz (1.7 Kts) | 59.2 Hz (3.3 Kts) |
| 10 | 36.9 Hz (2.1 Kts) | 73.8 Hz (4.2 Kts) | 147.4 Hz (8.3 Kts) | 294.8 Hz (16.6 Kts) |

3. Range measurement accuracy versus integration time.— Inspection of the waveform used to derive the range voltage (Fig. 13a) indicates that the worst case, the lowest frequency component present in the synchronously detected waveform will be at a frequency of $1/t_o$. For this reason, the AC ripple component on the range voltage is not felt to be a problem as serious as that in filtering the velocity information.

If it is assumed that the downward spikes as shown in Fig. 13a occur with a period $t_o$, the power in the AC component is found to be

$$P_{ac} \approx \frac{4}{3} \frac{\beta^2 \tau^3}{t_o} \left[1 + \frac{3}{4} \frac{\tau}{t_o}\right] \quad Hz^2 \quad . \tag{20}$$

Furthermore, if it is assumed that this total power is in the fundamental AC component, then the AC ripple as a function of a low-pass filter break frequency $\gamma$ is given approximately by

$$\text{rms ripple} \approx \frac{\beta\tau\gamma}{\pi} \left[\frac{2t_o\tau}{3}\right]^{1/2} \quad Hz \tag{21}$$

for $\gamma << 2\pi/t_o$.

The magnitude of the rms ripple in Hz is less than .3% of a 10 n.mi. range measurement value for a low-pass filter break frequency of 1 rad/sec and code parameters as given in Table 3. Since the 10 n.mi. case gives the largest value of ripple, the ripple on the range measurement at closer ranges can be considered negligible.

It should be noted that the DC level of the synchronously detected signal is approximately

$$E_{DC} \approx \beta\tau(1 - \frac{\tau}{t_o}) \quad , \tag{22}$$

hence the variation of the DC level with range is not linear. For small values of $\tau/t_o$, the deviation from linearity will be small.

### C. Application to Recognition Coding

The PN codes provide for multiple access by a spectrum spreading technique. The slow FM modulation of the carrier by the integrated PN code spreads the transmitted energy over a bandwidth corresponding to the peak-to-peak frequency deviation of the waveform. At the transponder, the signal is linearly amplified, shifted in frequency, and retransmitted in the same form. There is no problem with multiple access at the transponder since the transponder is linear up to a power output corresponding to the saturation level (approximately one watt or 30 dbm).

At the receiver, a sample of the transmitted signal is used in the first mixer to translate the input signal to an intermediate frequency. The IF bandwidth need only be wide enough to pass the single sideband Doppler signal, or approximately 13 KHz, for a receiver with a closing velocity coverage of 500 knots. Signals which were not transmitted from the ownship transmitter are noncoherent with the ownship transmitter signal and hence are spread over a bandwidth approximately twice the peak-to-peak deviation of the transmitted signal. This situation is shown pictorially in Fig. 14.

Passage of the signal and interfering signals through the relatively narrow band single sideband filter (assumed rectangular) removes a large part of the interfering energy while passing the ownship return with no attenuation. The signal-to-interference ratio out of the single sideband filter is related to the input signal-to-interference ratio as given in equation (23):

$$\left(\frac{S}{I}\right)_{IF} \approx \frac{2W_1}{BD}\left(\frac{S}{I}\right)_{in} \tag{23}$$

where $W_1$ is the one-sided peak deviation of the FM transmitted signal and BD is the bandwidth of the SSB filter.

For representative system parameters ($W_1 \approx 1.08$ MHz, BD = 13 KHz), the enhancement of desired signals over interfering signals is 166 or approximately 22.2 db. This degree of signal enhancement implies that it would take 166 interfering signals to equal the power level of a desired signal at the output of the single sideband filter (for equal range and transmitted power levels).

As mentioned in Section III, the signals in the IF are effectively differentiated twice in order to enhance the most hazardous signal. This double differentiation operation causes the signal-to-interference power ratio at the output of the double differentiator to be a function of the Doppler frequency shift. For a double differentiator in cascade with an ideal rectangular SSB filter with bandwidth BD, the signal-to-interference ratio at the output of the Doppler filter - double differentiator combination is derived as

$$\left(\frac{S}{I}\right)_{out} \approx \frac{10W_1}{BD}\left(\frac{f_d + f_o}{BD}\right)^4\left(\frac{S}{I}\right)_{in} \tag{24}$$

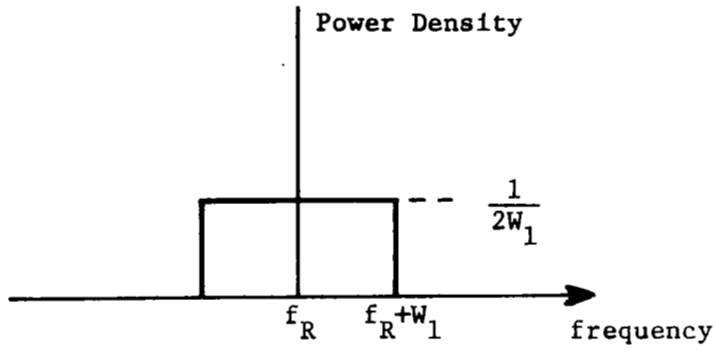


(a) Normalized power density at receiver input

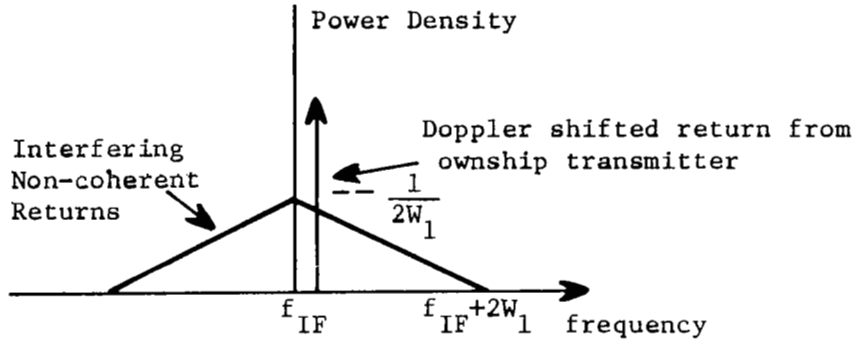


(b) Normalized power density out of 1st receiver mixer

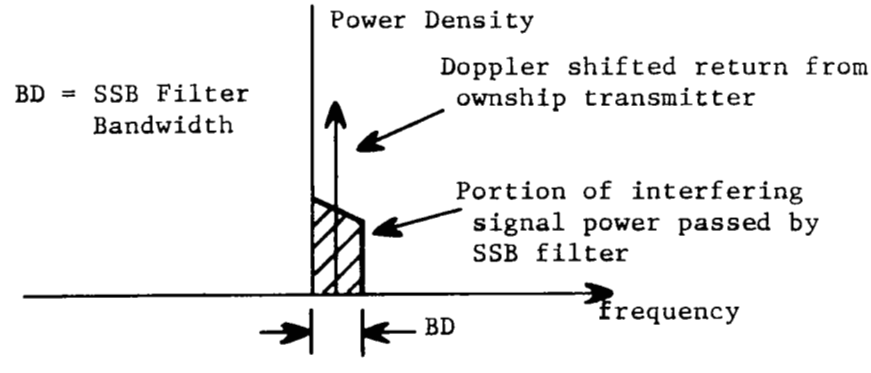


(c) Normalized power density out of SSB Filter

Fig. 14. Sketches of power density at various points in the receiver indicating the separation of ownship returns from interfering signals.

where $f_d$ is the Doppler frequency shift of the signal and $f_o$ is the frequency offset to provide the modified tau characteristic. In deriving this equation, the interfering power density is taken as $\frac{I}{2W_1}$ watts/Hz.

Note that for an input signal at a given frequency, the signal-to-interference ratio decreases by 50 db/decade as the bandwidth BD increases. This indicates the desirability of limiting the closing velocity coverage (and hence the necessary Doppler bandwidth) to the minimum consistent with that expected to be encountered.

In shaping the frequency characteristics of the receiver passband to achieve the effect of a SSB filter in cascade with a double differentiator, it is desirable from considerations of signal-to-noise plus interference ratios to use a passband shaped as shown in Figure 15a. This characteristic also approximates more closely the frequency vs. attenuation characteristics that can be attained in practice.

Figure 15b indicates the hazard region coverage in the range - closing velocity plane that corresponds to the passband shape of Figure 15a. Note that the coverage approximates a modified tau characteristic for closing velocities less than 380 knots and approaches a standard tau characteristic for closing velocities greater than 380 knots. This characteristic has been shown to be desirable (see Ref. [ 4 ]) to limit the number of alarms received under normal operating conditions while not adversely affecting the actual time available for avoidance of a hazardous situation.

For a receiver passband with a shape as in Figure 15a, the output signal-to-interference power ratio is calculated from the expressions,

$$\left(\frac{S}{I}\right)_{out} \approx \frac{10W_1}{(5B_2 - 4B_1)} \left(\frac{f_d + f_o}{B_1}\right)^4 \left(\frac{S}{I}\right)_{in}, \qquad 0 < f_d + f_o < B_1, \tag{25}$$

and

$$\left(\frac{S}{I}\right)_{out} \approx \frac{10W_1}{(5B_2 - 4B_1)} \left(\frac{S}{I}\right)_{in}, \qquad B_1 < f_d + f_o < B_2, \tag{26}$$

where $B_1$ and $B_2$ are the break frequencies defined in Fig. 15a and the remaining nomenclature is as given for equations (23) and (24).

For the evaluation of system performance in Section IV, equations (25) and (26) are used in the calculation of signal-to-interference ratios.

The above considerations have assumed that the desired return and the interfering returns are noncoherent or nonsynchronous. There exists a possibility that the PN codes in two different transmitters or in a transmitter and cooperating transponder are in synchronism. The chances of PN code synchronism and the effects caused by this phenomenon are considered in Section V.

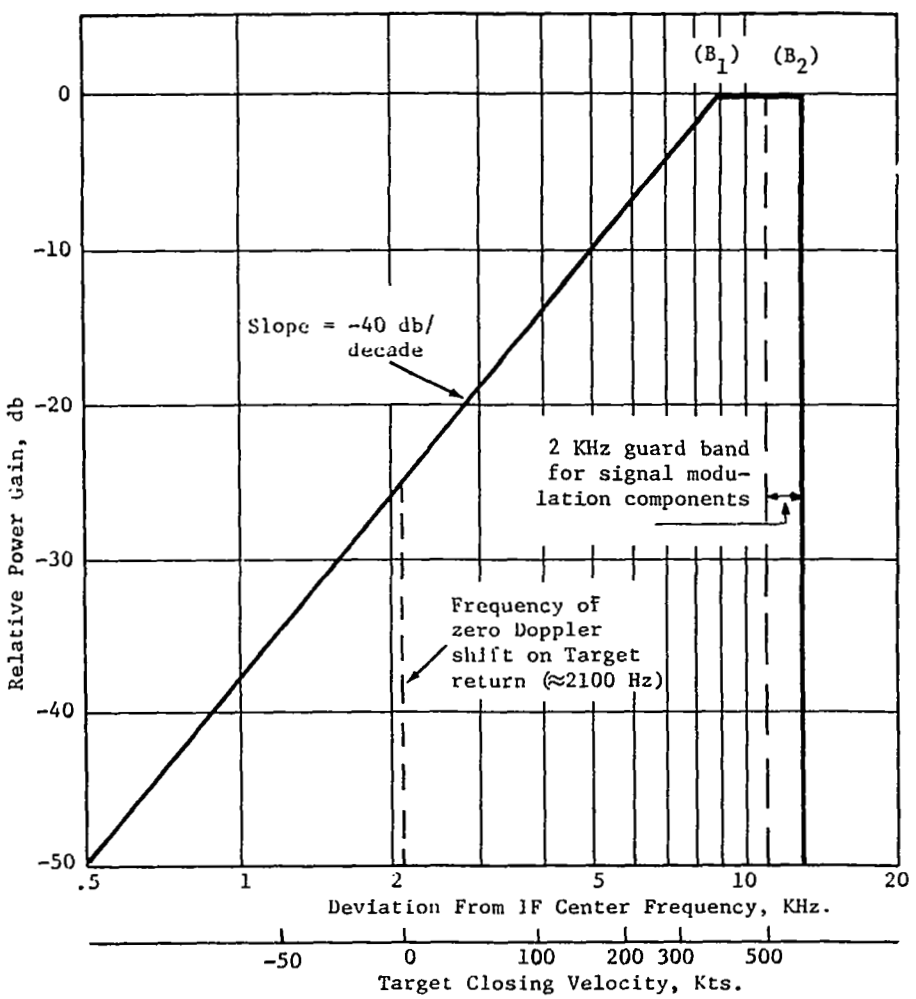


Fig. 15a. Idealized receiver IF passband characteristics (SSB) for system with 500 Kt. closing velocity coverage. The IF is offset by a frequency corresponding to a closing velocity of approximately 120 Kts. (≈ 2100 Hz.).

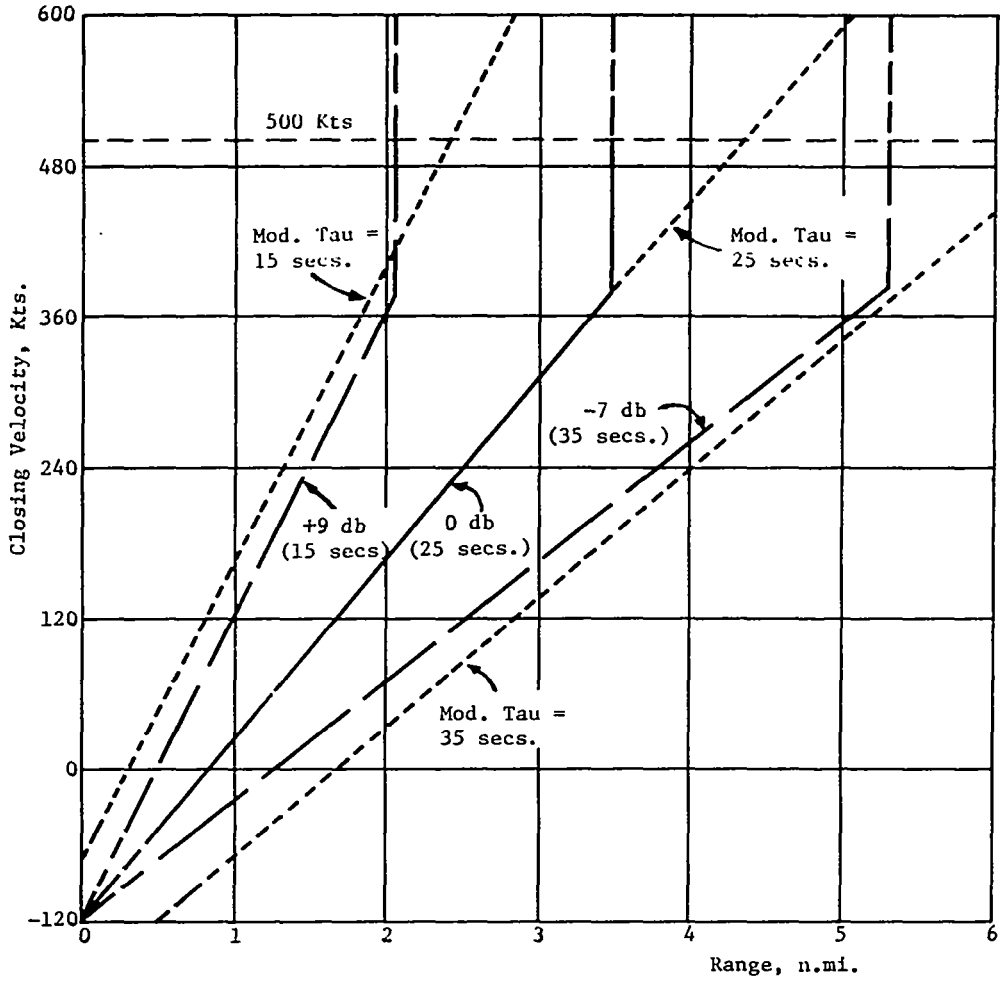


Fig. 15b. Constant signal power contours in the range-closing velocity plane for the receiver passband characteristic given in Fig. 15a. The db values are relative to the power level corresponding to a value of modified tau of 25 secs., and indicate approximations to the 15 and 35 sec. modified tau characteristics.

# V. EVALUATION OF SYSTEM PERFORMANCE

## A. Evaluation Techniques

A computer simulation approach has been used to determine the severity of the saturation and interference problems for the system under multiple aircraft conditions.

A detailed analytical model of the system has been developed (see Appendices B, C, and D). The simulation model is shown in flow diagram form in Fig. 16. The model accepts as inputs coordinates and coordinate rates of N aircraft, the set of system parameters, and the experimentally derived antenna patterns of the transmitter, transponder, and receiver.

The simulation outputs include statistics on system parameters of interest, including the signal, interference, and noise power levels at various points in the transponder and receiver. The statistics developed are given as "average percentage of flying time that a certain power level exceeded a specified level." This statistic provides an unbiased estimate of the probability that a randomly selected system will have a power level exceeding the specified level at any particular instant of time.

The input position data to the simulation consisted of (1) two aircraft, straight line encounter situations, (2) actual radar traffic data obtained from the Atlanta terminal during 1967, and (3) extended density traffic developed by a Monte Carlo technique described in Section V.D.

The Atlanta radar traffic data consisted of the three-dimensional position coordinates of each aircraft under radar track in the terminal area taken at four-second intervals. Twelve one-hour samples of data were taken over a five-day period. The data base is described in detail in Ref. [2 ]. For evaluation of the saturation and interference problem with the Atlanta data base, the most dense hour of the twelve hours of data was selected. This hour (hour 11), included 68 aircraft of which 50 were arrivals and 18 were departures. The average number of aircraft per radar scan (4-second interval) was approximately 12.7.

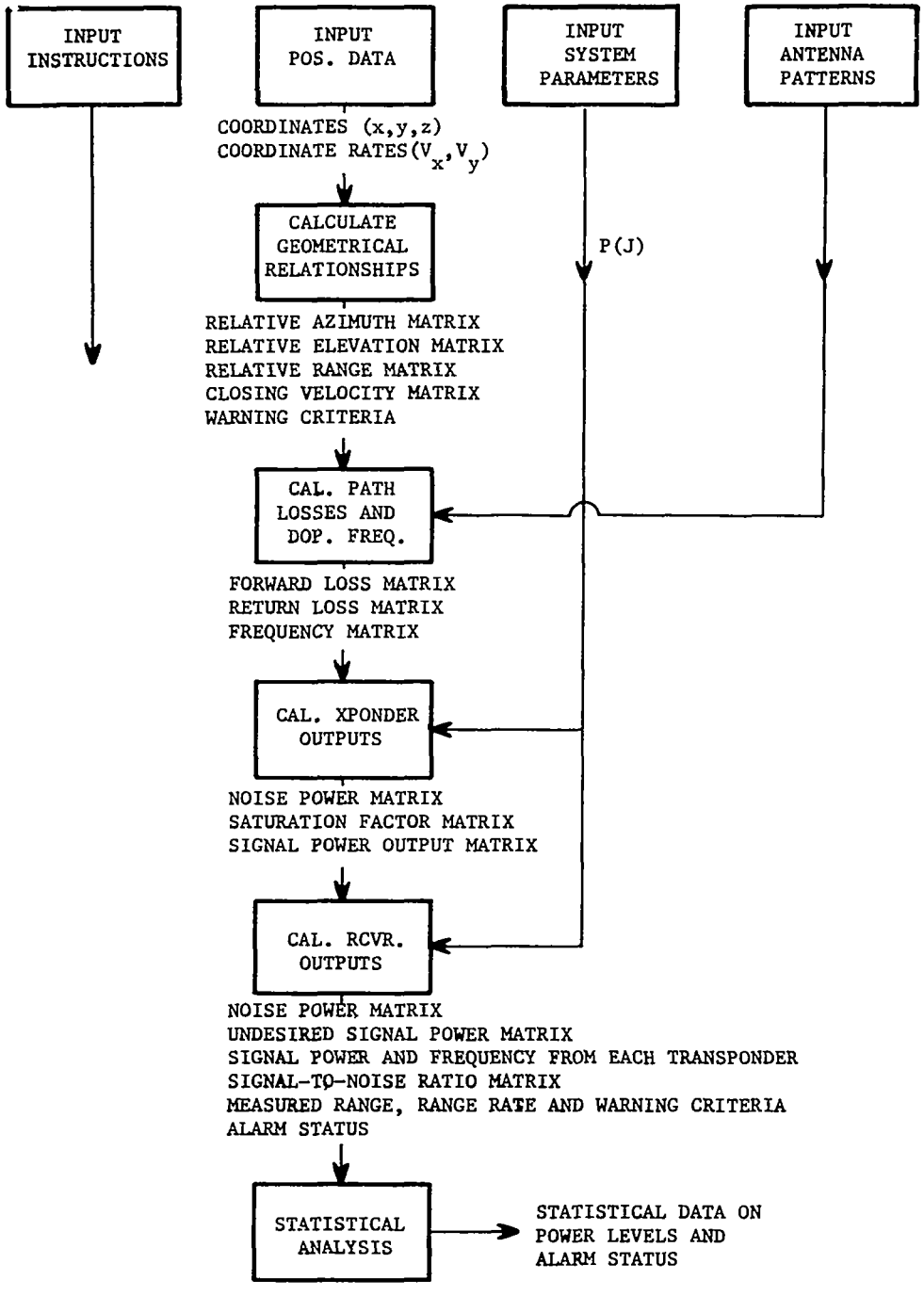


Fig. 16. Flow diagram of system simulations.

The maximum number of aircraft recorded in any one radar scan was 18. Fig. 17 shows a plot of the tracks of the aircraft in the Hour 11 data base.

The coverage volume of the data base generally included those aircraft under 6500 ft. in altitude and within a radius of 35 n.mi. of the Atlanta terminal.

The extensions of the Atlanta data to more dense situations (up to 40 aircraft simultaneously within a 35-mile radius), or roughly three times the Atlanta traffic density, are described in Section V.D.

### B. Simulated Two Aircraft Encounters

To investigate the alarm performance of the system under various conditions, a series of two aircraft encounters has been simulated. For each flight path condition, the power level vs. time of the power at the output of the double differentiator has been plotted. Also, the alarm status of the system is indicated (vs. time) on the plots.

The alarm status code used is as follows:

| Alarm Status Code | Signal-to-Noise Ratio Threshold Exceeded (13 db) | Modified Tau Threshold Exceeded(25 sec) | Power Level Threshold Exceeded |
|---|---|---|---|
| 0 | Yes or No | No | No |
| 1 | Yes | Yes | Yes |
| 2 | Yes | No | Yes |
| 3 | Yes | Yes | No |
| 4 | No | Yes | Yes |
| 5 | No | No | Yes |
| 6 | No | Yes | No |

The main purpose of this series of encounters was to determine the differences between alarm thresholds based on a power level threshold versus those based on a modified tau calculation from the geometry of the situation. The antenna pattern effect is thus made evident in the cases considered.

Since a signal-to-noise plus interference ratio of approximately

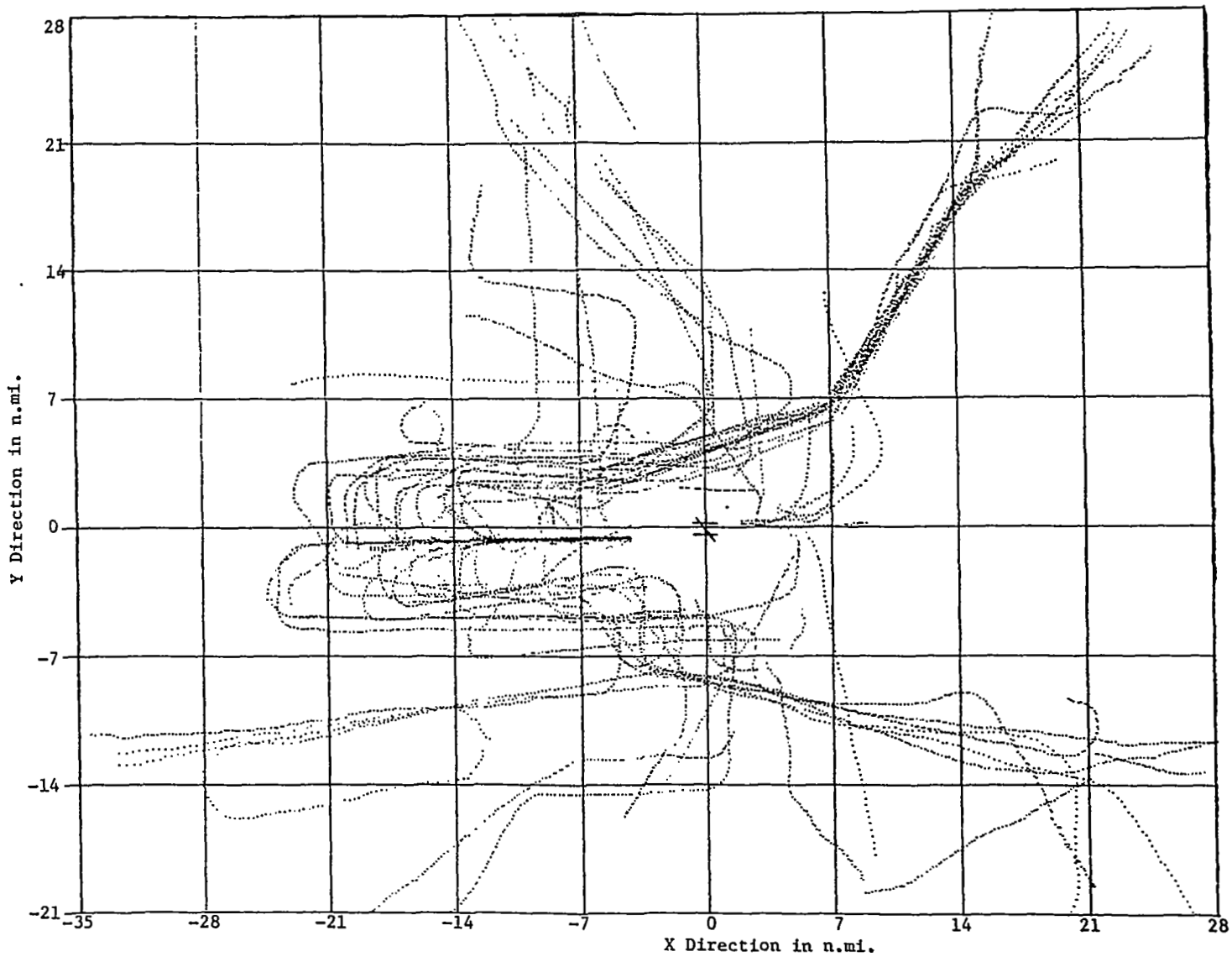


Fig. 17. Plot of the radar tracks taken from Hour 11 of the Atlanta data base. The Atlanta terminal is at the center of the coordinates.

13 db is required at the input of the FM detector for reliable demodulation, the threshold was set at this value. The geometrical modified tau threshold and the power level threshold were set at values corresponding to a modified tau of .25 seconds. The increment of time used in the calculations is .1 minute. The values of range and modified tau indicated on the plots are the values noted immediately after the alarm occurred.

Figures 18 through 24 show the flight paths, power levels, and alarm for the various conditions considered.

Under conditions 1, 2, and 3 (head-on approaches), the alarm status encountered indicated that all thresholds were exceeded (status #1). For conditions during which the intruding aircraft was approaching at an angle, the alarm status calculations indicate that in one case (condition #4) an alarm would have been received if a power threshold only was used, but the value of modified tau did not exceed a 25 second threshold during this simulated flight. In condition 5 the power threshold was exceeded before the geometrical threshold, whereas in condition 6, the opposite occurred. These periods of occurrence were short, however, and of minor significance.

In all cases, the signal-to-noise plus interference ratio was amply exceeded prior to the point of closest approach.

### C. Performance Under Multiple Aircraft Conditions Using the Atlanta Data Base

1. General Discussion.— To determine the severity of the saturation and interference problem for the PWI system, the simulated system has been "flown" on all aircraft in the radar traffic data from the Atlanta terminal (Hour 11). Statistics have been derived on the "average percent of flying time that a certain power level exceeded a specified level." It should be recalled that this statistic also provides an unbiased estimate of the probability that a randomly selected system will have a power level exceeding the specified level at any particular instant of time.

The system parameters used in this particular study are given in Section III.D. The antenna patterns used include the best available data

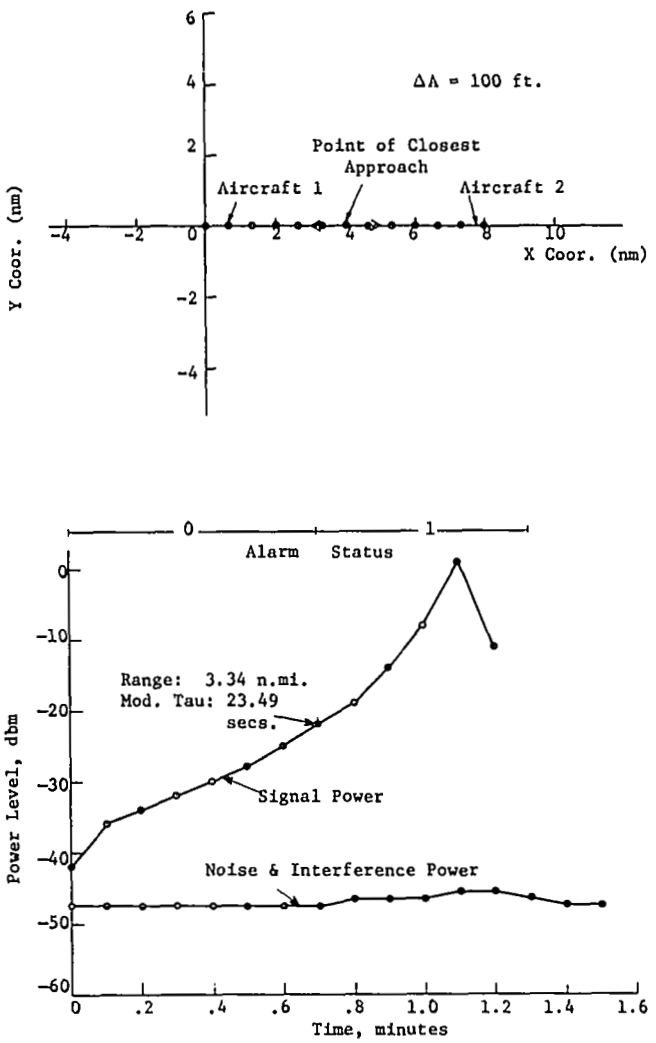


Fig. 18. Flight paths, power levels and alarm status for a head-on encounter with an altitude separation of 100 ft. (condition #1).

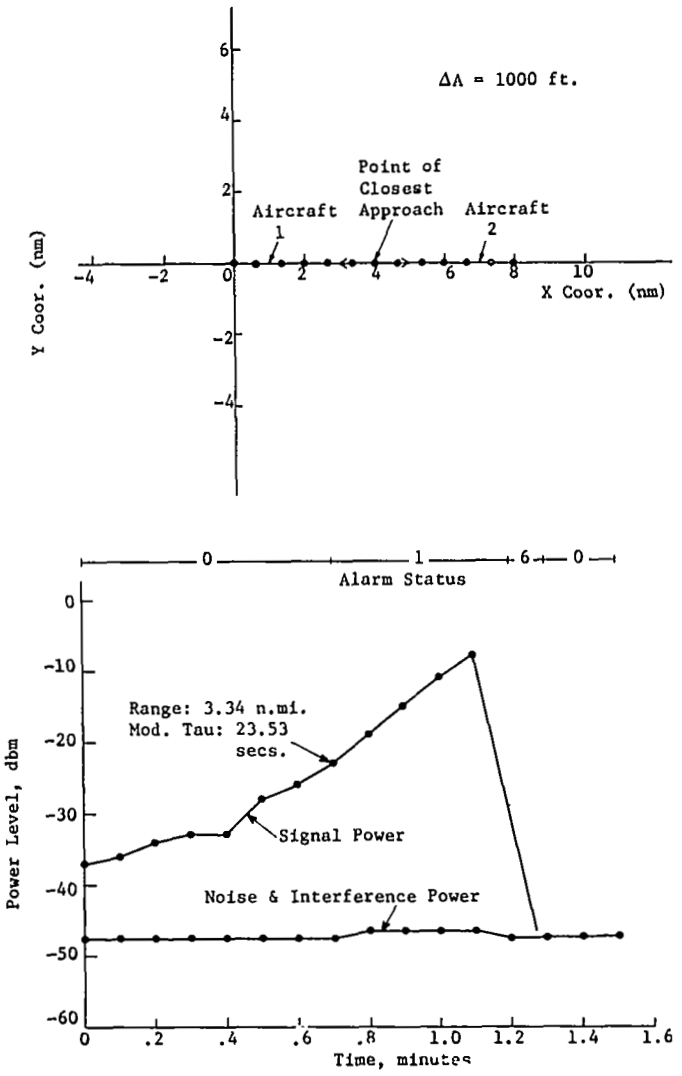


Fig. 19. Flight paths, power levels and alarm status for a head-on encounter with an altitude separation of 1000 ft. (condition #2).

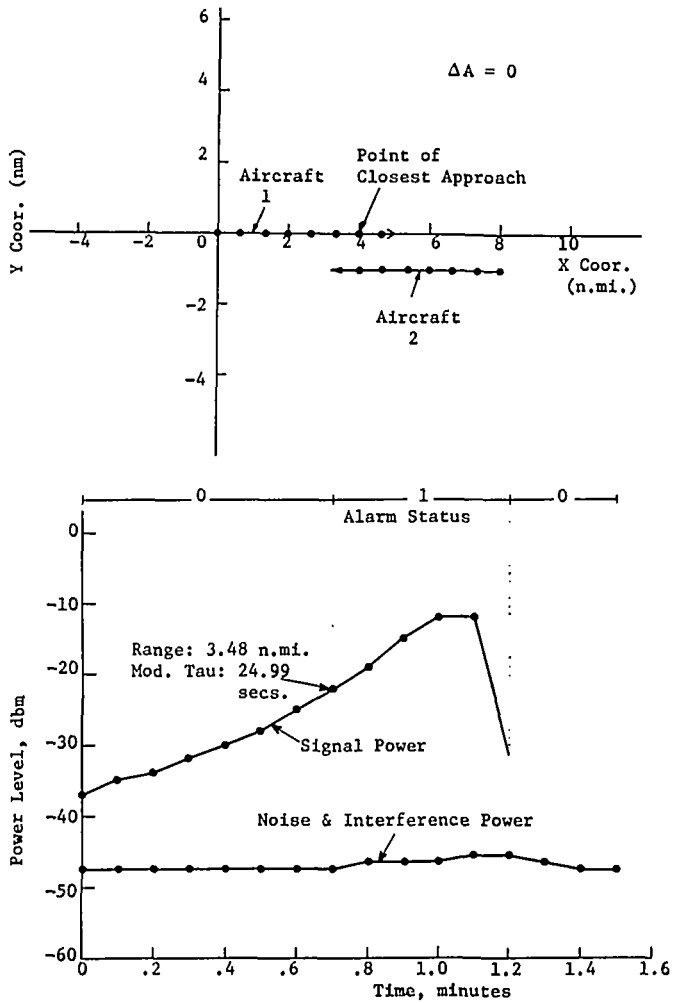


Fig. 20. Flight paths, power levels and alarm status for a 180° encounter with a lateral miss-distance of 1 n.mi. (condition #3).

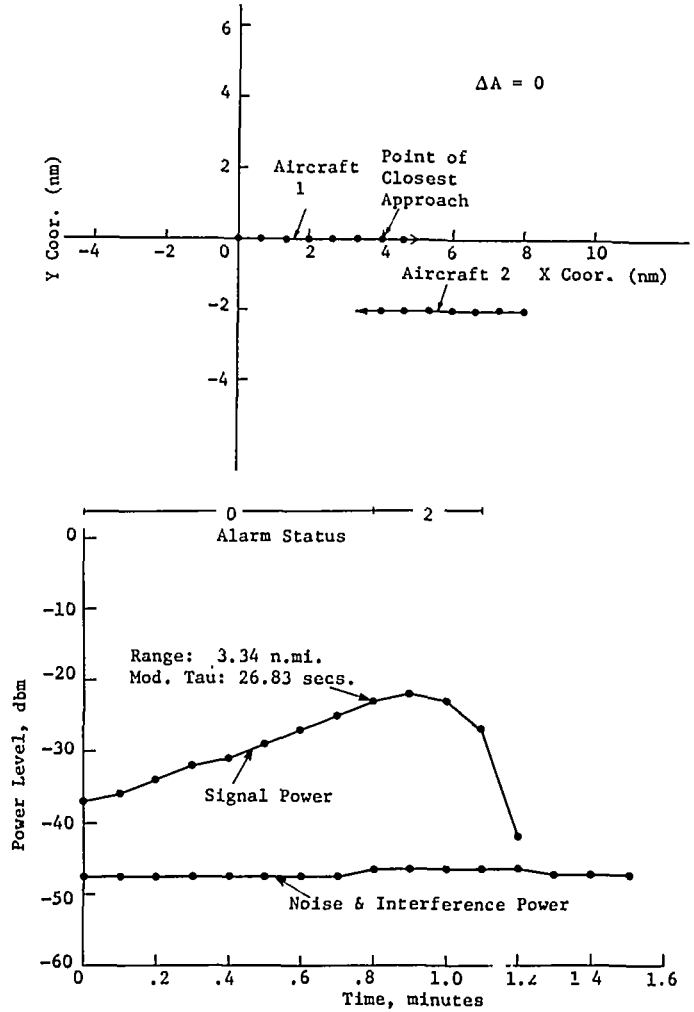


Fig. 21. Flight paths, power levels and alarm status for a 180° encounter with a lateral miss-distance of 2 n.mi. (condition #4).

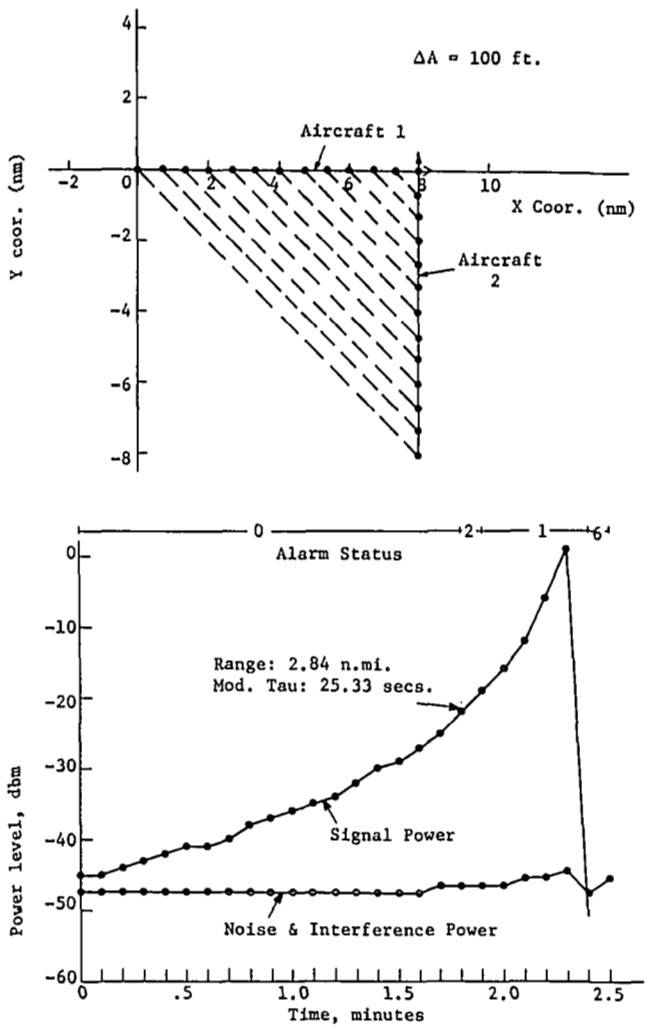


Fig. 22. Flight paths, power levels and alarm status for a 90° encounter with zero lateral miss-distance and an altitude of 100 ft. (condition #5).

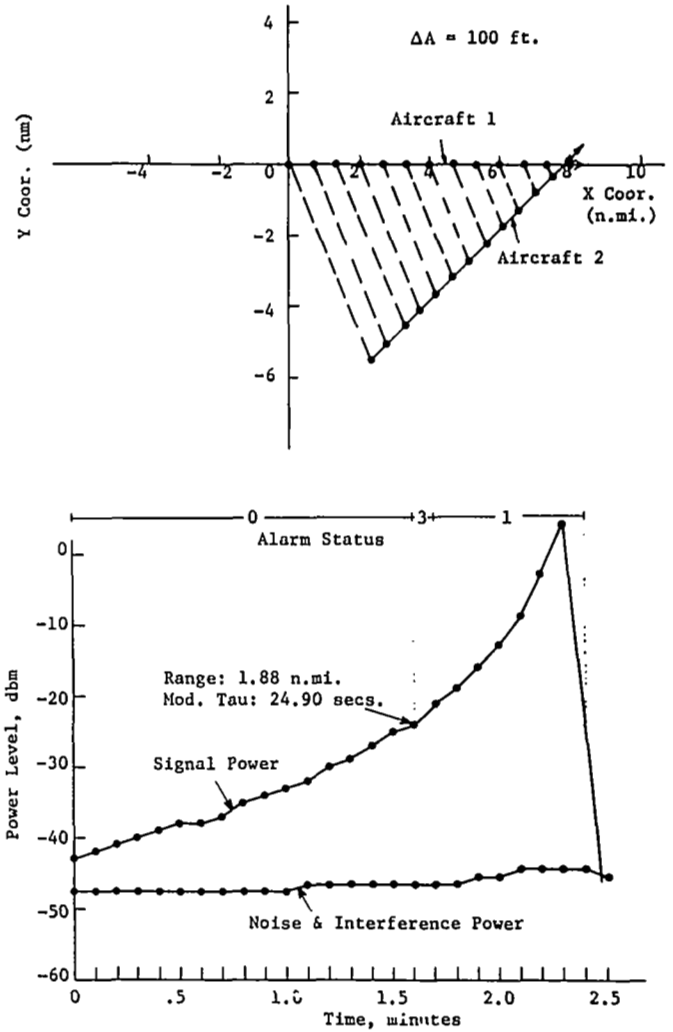


Fig. 23. Flight paths, power levels and alarm status for a 135° encounter with zero lateral miss-distance and an altitude of 100 ft. (condition #6).

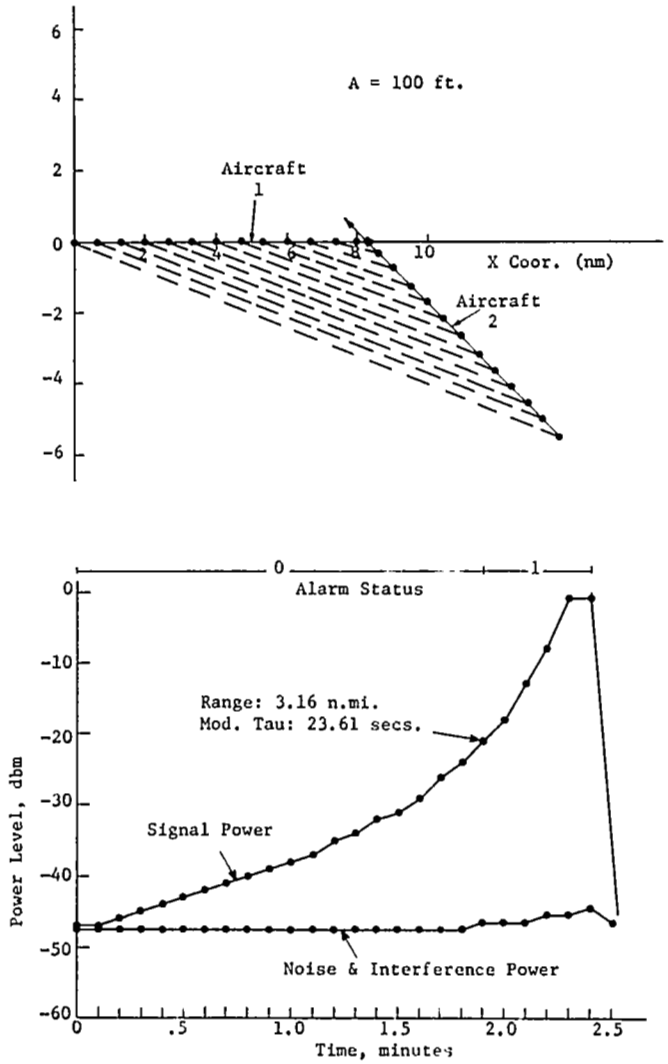


Fig. 24. Flight paths, power levels and alarm status for a 45° encounter with zero lateral miss-distance and an altitude of 100 ft. (condition #7).

existing at the present time on the antenna configuration. These included updated receiver patterns based on recent anechoic chamber measurements and the transmitter and transponder patterns that were measured for the two-frequency L-band system. The patterns are given in Appendix B.

2. Transponder characteristics.— Figure 25 indicates the average percent of time that the transponder saturation factor was greater than a value $S_k$ for the Hour 11 data base. The saturation factor is the ratio of the nominal transponder gain to the actual transponder gain. From the curve, we see that the saturation factor was greater than 1.45 approximately 1% of the time. In other words, there exists a probability of a gain reduction greater than approximately 1.4 db of .01. No cases were noted for which the saturation factor exceeded 2.6 db.

Figure 26 shows the average percentage of time that the power output of the transponder is greater than a value $P_k$ for various outputs. The total transponder output power exceeded 25 db approximately .7% of the time. Note also that the transponder signal-to-noise ratio for the largest signal is less than 0 db approximately 40% of the time. Because of the processing gain achieved in the receiver, the fact that the signal-to-noise ratio is less than 0 db should not be detrimental to the operation of the system.

From the power statistics on the transponder, we can conclude that with the system parameters used and with the Hour 11 data base, the transponder is not prone to saturation and is operating well within a power limitation of one watt or 30 dbm. Although the probability is high that the largest signal will be below the transponder noise level of approximately 13 dbm, this is not detrimental to the operation of the system. While the noise level of 13 dbm sounds excessive, it should be recalled that this power is spread over a bandwidth of approximately 4 MHz.

3. Receiver performance.— The signal levels at the receiver double differentiator output are shown in Fig. 27. A gain in the receiver to the limiter-discriminator output of approximately 86 db has been assumed. Approximately 45% of the time, the largest signal at the double differentiator output is below the noise plus the interference power level. The largest signal-to-noise plus interference power ratio exceeds 10 db only 9.5% of the time. This situation is also indicated in Fig. 28, which plots the signal-

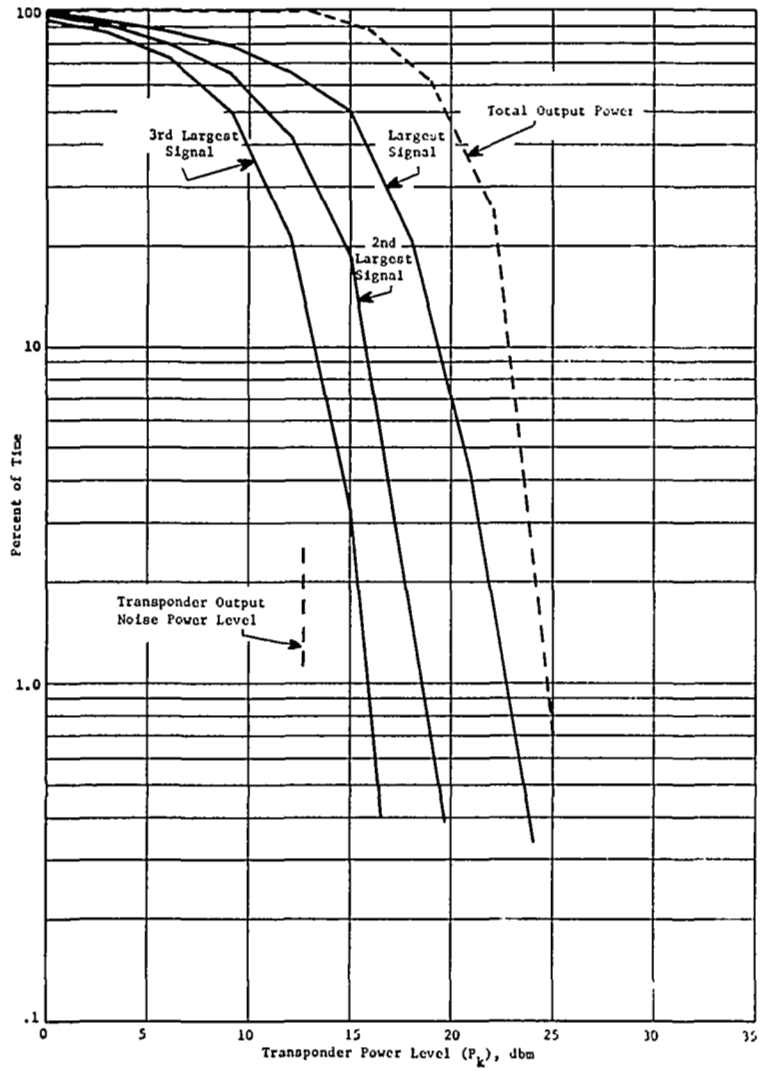


Fig. 25. Average percent of time that the transponder saturation factor is greater than $S_k$ for Hour 11 data.

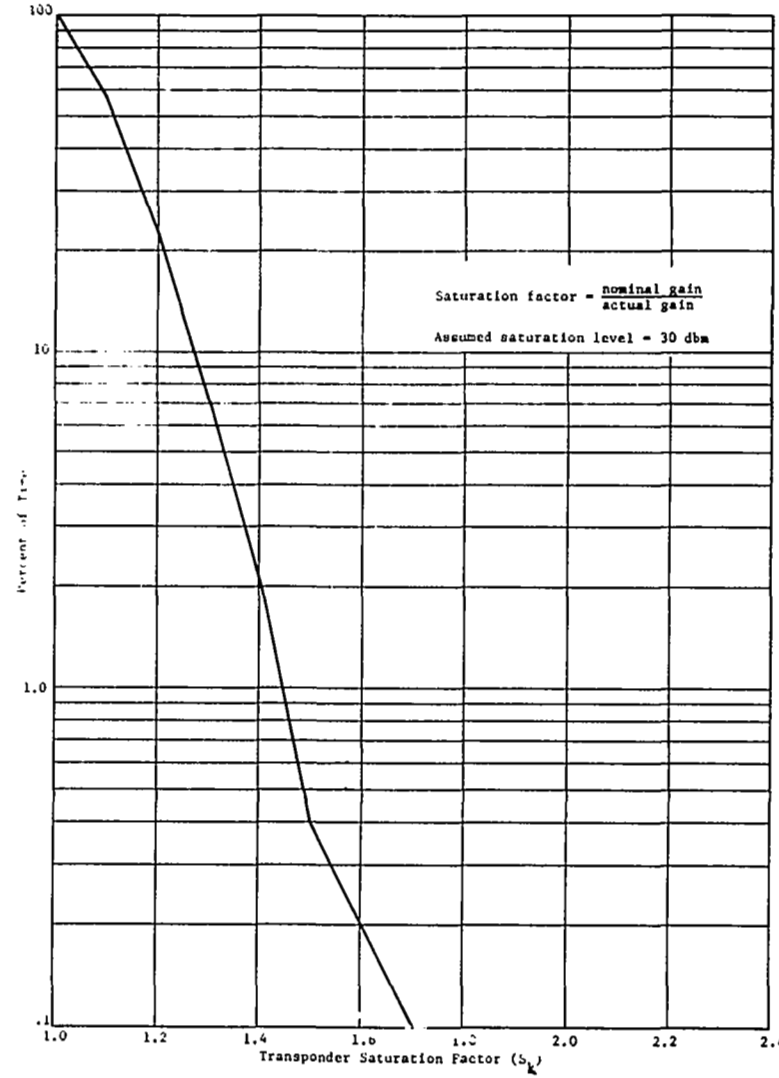


Fig. 26. Average percent of time that the power output of the transponder is greater than $P_k$ for various outputs, Hour 11 data.

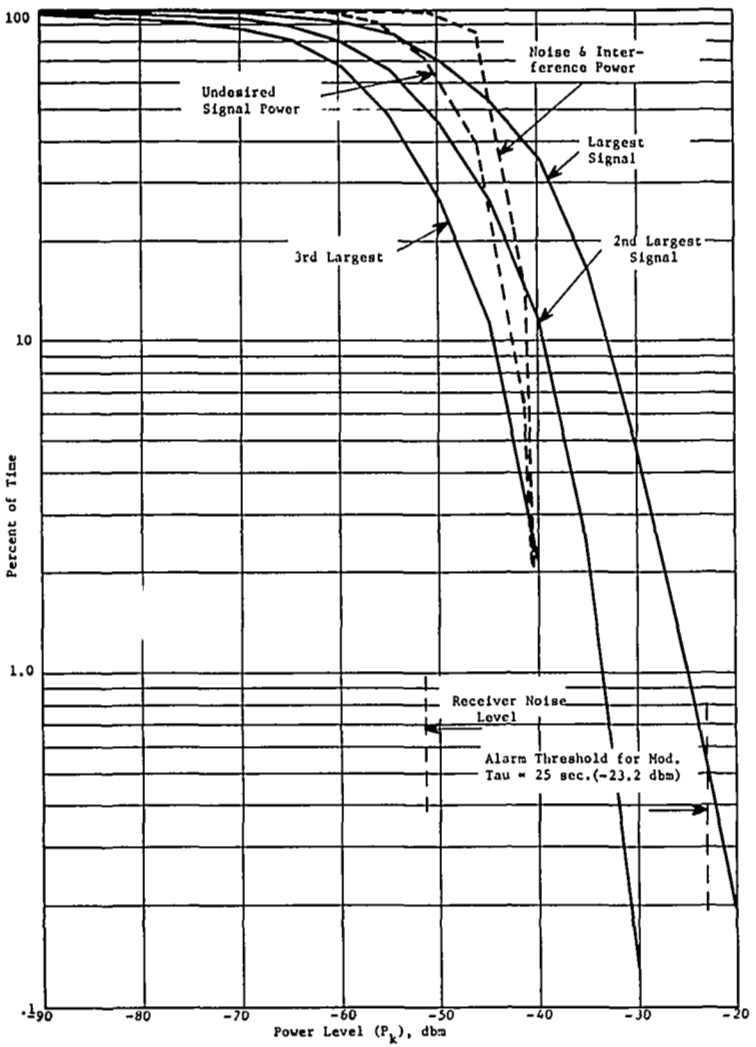


Fig. 27. Average percent of time that the power level at the double differentiator output is greater than $P_k$, Hour 11 data.

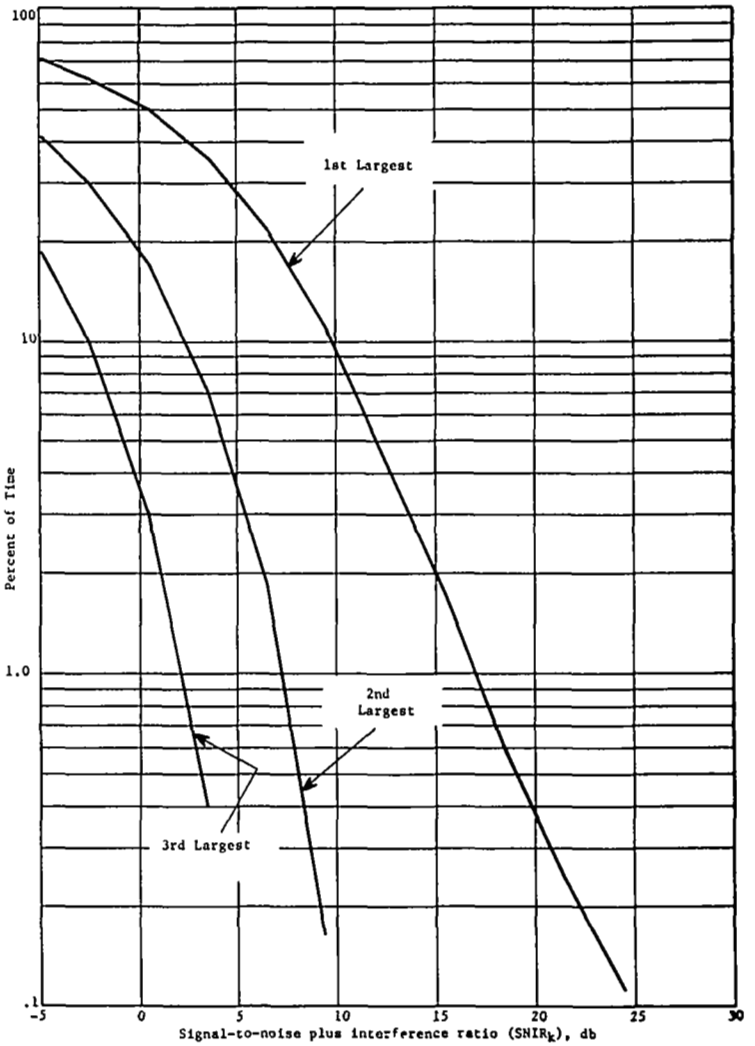


Fig. 28. Average percent of time that the signal-to-noise plus interference power ratio at the double differentiator output is greater than $SNIR_k$, Hour 11 data.

to-noise plus interference power ratios at the double differentiator output. The interference power (which arises from transponder outputs which are returns to receivers other than the receiver under consideration) is less than the receiver noise level approximately 36% of the time. These undesired signal returns effectively increase the noise level of the receiver by 10 db approximately 15% of the time. Very rarely, however, did the undesired signal returns increase the receiver threshold by as much as 15 db.

The indication that the receiver is operating with low signal-to-noise ratios for a large percent of the time is not necessarily detrimental to the system operation if the signal-to-noise ratio is high during the period when an alarm should be received. For a power threshold corresponding to a modified tau value of 25 seconds, Fig. 29 plots the largest signal power at the double differentiator output. The corresponding signal-to-noise plus interference ratios (SNIR) are shown in Fig. 30. The SNIR for the largest signal, or the signal causing the alarm, is in all cases greater than 16 db.

Signal levels using a 25 second alarm threshold based on a calculation of modified tau from the range and range rate of the aircraft providing the largest signal at the double differentiator output are given in Figs. 31 and 32. These power statistics compare well with those obtained using the corresponding power threshold (Figs. 29 and 30). When a signal-to-noise ratio constraint was added to this criterion such that the SNIR had to exceed 13.3 db before an alarm was registered, 5 alarm cases (out of 85 cases noted without this constraint) were dropped.

Figures 33 and 34 are plots of signal levels and SNIR while in an alarm status, with the power threshold corresponding to a modified tau value of 35 seconds. Figures 35 and 36 show similar plots of signal levels and SNIR while in an alarm status with the alarm threshold based on range and range rate measurements and for a modified tau value of 35 seconds. In this situation, the SNIR of the largest signal exceeded 3 db in all cases. This SNIR is less than the value required to make reliable measurements of range and range rate using the voltages derived from the FM signal. The probability of exceeding a 13.3 db SNIR threshold

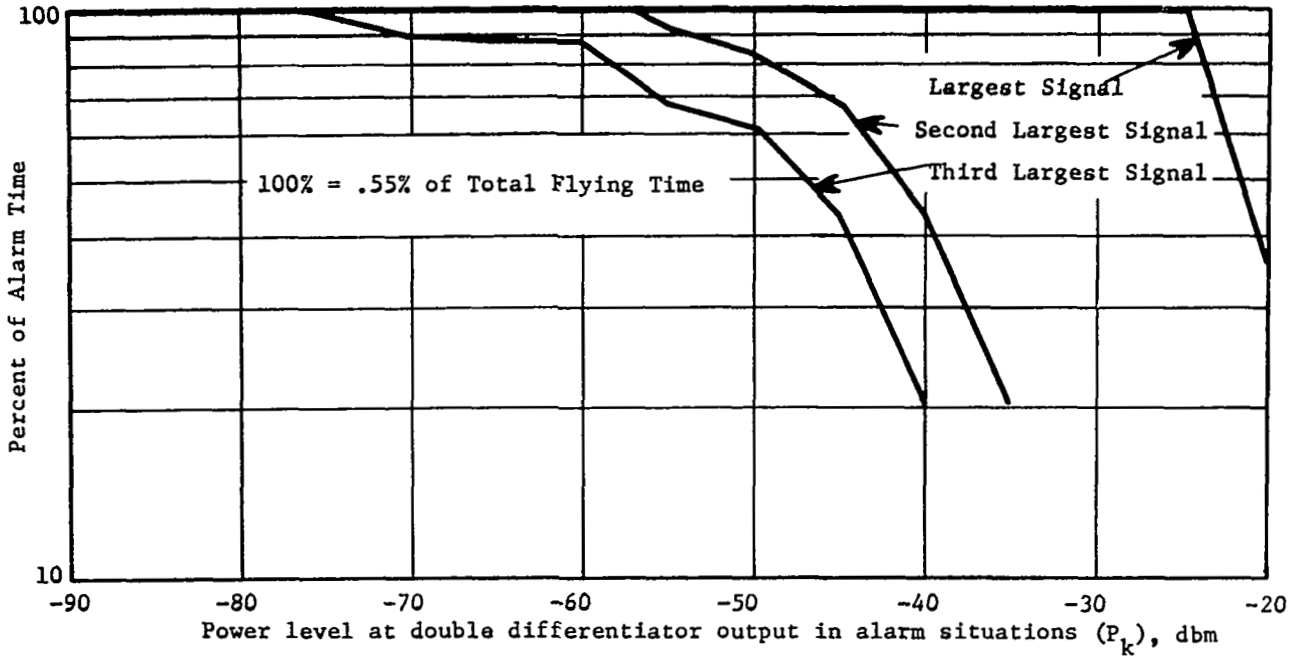


Fig. 29. Average percent of time that the received power level is greater than $P_k$ for alarm situations only, Hour 11 data. Power level threshold corresponding to modified tau = 25 secs.

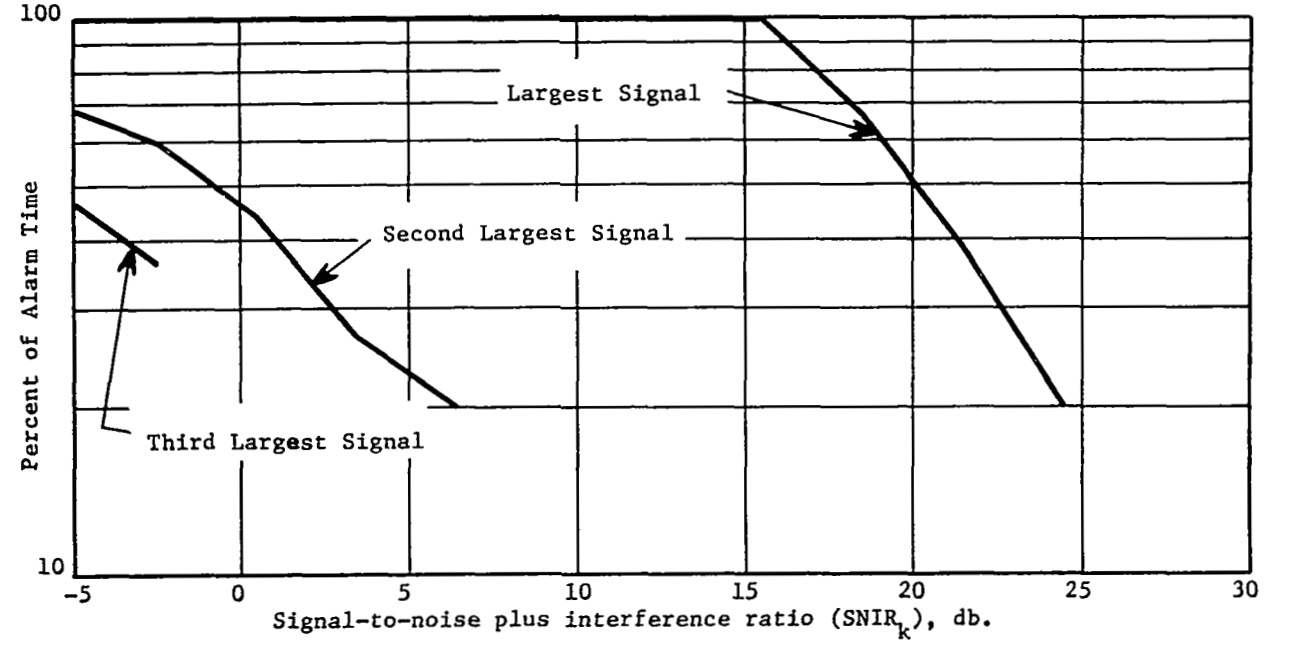


Fig. 30. Average percent of time that the signal-to-noise plus interference ratio at the double differentiator output is greater than $SNIR_k$ for alarm situations only, Hour 11 data. Power level threshold corresponding to modified tau = 25 secs.

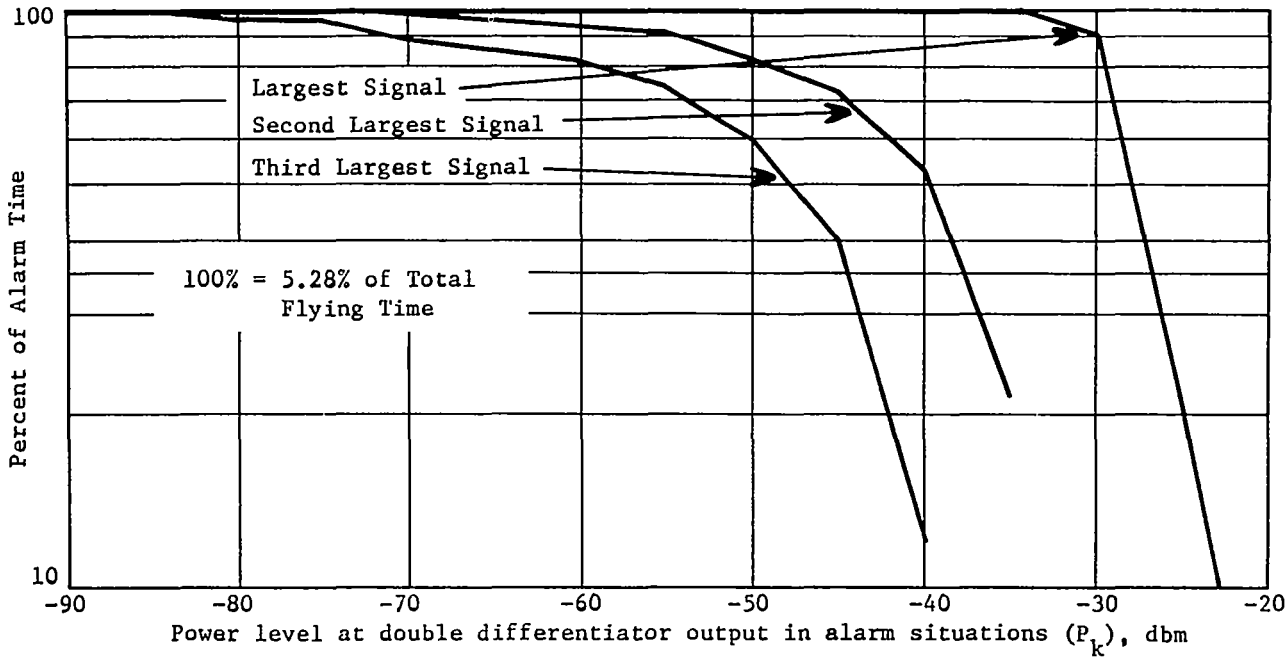


Fig. 31. Average percent of time that the receiver power level is greater than $P_k$ for alarm situations only. Threshold based on range and range rate and modified tau = 25 secs.

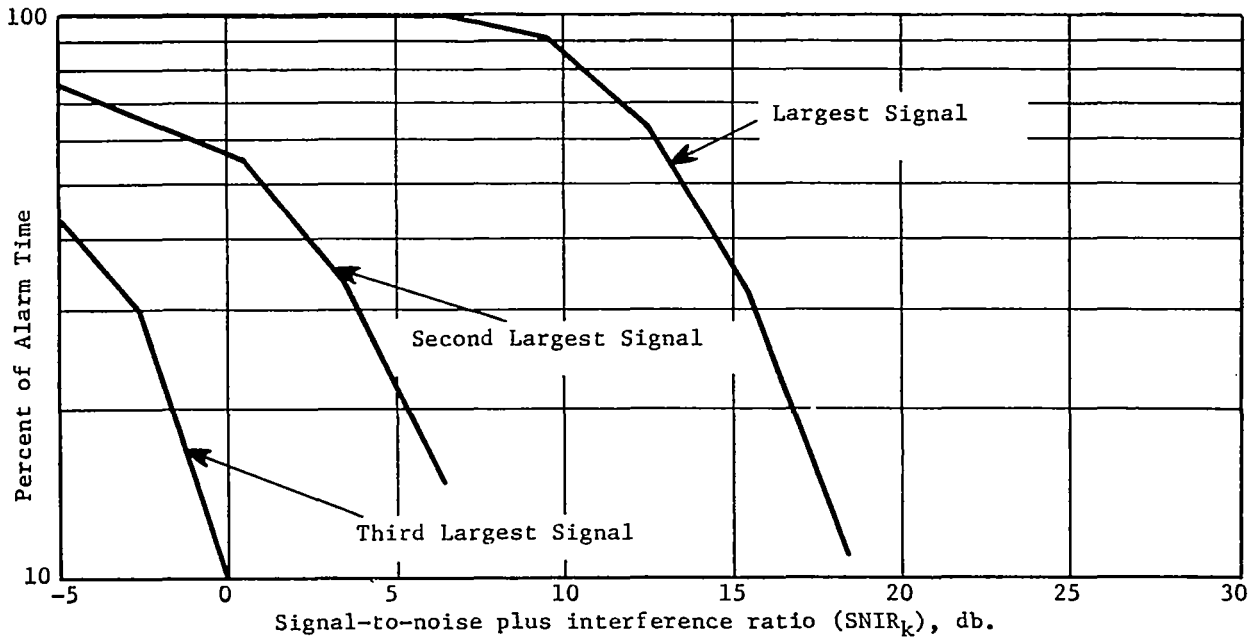


Fig. 32. Average percent of time that the signal-to-noise plus interference ratio at the double differentiator output is greater than $SNIR_k$ for alarm situations only. Threshold based on measured range and range rate and modified tau = 25 secs.

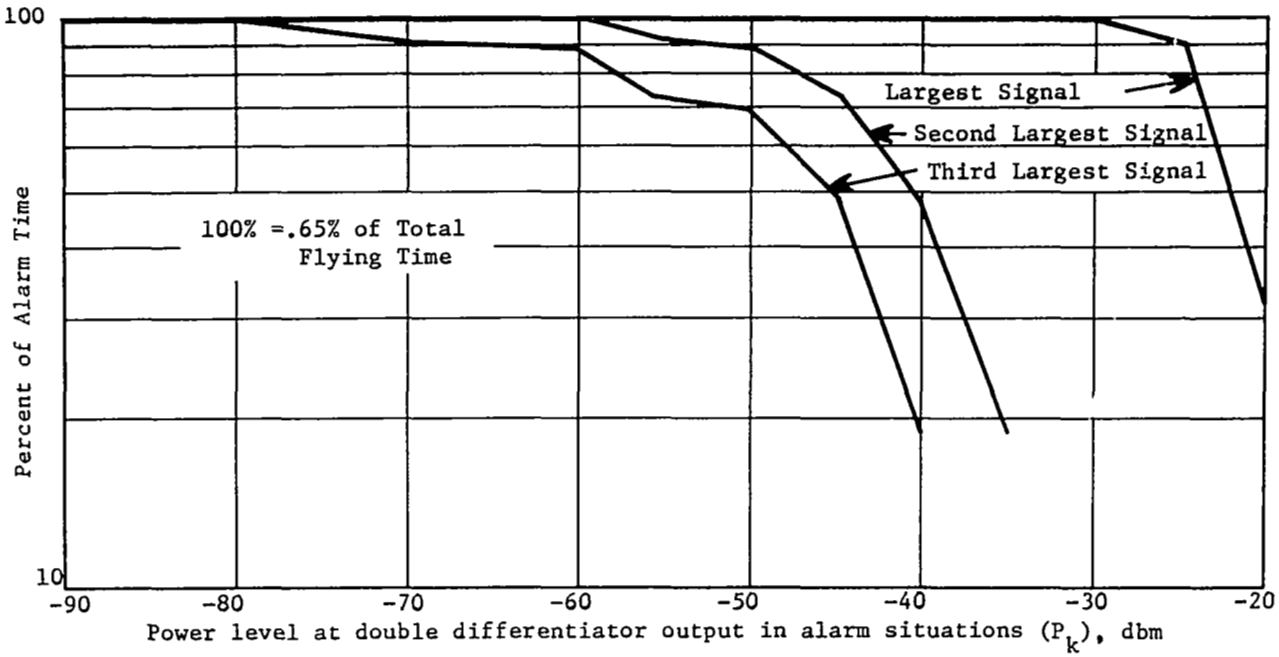


Fig. 33. Average percent of time that the receiver power level is greater than $P_k$ for alarm situations only. Power level threshold corresponding to modified tau = 35 secs.

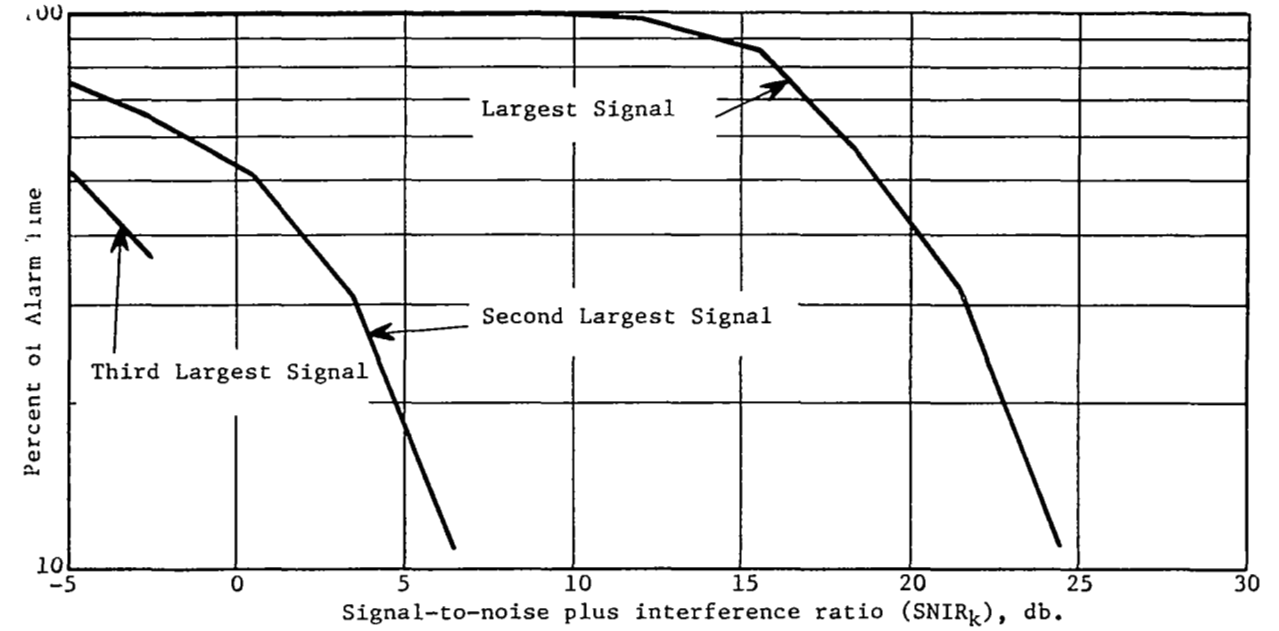


Fig. 34. Average percent of time that the signal-to-noise plus interference ratio at the double differentiator output is greater than $SNIR_k$ for alarm situations only. Power level threshold corresponding to modified tau = 35 secs.

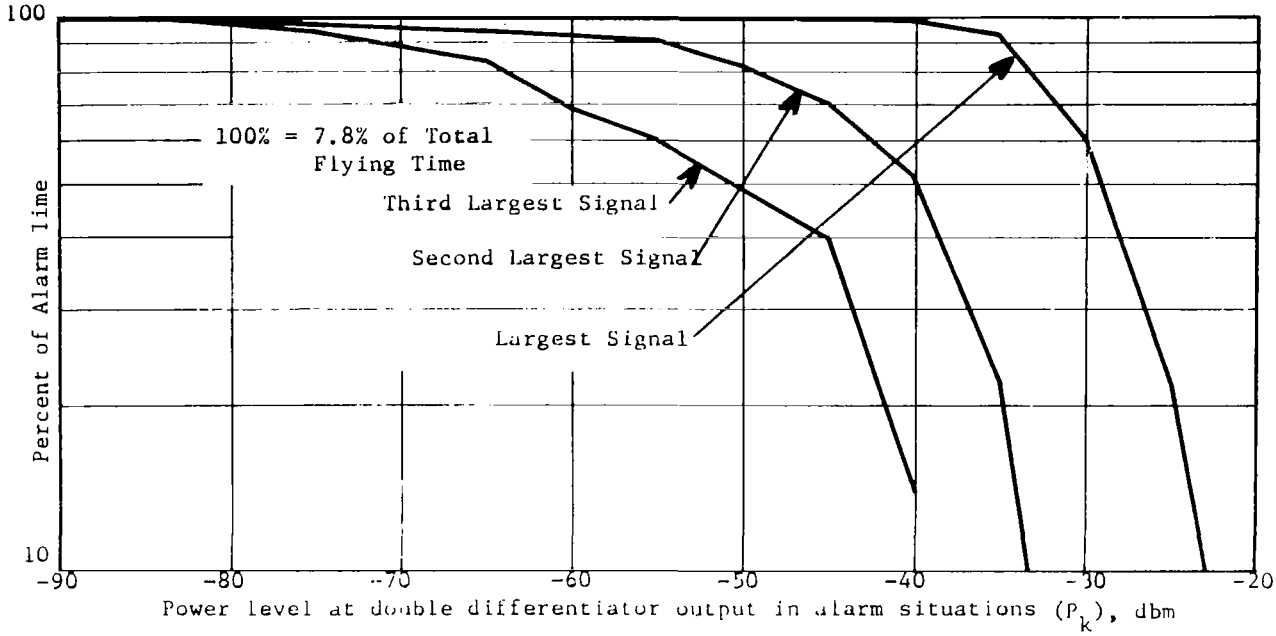


Fig. 35. Average percent of time that the received power level is greater than $P_k$ for alarm situations only. Threshold based on measured range and range rate and modified tau = 35 secs.

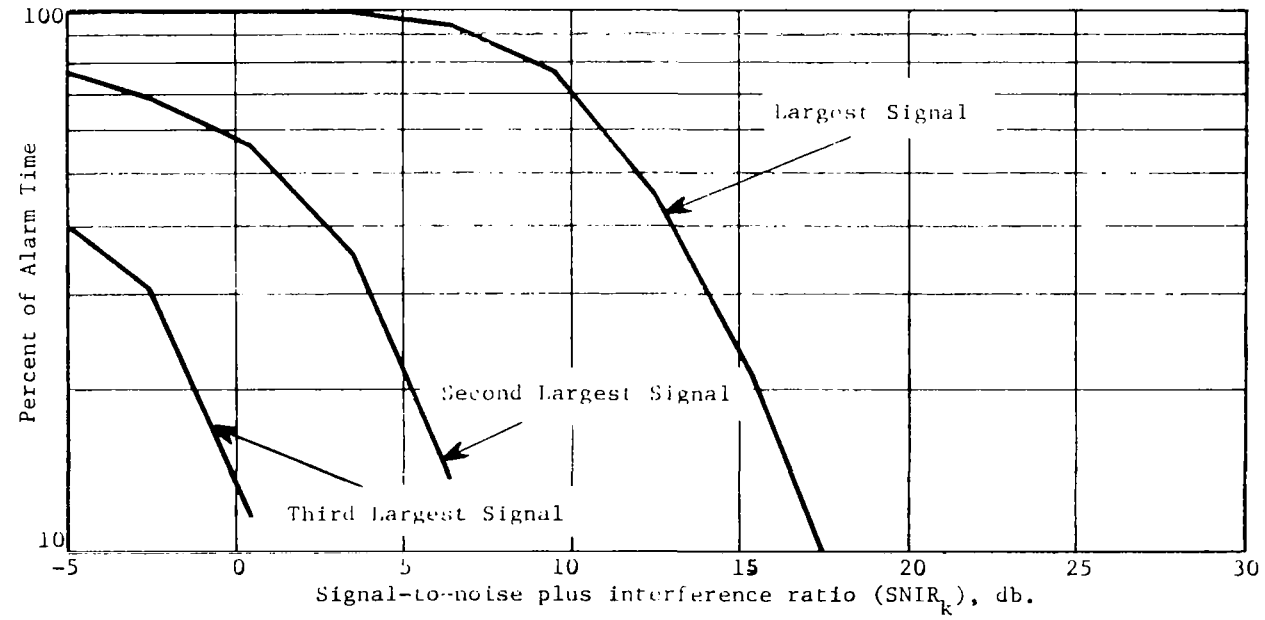


Fig. 36. Average percent of time that the signal-to-noise plus interference ratio at the double differentiator output is greater than $SNIR_k$ for alarm situations only. Threshold based on measured range and range rate and modified tau = 35 secs.

(the value calculated as required for reliable measurements) while in an alarm status is ≈.5. Thus, for an alarm threshold corresponding to a modified tau value of 35 seconds, the SNIR performance of the system is marginal and should be improved.

Another important measure of receiver performance is the ratio of the largest signal (i.e. the signal causing the alarm) to the second largest signal into the receiver limiter. Since the receiver is designed so that the largest signal is the most hazardous signal, it should be greater by approximately 3 db to capture the limiter and to permit reliable FM demodulation. The signal-to-signal ratios are plotted in Fig. 37 for alarm thresholds corresponding to values of modified tau of 25 and 35 seconds. As may be seen, the ratio exceeded 6 db in all cases for the 25 second threshold, and exceeded 3 db 93% of the alarm time for the 35 second threshold.

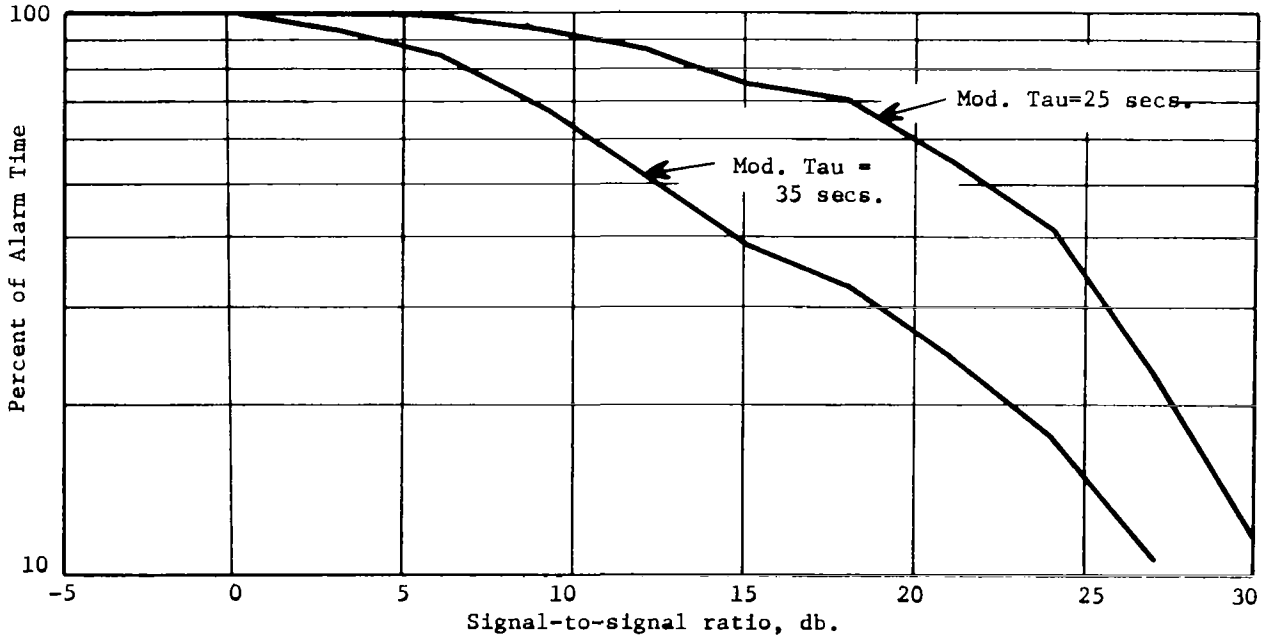


Fig. 37. Average percent of time that the ratio of the largest signal to the second largest signal into the receiver limiter is greater than the value given along the horizontal axis for alarm thresholds of 25 and 35 seconds (Hour 11 data).

4. Summary.— For the system parameters used in this particular simulation, and using the Hour 11 data base, the transponder is operating well within an assumed power limitation of 30 dbm. The total transponder output power exceeded 25 db only .7% of the time.

In the receiver, the interference level is not excessive. For an alarm threshold corresponding to a modified tau value of 25 seconds, the signal-to-noise plus interference ratio for the signal causing the alarm was greater than 16 db in all cases. For an alarm threshold of 35 seconds, the signal-to-noise plus interference ratio exceeded 3 db in all cases.

The low SNIR values encountered for a threshold based on 35 seconds are largely due to the interference level, rather than the receiver noise level.

Ratios of the largest signal to the second largest signal into the limiter-discriminator exceeded 6 db in all cases for a 25 second alarm threshold and exceeded 3 db 93% of the time for a 35 second alarm threshold.

## D. Performance Under Multiple Aircraft Conditions Using An Extended Density Data Base

1. General discussion.— The saturation studies discussed in the previous section were carried out using Hour 11 of the Atlanta radar data base. It is anticipated that future aircraft densities may well be greater than that encountered in the Atlanta data, although the Atlanta data were for near-capacity operations at that terminal. To provide for variable aircraft density, the Atlanta data base has been extended to provide higher numbers of aircraft within the terminal area. The techniques for making the extensions to the data base are discussed in the following.

2. Extensions of the Atlanta data base.— In developing an extended density data base, it is highly desirable that the data base be representative of the present ATC operational procedures and separation standards. That is, one cannot just insert more aircraft in a certain volume without careful consideration of the spacing of these aircraft.

In order to provide a realistic extension of the Atlanta data, a Monte Carlo technique was used as illustrated in Fig. 38 (see Appendix E). Analyses of the Atlanta data were conducted to determine the joint probability distribution of relative range and closing velocity between pairs of aircraft (see

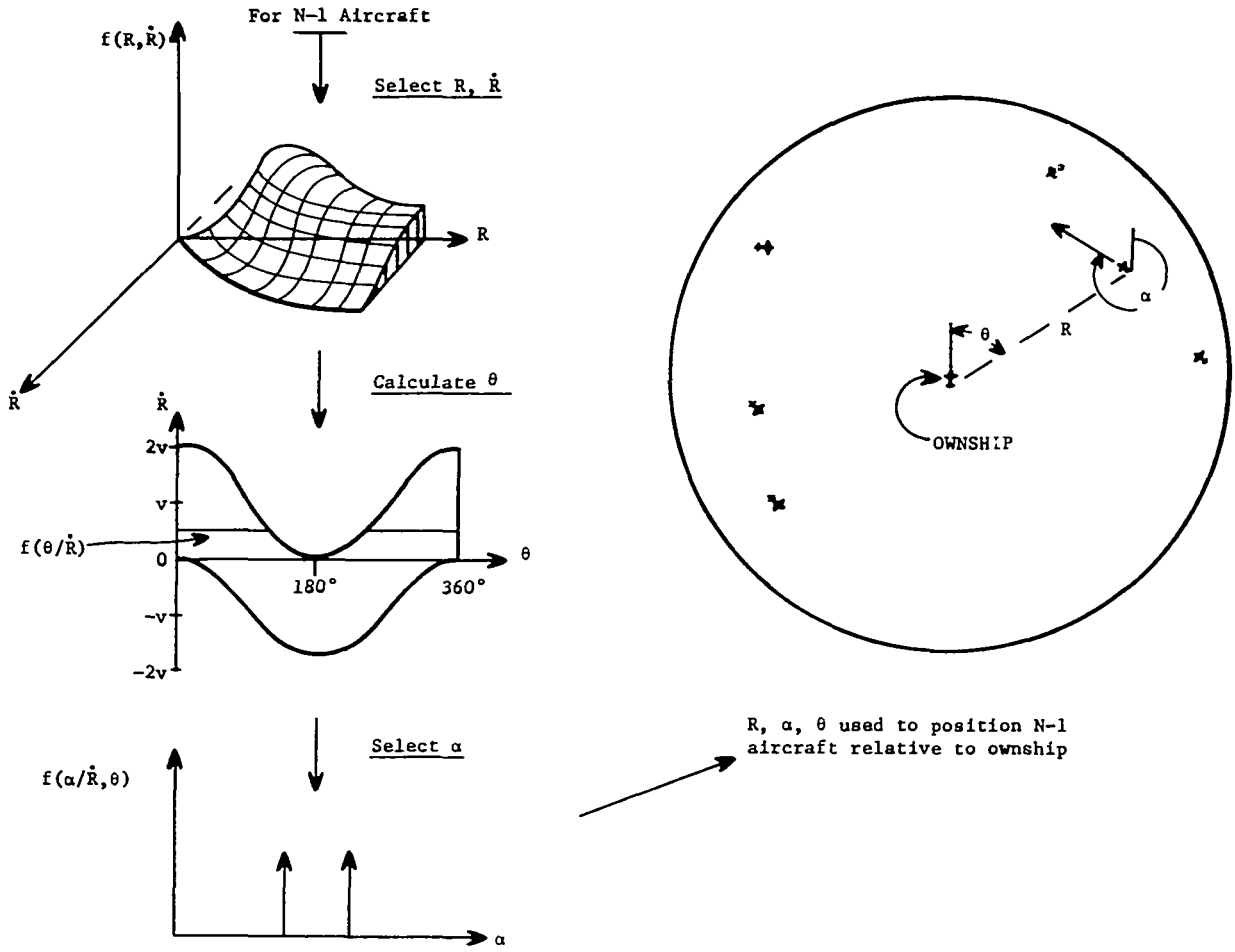


Fig. 38. Technique for extension of data base to higher density situations.

Appendix F). This joint distribution was then used to position the aircraft relative to ownship and to select the propoer bearing to the target and the heading angle of the target relative to the ownship.

For one calculation increment, a random number generator is used to select a value of relative range and closing velocity in accordance with the joint distribution obtained from the Atlanta data. Based on geometrical constraints that exist under an hypothesis that all aircraft have nearly the same velocity (i.e., there is a speed limit in the terminal area), the value of closing velocity selected is used to position each of (N-1) aircraft relative to ownship. Next, based on the particular value of closing velocity and relative bearing, one of two possible headings is selected with a .5 probability of each. These parameters are then used to position N aircraft to calculate the system outputs for one particular simulated radar scan (see Appendix E).

Repetitive calculations are then used to determine the statistics such as those calculated in the previous section.

This technique for extension of the data base in effect assumes that the ATC separation requirements remain similar to those existing in the Atlanta data base. It is also possible, using this technique, to simulate the effects of changing the FAA minimum separation requirement between aircraft, the size of the terminal area, or the speed limit of aircraft in the terminal area. Because of time limitations, however, these effects were not investigated during the present study.

3. Verification of the extended data base.— In order to verify that the technique for the generation of extended data was valid, simulation runs were conducted using the average number of aircraft present in the Atlanta data (12.7 aircraft per scan) in the extended simulation model and the resulting outputs compared. The outputs compared very favorably under these conditions. An example of the degree of similarity between the results using the Atlanta data base and the results using the Monte Carlo model are shown in Fig. 39. This particular curve is for the average percent of time that the signal-to-noise plus interference ratio into the receiver limiter exceeded a given value. The other results compared equally favorably.

This comparison of results from the actual data base and the extended data base model gave confidence in the results obtained from the extended data base model. These results are discussed in the following section.

4. Results of simulations using the extended data base model.— Figures 40 through 46 present results similar to those in Section V.C. except that the extended density data base is used. For simplicity, the curves for the second, third, etc. aircraft are not shown on these plots. The aircraft densities considered were 13, 20, 30 and 40 aircraft within a radius of roughly 35 n.mi. of the terminal.

Inspection of the performance curves indicates that even with extended densities, the transponder did not in any case exceed a power level of one watt. The signal-to-noise ratios at the receiver in alarm situations degraded somewhat as would be expected. However, the signal-to-interference ratios during alarm situations exceeded 11 db for the extended density results for at least 90 percent of the alarm time, for a warning time

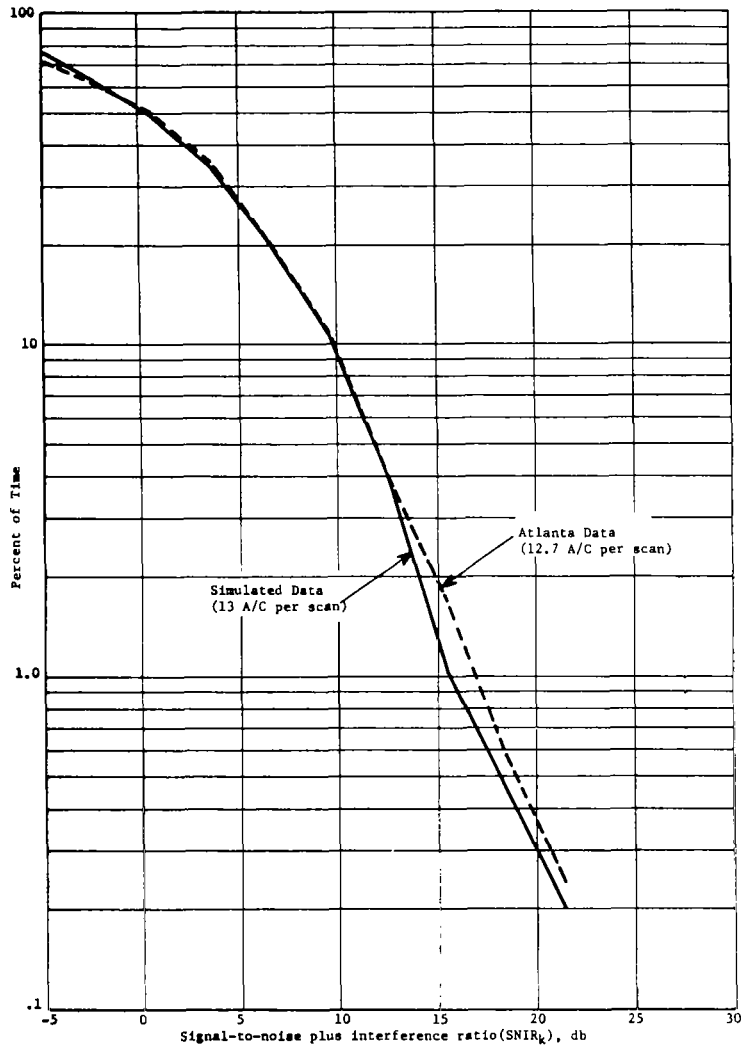


Fig. 39. Comparison of results using actual data and simulated data. Percent of total flying time that the signal-to-noise plus interference ratio into the receiver limiter exceeds $SNIR_k$.

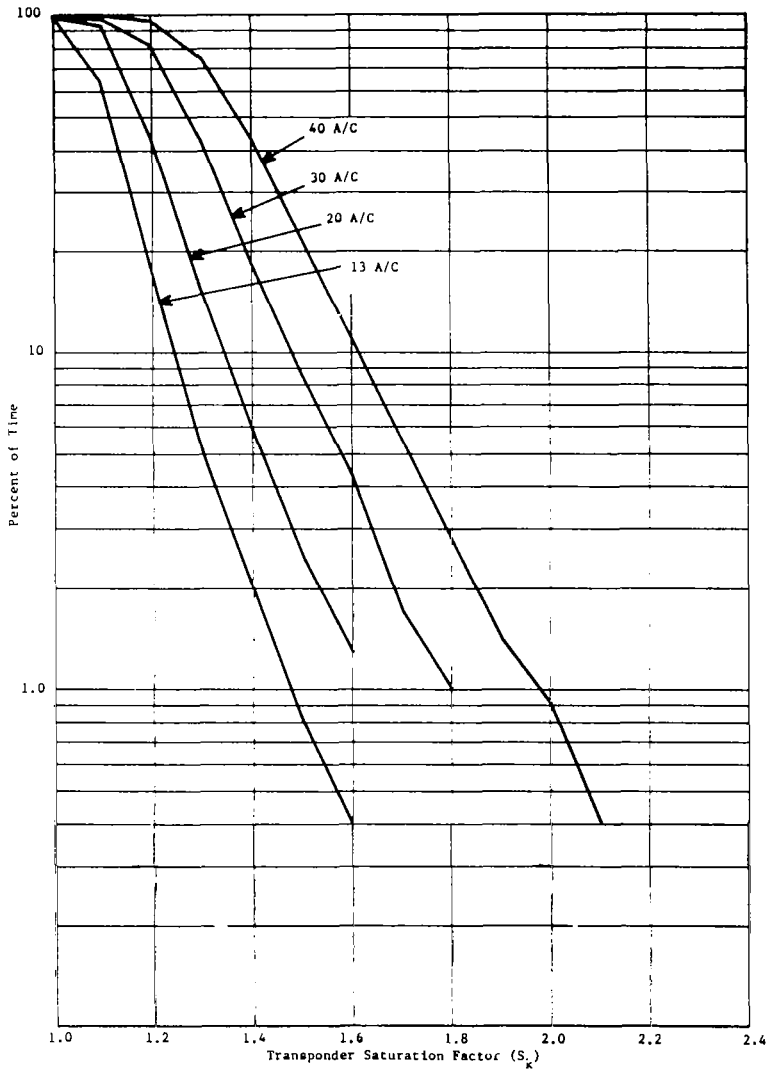


Fig. 40. Average percent of time that the transponder saturation factor is greater than $S_k$ for extended density data.

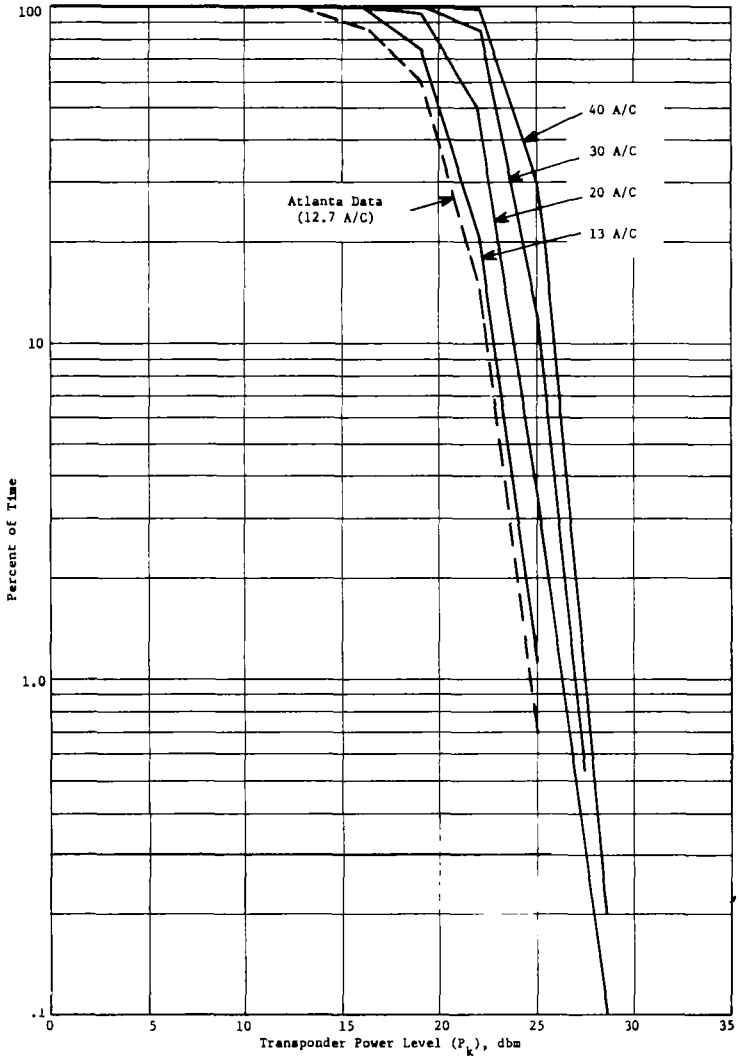


Fig. 41. Average percent of time that the power output of the transponder is greater than $P_k$ for various aircraft densities in extended density model.

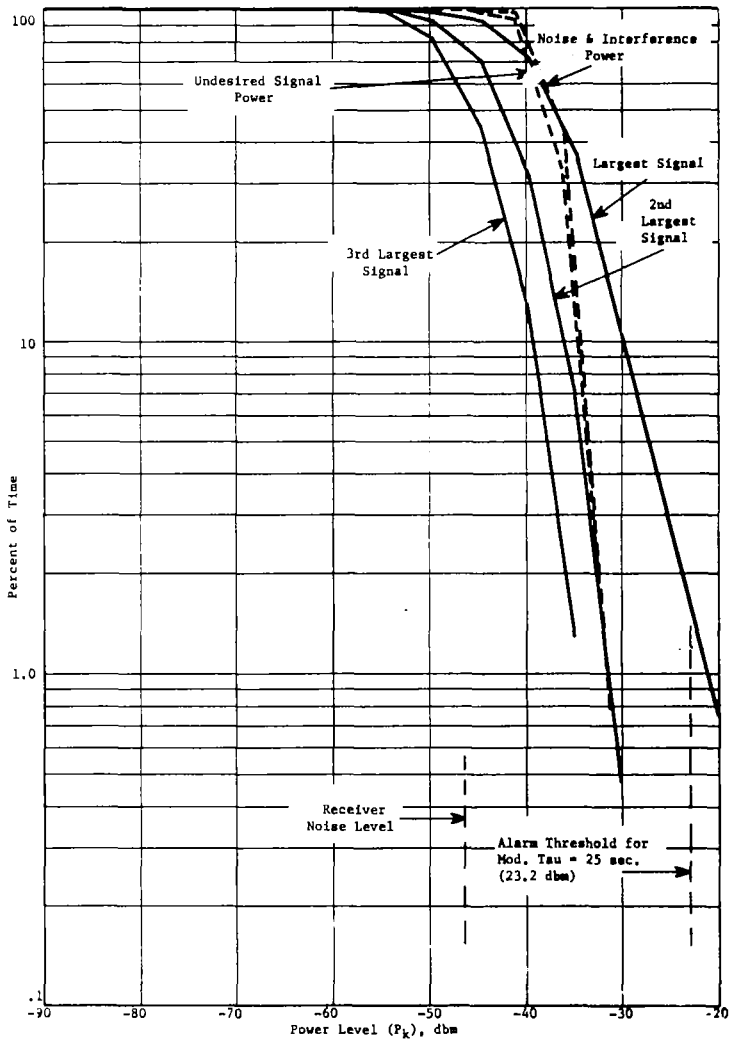


Fig. 42. Average percent of time that the power level at the double differentiator output is greater than $P_k$ for extended density data (40 aircraft).

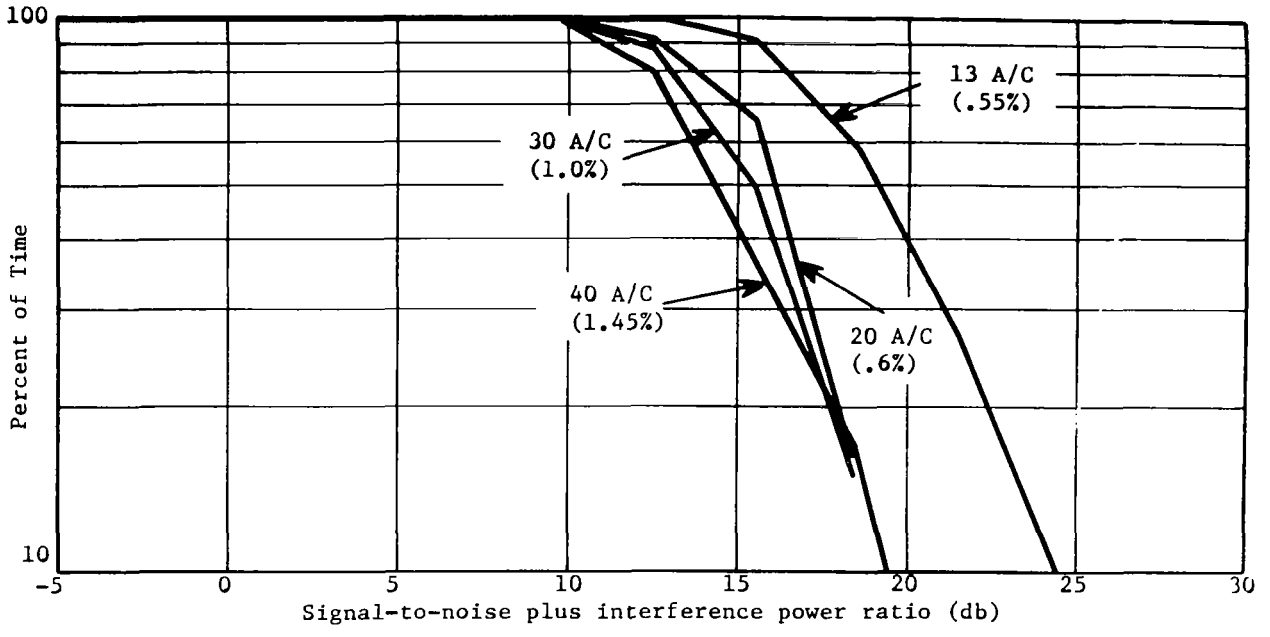


Fig. 43. Receiver signal-to-noise plus interference power ratios in alarm situations (modified tau = 25 secs.) extended data base.

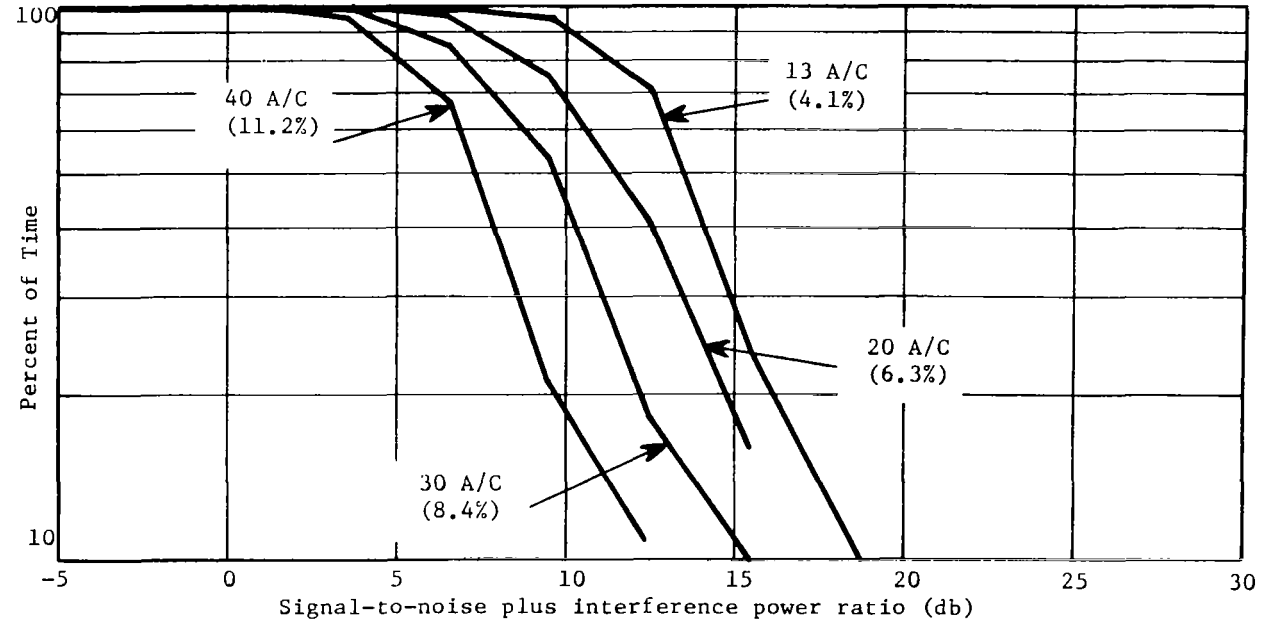


Fig. 44. Receiver signal-to-noise plus interference power ratios in alarm situations (modified tau = 35 secs.) extended data base.

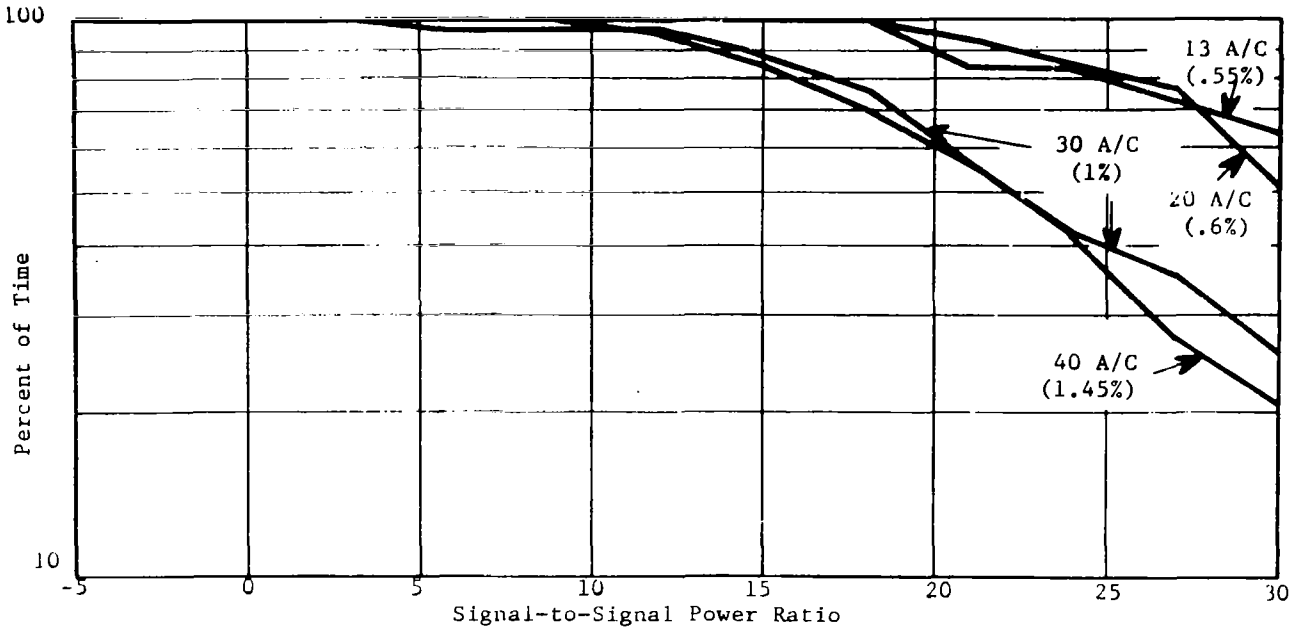


Fig. 45. Ratio of largest received signal to second largest received signal in alarm situations (modified tau = 25 secs.)

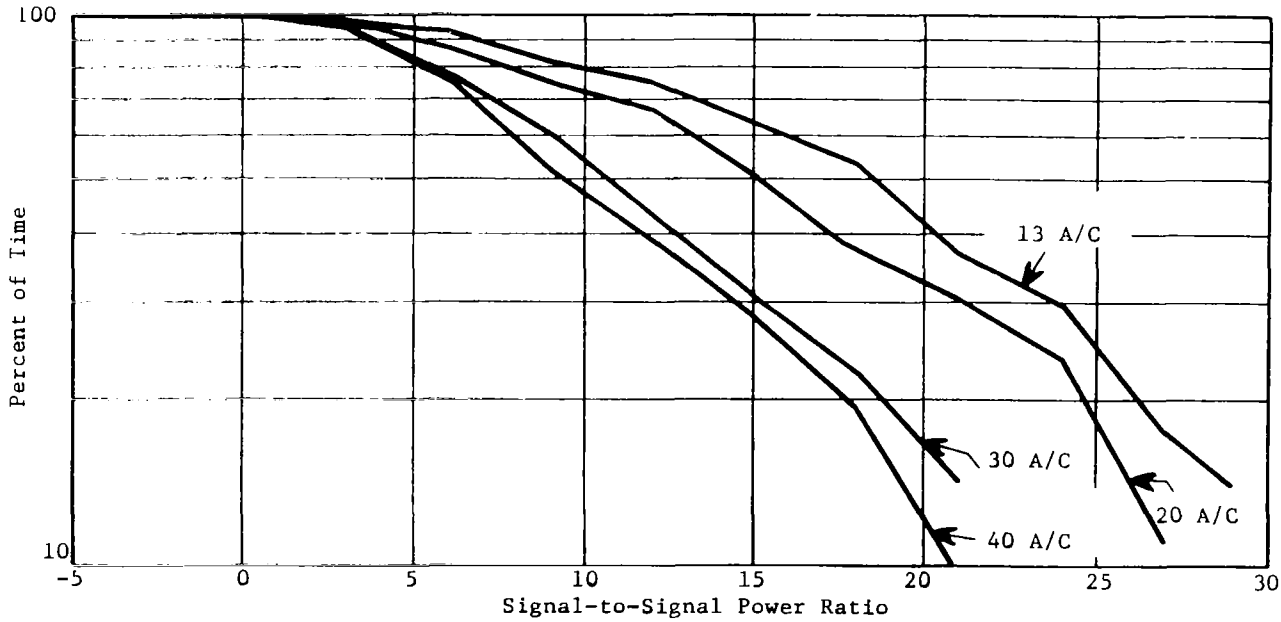


Fig. 46. Ratio of largest received signal to second largest received signal in alarm situations (modified tau = 35 secs.)

(modified tau) of 25 seconds.

For alarm thresholds corresponding to modified tau of 15 seconds, very few alarm cases were noted. Hence, curves of signal-to-noise plus interference ratios and power levels were not plotted for this case. In all alarm situations noted, however, the signal-to-noise plus interference ratio was greater than 16 db. using the 15 second threshold (40 A/C density case).

The percent of time spent in an alarm status increased with increasing aircraft density, as would be expected. Table 4 provides a summary of these times for various densities and alarm thresholds. The approximate number of alarms per arrival at the terminal has also been estimated by assuming values for average flying time in the terminal area (13 minutes) and average alarm duration (15 seconds). These statistics again indicate the desirability of using warning times on the order of 25 seconds (modified tau) in congested areas.

The results from the extended density simulations, then, do not significantly change the conclusions drawn from the simulations using the Atlanta data base. The system with parameters as presently selected appears to perform satisfactorily even in extremely dense traffic situations. If it is anticipated that alarm thresholds of 35 seconds are to be used in the terminal area, the system transmitted power should be increased such that the signal-to-noise plus interference ratio is not marginal at ranges and closing velocities corresponding to this threshold condition.

## E. Probability of a Communications Loss Due to PN Code Synchronization

1. General discussion.— As mentioned in Section IV.C., there exists the possibility that the PN code in a given transponder will be in synchronism with an interrogating signal. If this occurs, a loss of communications will result. Even though the signals are not in synchronism, the difference signal out of the first mixer in the transponder will sweep through the notch filter periodically. This situation is shown in Fig. 47.

Table 4. Alarm Statistic Summary

| Threshold Setting (Modified Tau) | Aircraft Density (≈ 40 n.mi. radius) | Percent of Time in Alarm Status | Approx. No. of Alarms Per Arrival* |
|---|---|---|---|
| 35 sec. | 13 (Atlanta Density) | 4.1 | 2.1 |
| | 20 | 6.3 | 3.2 |
| | 30 | 8.4 | 4.3 |
| | 40 | 11.2 | 5.7 |
| 25 sec. | 13 (Atlanta Density) | .6 | .3 |
| | 20 | .6 | .3 |
| | 30 | 1.0 | .5 |
| | 40 | 1.5 | .8 |
| 15 sec. | 13 (Atlanta Density) | .2 | .1 |
| | 20 | .25 | .13 |
| | 30 | .3 | .15 |
| | 40 | .4 | .2 |

*Based on 13 minutes flying time in area and alarm duration of 15 seconds.

The following sections develop the relationships required to estimate the effects of the notch filter on the retransmitted signals and the probability of a complete communications loss.

2. Transponder synchronization and notch filter effects.— The return signal from the transponder will effectively drop out each time the difference function passes through the notch filter. This will provide a strong amplitude modulation component at a frequency which may be determined from the average number of zero crossings of the difference function and the code length. For example, for a 31 bit code 403 milliseconds long, the AM modulation component is approximately 13 Hz. For a 63 bit code 819 milliseconds long, the dropout frequency is approximately 10 Hz.

The probability that a transponder will be in synchronism with the interrogating transmitter such that no return at all is received from the transponder is given by the expression, for exactly equal clock frequencies,

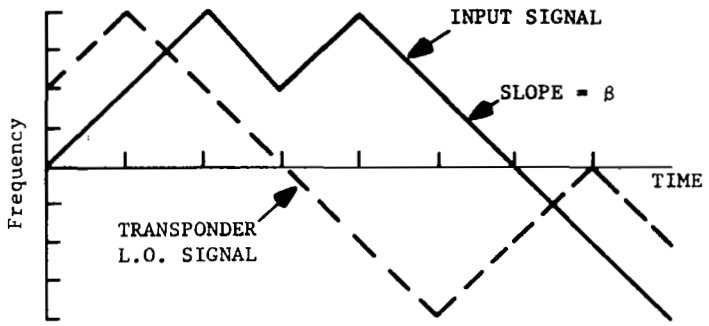


(a) Received and L.O. Signals

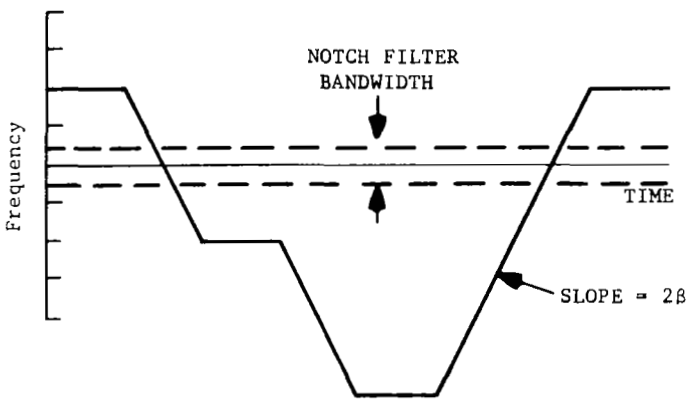


(b) Difference Signal from Transponder
1st Mixer

Fig. 47. Sketch indicating how the difference signal at the transponder 1st mixer output sweeps through the notch filter bandwidth for an input signal non-synchronous with the transponder L.O. signal.

$$\text{PROB.(no return)} = \frac{2\Delta f_n}{\beta T} \tag{25}$$

where $\Delta f_n$ is the width of the notch filter in the transponder, $\beta$ is the frequency slope, and T is the total length of the code. The above equation assumes that the clocks in the transponder and transmitter are running at the exact same rate. For example, a 127 bit code of length 1270 milliseconds with a slope of 16.6 MHz/sec. and a notch width of 10 KHz will have a probability of no output on the order of $10^{-3}$.

If the clocks in the transmitter and transponder are not running at exactly the same rate, a beat phenomenon will take place and dropouts will occur at the beat frequency. If the clocks differ by a frequency $\Delta f_c$ Hz, then the beat will occur at a frequency $\Delta f_c/p$, where p is the number of bits in the code. Thus, there will be a dropout of approximate duration $2\Delta f_n/\beta t_o \Delta f_c$ every $p/\Delta f_c$ seconds. For example, if a one Hz difference exists between the clocks, a 127 bit code with a bit period of 10 milliseconds and slopes and notch widths as given in Section III.F. would have a .12 second dropout every 127 seconds.

Note that if we divide the dropout duration by the dropout period to obtain a probability of no return signal, we get equation (25). Thus, small differences in the clock rates do not affect the probability of no return signal at any particular instant of time. This probability is strictly a function of the notch width, the slope, and the total length of the code.

It is also possible to observe dropouts of smaller duration than that considered above. For example, there are certain values of delay where a dropout will occur of a length equivalent to six bit units in the case of a 127-bit code. For the 127-bit codes, the probability of a dropout of a duration greater than a given value has been computed and is shown in Fig. 48. For the other 127-bit codes, the cumulative probability curves appear to have generally the same form. All of the curves approach an asymptotic value given by equation (25).

The dropouts of duration greater than that corresponding to a single sweep through the filter and less than that corresponding to a total dropout will also cause an AM modulation of the signal if a difference exists between the clock rates in the transmitter and transponder. The dropouts in this class occur approximately every bit unit. Thus, an AM modulation component will exist at a frequency of $\Delta f_c$, as well as at the frequencies mentioned previously. Hence, there will exist AM modulation of the return signal at the following frequencies and with the approximate durations as noted:

Table 5. AM modulation of return signal due to the transponder notch filter.

| Dropout Frequency (Hz) | Approximate Duration (sec.) | Cause |
|---|---|---|
| $Nz/T$ | $\Delta f_n/\beta$ | Difference function sweeping through notch |
| $\Delta f_c/p$ | $2\Delta f_n/\beta t_o \Delta f_c$ | Periodic total synchronization due to difference in clock rate |
| $\Delta f_c$ | less than smaller of $nt_o$ or $2\Delta f_n/\beta t_o \Delta f_c$ | Periodic partial synchronization due to difference in clock rate |

Where: Nz = No. of zero crossings of the difference function, n = length of shift register, and $t_o$, p, $\beta$, $\Delta f_n$, T, $\Delta f_c$ were defined previously.

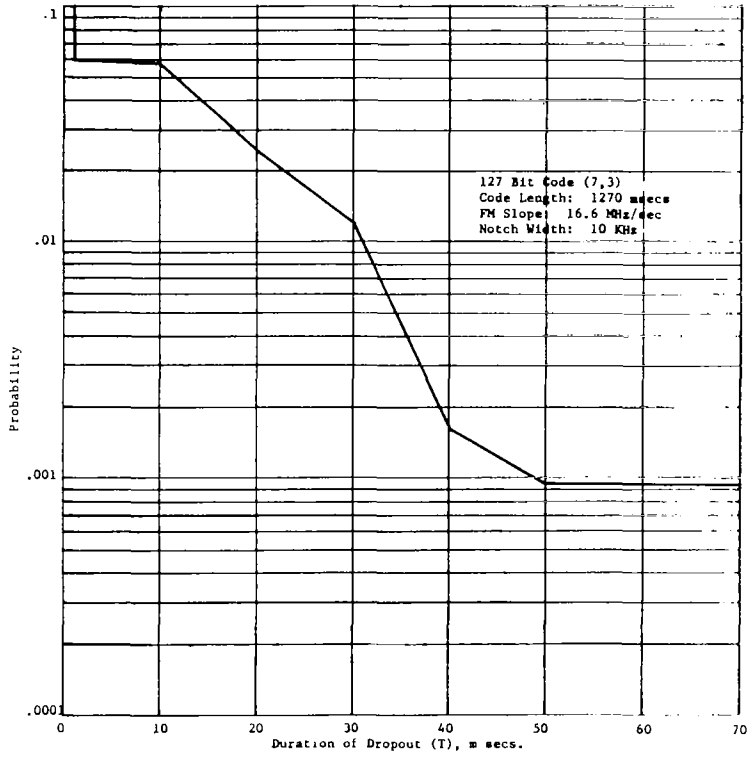


Fig. 48. Probability of a signal dropout of duration greater than T for the specific 127 bit code specified. This plot assumes the separate clocks generating the PN codes are run at exactly the same rate and that the transmitter center frequencies are exactly the same.

In the following section, the probability of a complete communications loss is considered for given variations in clock and transmitter center frequencies.

3. The probability of a communications loss (missed alarm) due to transponder-transmitter synchronism.— System dropout is defined here as communication time when no return is transmitted from the transponder, due to the presence of the notch filter in the transponder. Any time the difference between the received frequency and the local transmitter frequency is less than $\Delta f_n$, dropout will occur. Total dropout is loss of communications during all of a specified time interval, $T_c$.

The probability that a transponder will be in phase synchronism with the interrogating transmitter such that no return is received from the transponder during any time interval is termed the probability of total dropout, given by equation (25). Equation (25) assumes that the transponder and transmitter have identical clock rates. Variation in clock frequency as well as transmit frequency should enhance the total dropout probability to the extent that this probability is reduced. This section presents a discussion of the effects of such variations.

In deriving equation (25), clock frequency is considered stable to the extent that if $\Delta f \leq \Delta f_n$ at the beginning of the code sequence this condition remains true. It can be seen in Fig. 49 that if the phase delay time, $t_\phi$, is such that $\Delta f \leq \Delta f_n$ for all t, then total dropout occurs. However, even if $t_\phi$ is large enough that total dropout does not result, there are still generally some periods of dropout during the communication time, as given in Table 5. For the codes actually used for modulation in this system, computer results show that these isolated dropouts are of short duration and do not affect the total dropout probability.

Figure 48 has shown the probability of a dropout for various 127-bit codes with all values of phase delay between the two signals considered equally likely. It can be seen that the probability of a dropout of duration greater than 70 msec. is on the order of $10^{-3}$ for the (7,3), 127-bit code. (This curve is representative of all 127-bit codes--variation between specific codes is minor.) Since communication dropouts of concern will only involve total times greater than about 10 seconds, these short duration dropouts do not appreciably affect

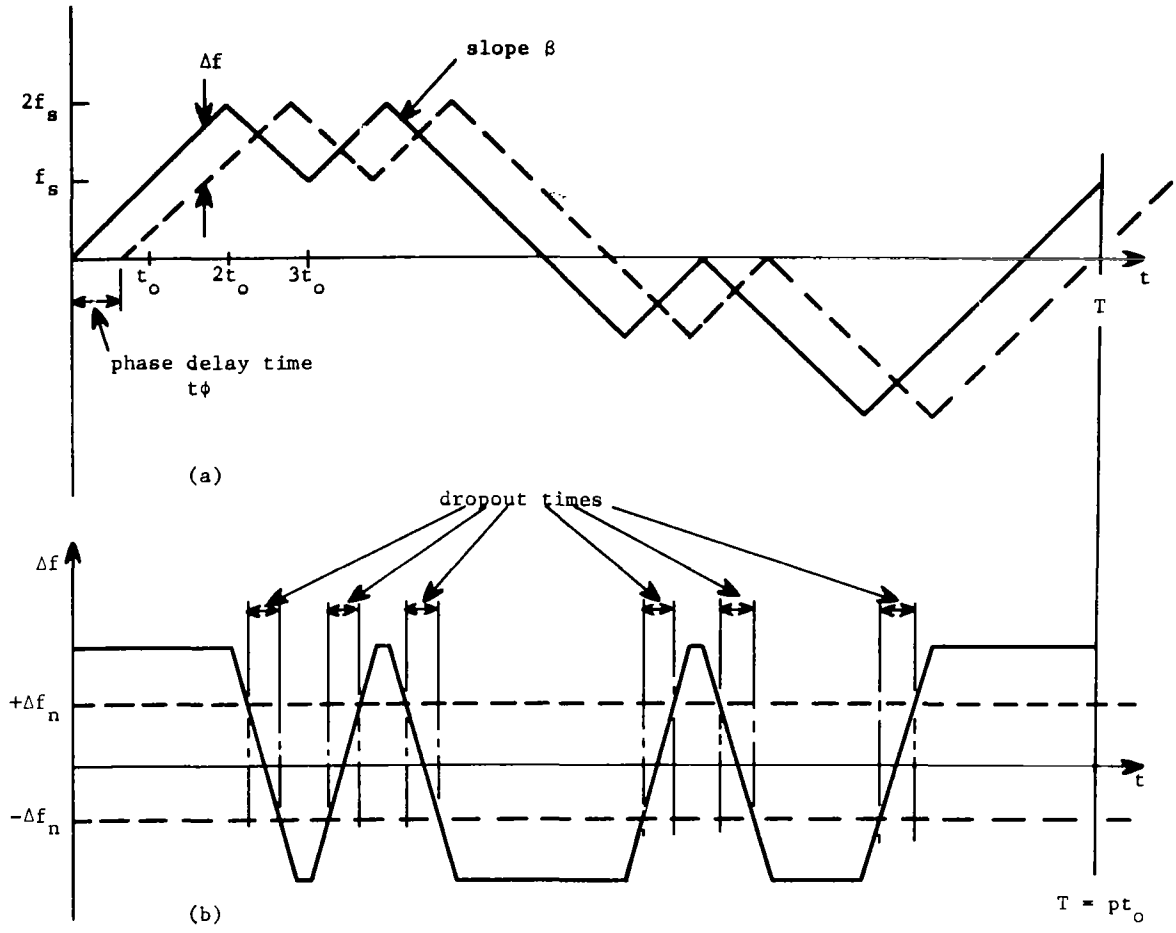


Note: The width of the notch filter is exaggerated on the frequency scale.

Fig. 49. (a) f-t plot of transponder signal (solid line) and received signal (dotted line) for a typical 13 bit code. (b) difference frequency versus time showing the notch filter and various short duration dropout times.

the total dropout situation, but cause AM modulation, as previously discussed.

Considering variations in carrier frequency f and clock frequency $f_c$, the total dropout probability can be expressed as

$$\text{Prob.(total dropout)} = \text{Prob.}(\Delta f \leq \Delta f_n, \text{ dropout with } \Delta f_c \leq \Delta f_{c_1}). \qquad (26)$$

where $\Delta f$ is the difference in transmitter and transponder carrier frequencies,

$\Delta f_c$ is the difference in transmitter and transponder clock frequencies,

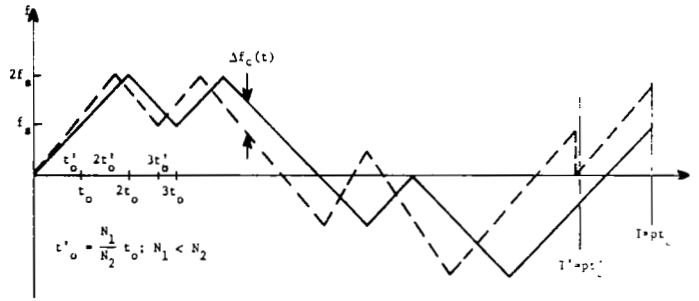


Fig. 50(a). f-t plot of transponder signal (solid line) with clock frequency $f_c = 1/t_o$ and synchronous received signal (dotted line) with clock frequency $f_c = 1/t'_o$ for a typical 13-bit code.

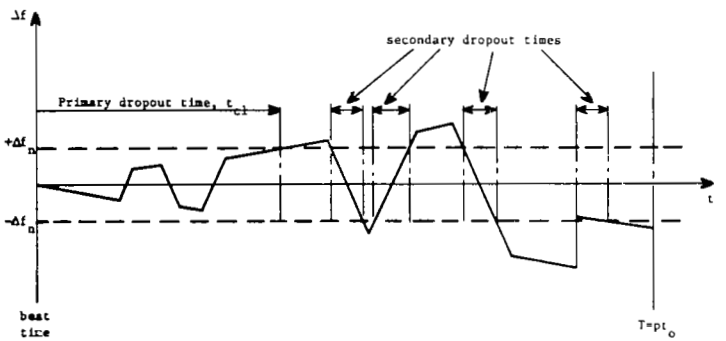


Fig. 50(b). f-t plot of difference frequency for (a) showing the notch filter and the primary dropout time $t_{c1}$, which is the time period near the beat time and several secondary dropout times of shorter duration.

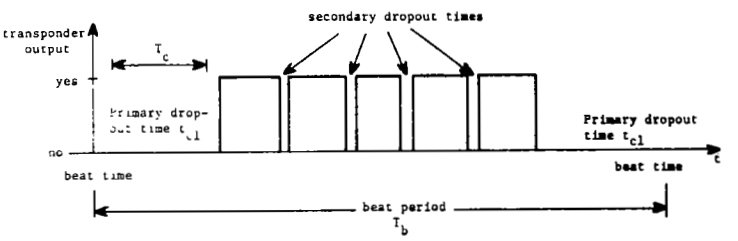


Fig. 50(c). Typical situation showing the occurrence of a primary dropout time $2t_{c1}$ each beat period where the beat frequency $f_b = |\Delta f_c|/p$. Several secondary dropout times are illustrated also.

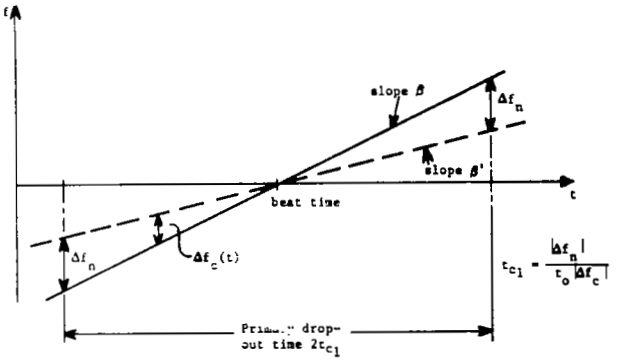


Fig. 50(d). Analysis of $\Delta f_c(t)$ (difference frequency as a function of time) near the beat time.

Fig. 50. f-t analysis of transponder output when clock frequencies vary.

$\Delta f_{c_1}$ is $2\Delta f_n/\beta t_o T_c$, the critical clock frequency above which total dropout is not possible (see Fig. 50), and

$\Delta f_n$ is the notch filter bandwidth in Hz (10 KHz).

Also, Prob.($\Delta f \leq \Delta f_n$, dropout with $\Delta f_c \leq \Delta f_{c_1}$) is the joint probability of dropout due to the difference in carrier frequencies being less than the notch filter bandwidth (see Fig. 51) and dropout due to the fact that the communication time $T_c$ is less than the dropout time caused by clock frequency differences.

It will be assumed here that clock variations and transmitter carrier variations are statistically independent. Then

$$\text{Prob.}(\Delta f \leq \Delta f_n, \text{ dropout with } \Delta f_c \leq \Delta f_{c_1}) = \text{Prob.}(\Delta f \leq \Delta f_n) \cdot \text{Prob.}(\text{dropout with } \Delta f_c \leq \Delta f_{c_1}). \quad (27)$$

The event "dropout with $\Delta f_c \leq \Delta f_{c_1}$" will involve situations where the communication time $T_c$ falls totally within the primary dropout time defined in Fig. 50. The secondary dropout times are neglected on the assumption that these are short compared to $T_c$ as was the situation with the short duration dropout times experienced when considering only phase differences in the two signals as illustrated in Fig. 49. Thus,

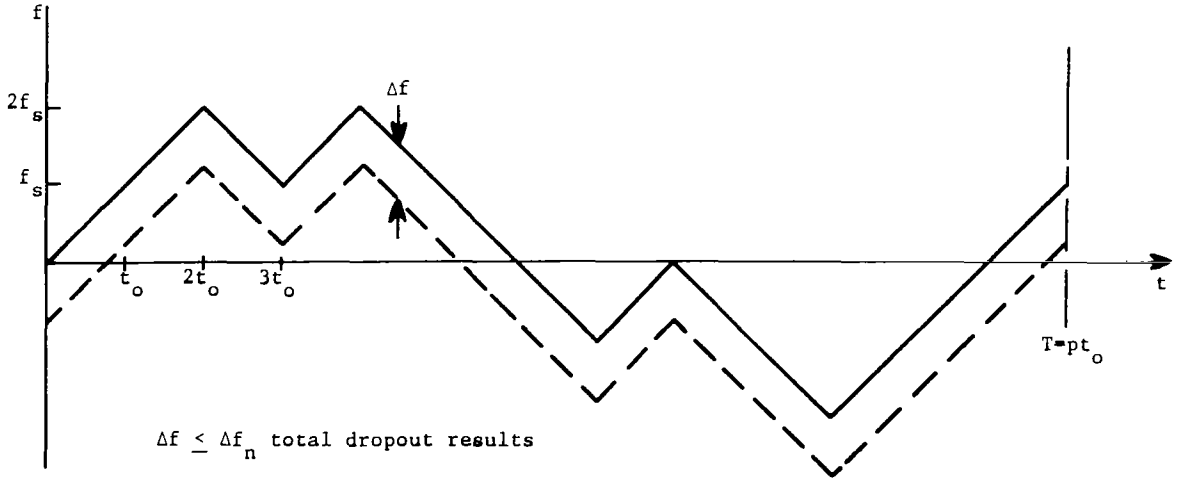


Fig. 51. f-t plot of transponder signal (solid line) and received signal (dotted line) for a typical 13-bit code where there is a difference $\Delta f$ in carrier frequencies.

$$\text{Prob.(dropout with } \Delta f_c \leq \Delta f_{c_1}) = \text{Prob}(T_c \in 2t_{c_1} | \Delta f_c \leq \Delta f_{c_1}) \text{Prob}(\Delta f_c \leq \Delta f_{c_1}) \tag{28}$$

where $\text{Prob.}(\Delta f_c \leq \Delta f_{c_1})$ is just the marginal probability that the communication time is less than the primary dropout time $2t_{c_1}$, and $\text{Prob.}(T_c \in 2t_{c_1} | \Delta f_c \leq \Delta f_{c_1})$ is the probability that the time of communication $T_c$ falls totally within the primary dropout time $2t_{c_1}$ conditioned on $T_c \leq 2t_{c_1}$. Therefore, equation (27) becomes

$$\text{Prob.(total dropout)} = \text{Prob.}(\Delta f \leq \Delta f_n)\text{Prob.}(\Delta f_c \leq \Delta f_{c_1}) \text{Prob.}(T \in 2t_{c_1} | \Delta f_c \leq \Delta f_{c_1}). \tag{29}$$

Assume that the variation in transmitter carrier frequency of each transmitter is normally distributed with mean f* and standard deviation $\sigma_t$, $[N(f^*,\sigma_t)]$. Then the difference in carrier frequencies $\Delta f$ is also distributed normally with zero mean and standard deviation $\sigma_t\sqrt{2}$, $[N(0,\sigma_t\sqrt{2})]$. Thus, from (29)

$$\text{Prob.}(\Delta f \leq \Delta f_n) = \int_{-\Delta f_n}^{\Delta f_n} g(\Delta f)d\Delta f = \text{erf}\left(\frac{\Delta f_n}{\sqrt{2\sigma_t^2}}\right). \tag{30}$$

Here erf(·) is the error function where

$$\text{erf}(x) = \frac{2}{\sqrt{\pi}} \int_0^x e^{-t^2} dt.$$

For the system parameters selected, the notch width $\Delta f_n$ is 10 KHz such that if $\sigma_t \leq 10$ KHz, then $\text{Prob.}(\Delta f \leq \Delta f_n) \approx 1.0$.

Furthermore, assume that each transmitter clock frequency is normally distributed with mean $f_c^*$ and standard deviation $\sigma_c$. Then,

$$\text{Prob.}(\Delta f_c \leq \Delta f_{c_1}) = \text{erf}\left(\frac{2\Delta f_n}{\beta t_o T_c \sqrt{2\sigma_c^2}}\right). \tag{31}$$

Also, assuming that the starting time of the communication time $T_c$ is evenly distributed throughtout the beat period $T_b$, then

$$\text{Prob.}(T_c \in 2t_{c_1} | \Delta f_c \leq \Delta f_{c_1}) = \frac{2|\Delta f_n|}{\beta T} - \frac{T_c |\Delta f_c|}{p} \quad . \tag{32}$$

Therefore,

$$\text{Prob.}(T_c \in 2t_{c_1} | \Delta f_c \leq \Delta f_{c_1}) \leq \frac{2|\Delta f_n|}{\beta T} \quad . \tag{33}$$

Substituting equations (30), (31), and (33) into (29) yields

$$\text{Prob.}(\text{total dropout}) \leq \left[ \text{erf}\left( \frac{\Delta f_n}{\sqrt{2\sigma_t^2}} \right) \text{erf}\left( \frac{2\Delta f_n}{\beta t_o T_c \sqrt{2\sigma_c^2}} \right) \right] \left[ \frac{2\Delta f_n}{\beta T} \right] \quad . \tag{34}$$

Using the approximation $\text{erf}(x) = (2/\sqrt{\pi})x$; $x \ll 1$, equation (34) can be written as

$$\text{Prob.}(\text{total dropout}) \leq \frac{8}{\pi} \frac{(\Delta f_n)^3}{\beta^2 t_o T \sigma_t \sigma_c T_c} \qquad \begin{Bmatrix} \sigma_t \geq 10 \text{ KHz} \\ \sigma_c > 1.0 \text{ Hz} \end{Bmatrix} \quad . \tag{35}$$

Note that if $\sigma_t < 10$ KHz, then $\text{Prob.}(\Delta f \leq \Delta f_n) \approx 1$, and

$$\text{Prob.}(\text{total dropout}) \leq \frac{8}{\sqrt{2\pi}} \left( \frac{\Delta f_n}{\beta} \right)^2 \frac{1}{t_o T T_c \sigma_c} \qquad \{\sigma_c > 1.0 \text{ Hz}\} \quad . \tag{36}$$

And for the case where $\sigma_t < 10$ KHz and $\sigma_c < 1$ Hz,

$$\text{Prob.}(\text{total dropout}) \leq \frac{2\Delta f_n}{\beta T} \text{erf}\left( \frac{2\Delta f_n}{\beta t_o T_c \sqrt{2\sigma_c^2}} \right) \quad , \tag{37}$$

where in the above,

$\beta$ is the slope of integrated waveform in Hz per second ($16.6 \times 10^6$),
$\Delta f_n$ is the notch filter bandwidth in Hz (10 KHz),
$\sigma_c$ is the rms deviation in clock oscillators,
$\sigma_t$ is the rms deviation in transmitter carrier frequency oscillators
$T$ is the code length in seconds (1.27),
$t_o$ is the bit period in seconds ($10^{-2}$),

$2t_{c_1}$ is the primary dropout time ($\Delta f \leq \Delta f_n$, $t \in 2t_{c_1}$) due to differences in clock frequencies ($2\Delta f_n / \beta t_o |\Delta f_c|$), and

$T_c$ is the time of communications.

Figure 52 provides a plot of the total dropout probability bounds given by equation (34) as a function of $T_c$ for various values of $\sigma_t$ and $\sigma_c$ when a 127-bit code is used. For $T_c > 1$, the bound as given by equation (35) is shown for the various values of the product $(\sigma_t \sigma_c)$ where $\sigma_t \geq 10^4$, $\sigma_c \geq 1$ in all cases. Also included is the curve for no clock or transmitter errors, i.e., $\sigma_t = \sigma_c = 0$ (see Fig. 48).

4. Summary.— As shown in the above, variations in clock oscillators and transmitter oscillators can serve to reduce considerably the probability of total dropout in communications. In fact, the greater the rms variation in these oscillators the less the chance of loss of communications in an alarm situation. For clock oscillator stability on the order of 1 part in $10^2$ (rms error 1 Hz. at 100 KHz clock oscillator frequency) and transmitter oscillator stability on the order of 2 parts in $10^6$ (rms error 10 KHz. at 5200 MHz. transmitter oscillator frequency), the probability of a 10-second loss of communications is on the order of $1 \times 10^{-6}$.

Furthermore, by varying the transmitter frequency assignments over the allowable range, and by using different PN codes at different transmitters, the total dropout probability can be reduced even further.

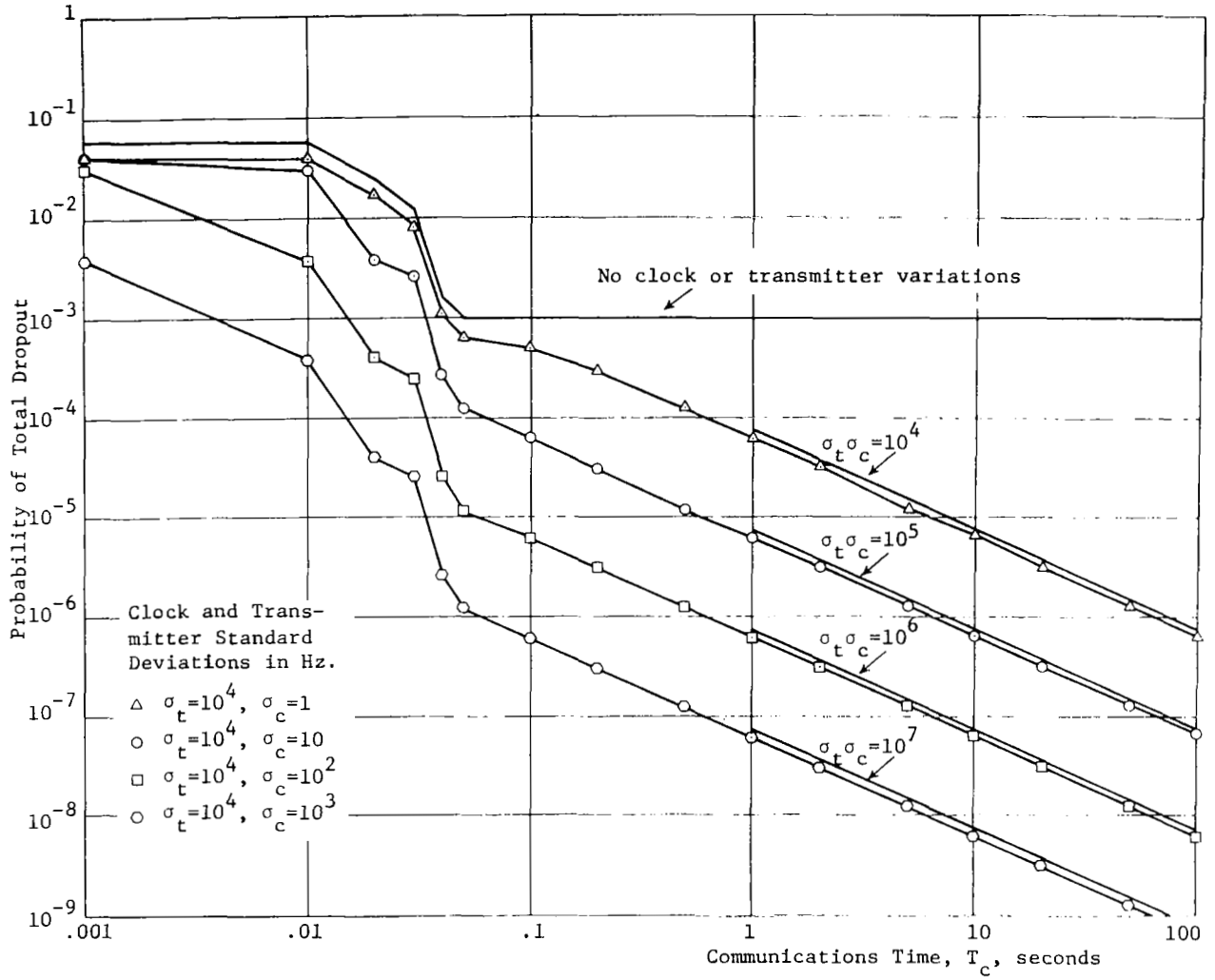


Fig. 52. The probability of a loss of communications of duration $T_c$ due to the notch filter in the transponder as a function of (rms) PN code clock variations ($\sigma_c$) and transmitter frequency variations ($\sigma_T$). The curves are for a 127 bit PN code with a period of 1.27 seconds. The asymptotes shown are calculated from equation (35).

# APPENDICES

## APPENDIX A

### PN Code Characteristics

During the course of the program, a large number of specific PN codes were investigated to determine the characteristics of importance for system design. These characteristics include the peak deviation for given slopes, the duration that the waveform spends within the bandwidth of the notch filter, the average number of zero crossings, and the amplitude distribution of the integrated code. Computer programs were developed to determine these and other characteristics of desired codes.

Table A-1 summarizes certain characteristics of 31, 63, and 127 bit codes for a bit period of 10 m sec and an FM slope of 16.6 MHz/second. Since the frequency deviation is a linear function of the product of bit period and FM slope, the deviation figures are easily converted into different bit period-FM slope products.

Figure A-1 plots the set of integrated 127 bit codes that are of interest for system design. (The 127 bit code (7,3) is given in Fig. A-1a.)

Figure A-2 plots the amplitude distribution of the 127 bit integrated PN sequences. Also plotted is the amplitude distribution of the difference function (i.e. the amplitude of the difference between the PN code and a time shifted replica of the code averaged over all time lags). The amplitudes may be converted to frequency deviations by multiplying the horizontal axes by the $\beta$-$t_o$ product, where $\beta$ is the FM slope and $t_o$ is the period of one bit of the code.

Figure A-3 plots the probability of a dropout of a duration greater than the value given along the horizontal axes in m sec for a notch filter width of 10 KHz. The dropout probability for the (7,3) code is also given in the text in Fig. 48.

Table A-1. Summary of Integrated PN Code Characteristics

Bit period = 10 m sec, Slope = 16.6 MHz/sec, Notch width = 10 KHz

| Code | Bits | Length (m sec) | Peak Dev.[1] + | Peak Dev.[1] − | Total Dev. (MHz) | Peak Dev. of Difference (MHz) | Avg. no. of zero crossings[2] | Maximum duration in notch[2] (m sec) | Average duration in notch[2] (m sec) | Avg. % of total time in notch[2] (%) |
|---|---|---|---|---|---|---|---|---|---|---|
| (5,2) | 31 | 310 | +.33 | -.66 | .99 | .92 | 5.2 | .30 | .30 | .52 |
| (5,3) | 31 | 310 | +.17 | -.83 | 1.00 | .92 | 5.2 | .30 | .30 | .52 |
| (5,4,3,2) | 31 | 310 | +.33 | -.83 | 1.16 | 1.11 | 5.4 | .30 | .30 | .54 |
| (5,3,2,1) | 31 | 310 | +.33 | -.83 | 1.16 | 1.11 | 5.3 | .30 | .30 | .54 |
| (5,4,2,1) | 31 | 310 | +.17 | -1.00 | 1.17 | 1.09 | 5.5 | .30 | .30 | .54 |
| (5,4,3,1) | 31 | 310 | +.50 | -.66 | 1.16 | 1.09 | 5.4 | .30 | .30 | .54 |
| (6,1) | 63 | 630 | +1.00 | -.83 | 1.83 | 1.71 | 8.8 | .30 | .30 | .43 |
| (6,5) | 63 | 630 | +.17 | -1.66 | 1.83 | 1.71 | 8.9 | .30 | .30 | .43 |
| (6,5,2,1) | 63 | 630 | +.83 | -.83 | 1.66 | 1.58 | 9.2 | .30 | .30 | .45 |
| (6,5,4,1) | 63 | 630 | +.17 | -1.50 | 1.67 | 1.58 | 9.3 | .30 | .30 | .45 |
| (6,5,3,2) | 63 | 630 | +.83 | -.83 | 1.66 | 1.55 | 7.5 | .30 | .30 | .37 |
| (6,4,3,1) | 63 | 630 | +.17 | -1.50 | 1.67 | 1.55 | 7.6 | .30 | .30 | .37 |
| (7,3) | 127 | 1270 | +.83 | -1.33 | 2.16 | 2.07 | 13.0 | 60.30 | .46 | .71 |
| (7,3,2,1) | 127 | 1270 | +1.00 | -1.99 | 2.99 | 2.44 | 10.7 | 60.30 | .46 | .65 |

[1] Initial conditions = 0 ... 001.

[2] Averaged over all delays except zero delay.

Table A-1. Continued.

| Code | Bits | Length (m sec) | Peak Dev. + | Peak Dev. - | Total Dev. (MHz) | Peak Dev. of Difference (MHz) | Avg. No. of zero crossings | Maximum duration in notch (m sec) | Average duration in notch (m sec) | Avg. % of total time in notch (%) |
|---|---|---|---|---|---|---|---|---|---|---|
| (7,4,3,2) | 127 | 1270 | +.33 | -1.99 | 2.32 | 2.27 | 11.0 | 60.30 | .46 | .66 |
| (7,6,5,4,2,1) | 127 | 1270 | +.66 | -1.66 | 2.32 | 2.26 | 11.4 | 60.30 | .46 | .67 |
| (7,5,4,3,2,1) | 127 | 1270 | +.83 | -1.66 | 2.49 | 2.37 | 14.3 | 60.30 | .46 | .74 |
| (7,6,4,2) | 127 | 1270 | +.17 | -2.49 | 2.66 | 2.56 | 13.7 | 60.30 | .46 | .72 |
| (7,1) | 127 | 1270 | +1.49 | -1.00 | 2.49 | 2.38 | 12.7 | 60.30 | .46 | .70 |
| (7,6,3,1) | 127 | 1270 | +1.16 | -1.00 | 2.16 | 2.13 | 11.4 | 60.30 | .46 | .67 |
| (7,6,5,2) | 127 | 1270 | +1.16 | -1.00 | 2.16 | 2.08 | 10.7 | 60.30 | .46 | .66 |

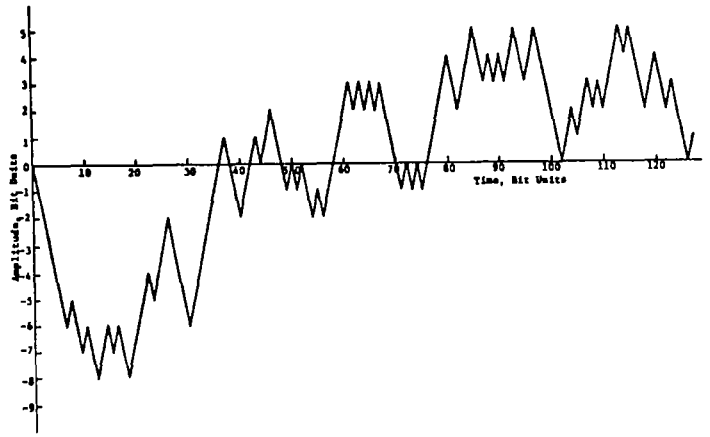


Fig. A-1a. 127 bit code (7,3).

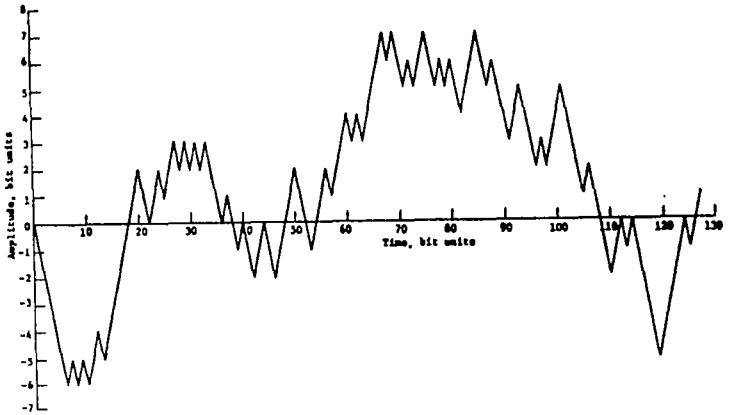


Fig. A-1b. 127 bit code (7,6,5,2).

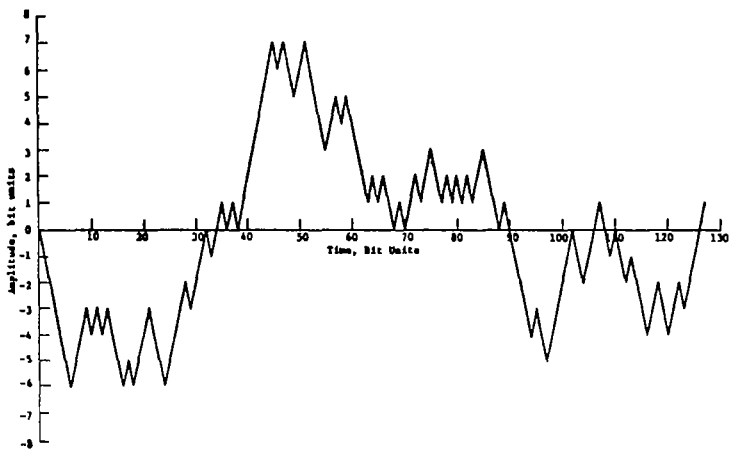


Fig. A-1c. 127 bit code (7,6,3,1).

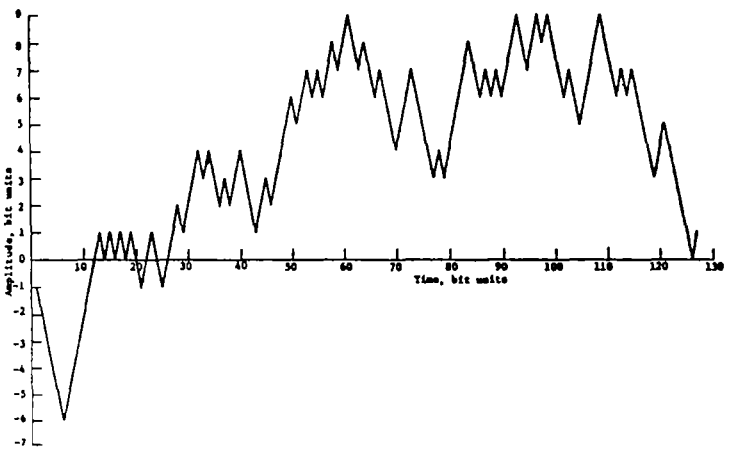


Fig. A-1d. 127 bit code (7,1).

Fig. A-1. Integrated PN sequence for the code as indicated.

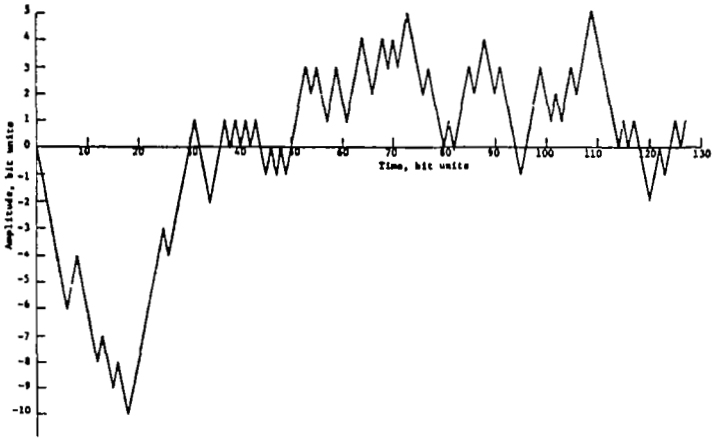


Fig. A-1e. 127 bit code (7,5,4,3,2,1).

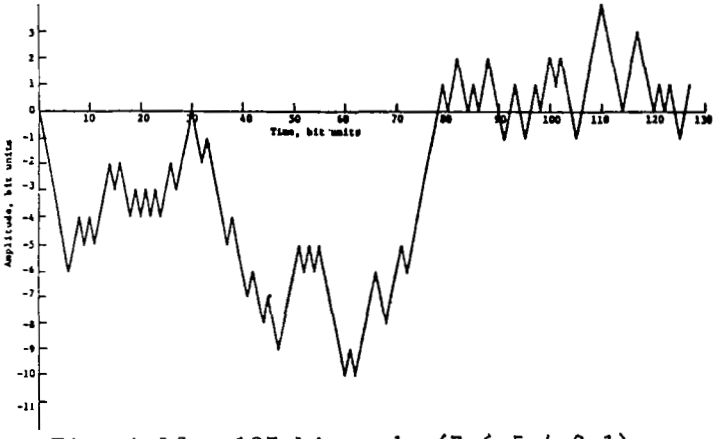


Fig. A-1f. 127 bit code (7,6,5,4,2,1).

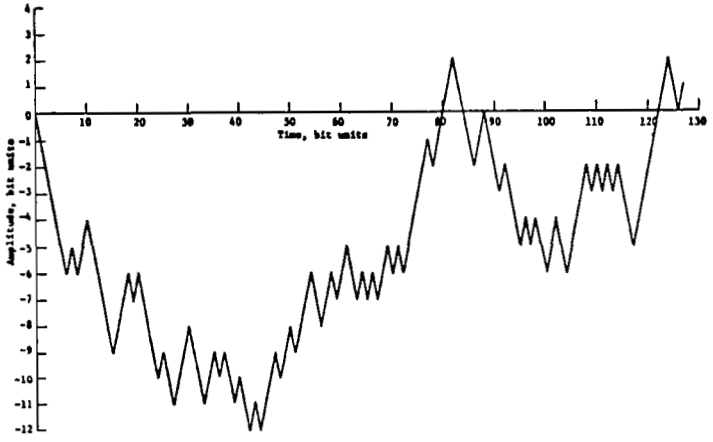


Fig. A-1g. 127 bit code (7,4,3,2).

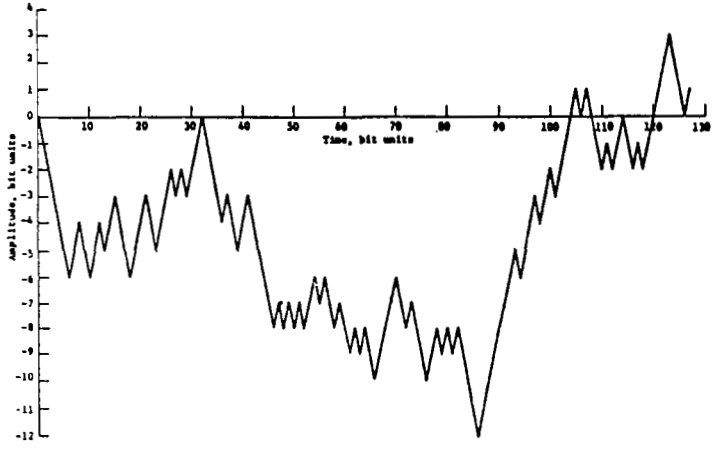


Fig. A-1h. 127 bit code (7,3,2,1).

Fig. A-1. Concluded.

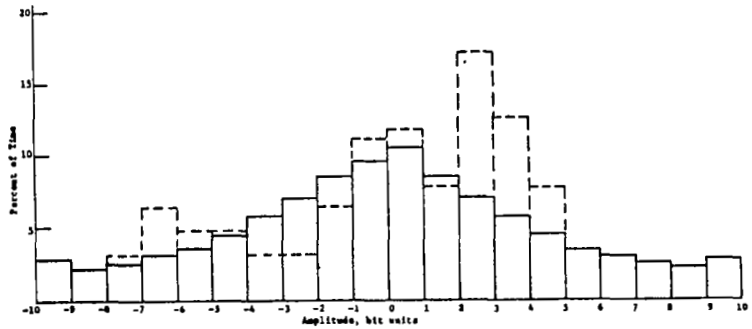

Fig. A-2a. 127 bit code (7,3).

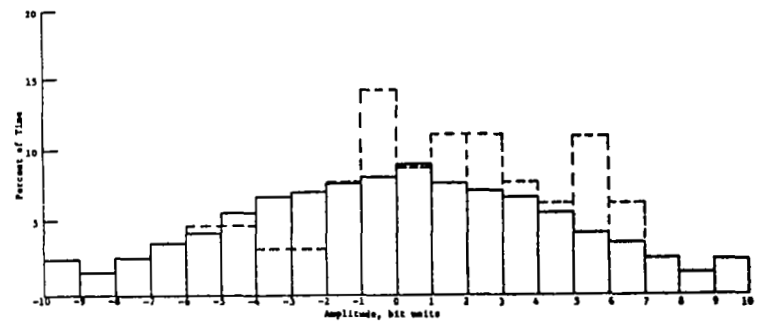

Fig. A-2b. 127 bit code (7,6,5,2).

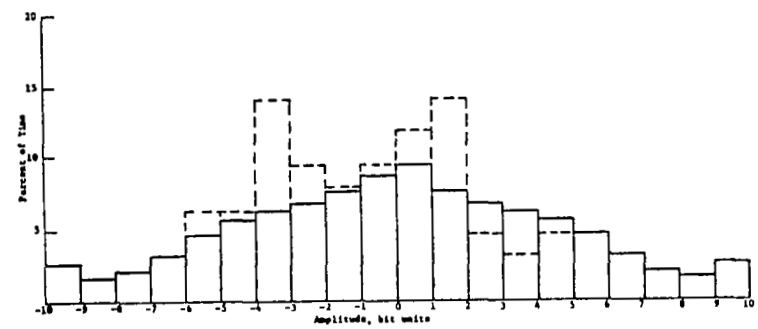

Fig. A-2c. 127 bit code (7,6,3,1).

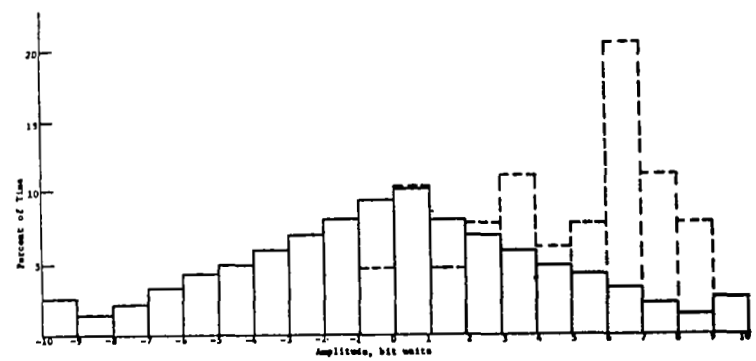

Fig. A-2d. 127 bit code (7,1).

Fig. A-2. Amplitude distribution of the integrated PN sequence (dotted lines) and the difference function (solid lines) for the code as indicated.

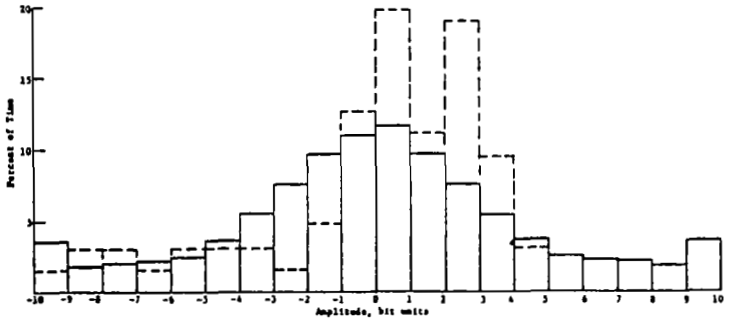

Fig. A-2e. 127 bit code (7,5,4,3,2,1).

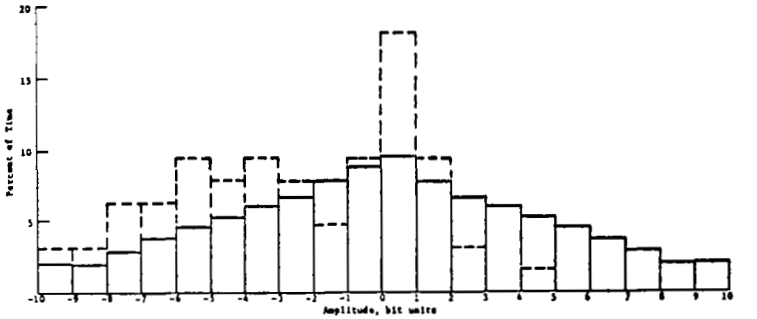

Fig. A-2f. 127 bit code (7,6,5,4,2,1).

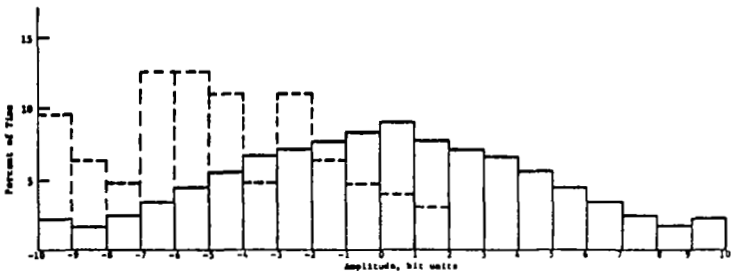

Fig. A-2g. 127 bit code (7,4,3,2).

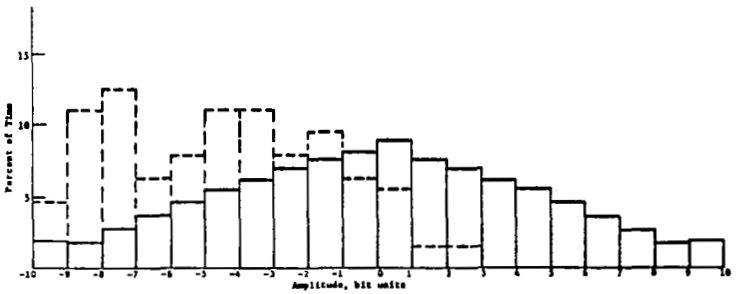

Fig. A-2h. 127 bit code (7,3,2,1)

Fig. A-2. Concluded.

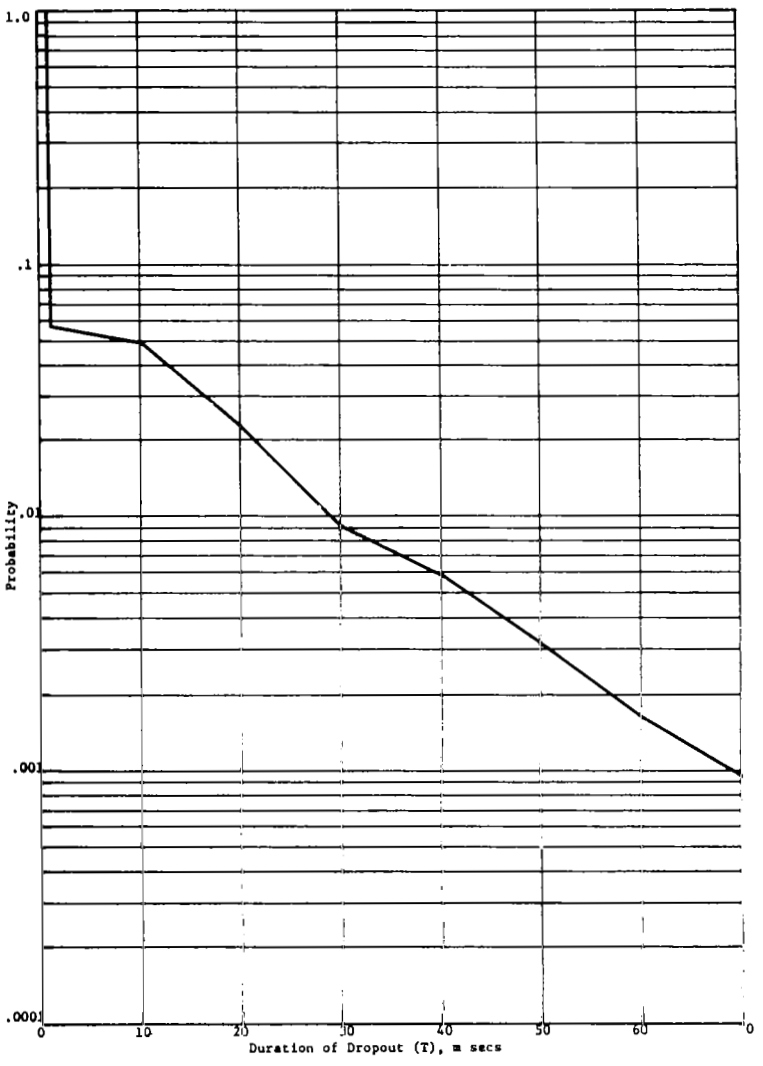


Fig. A-3a. 127 bit code (7,3).

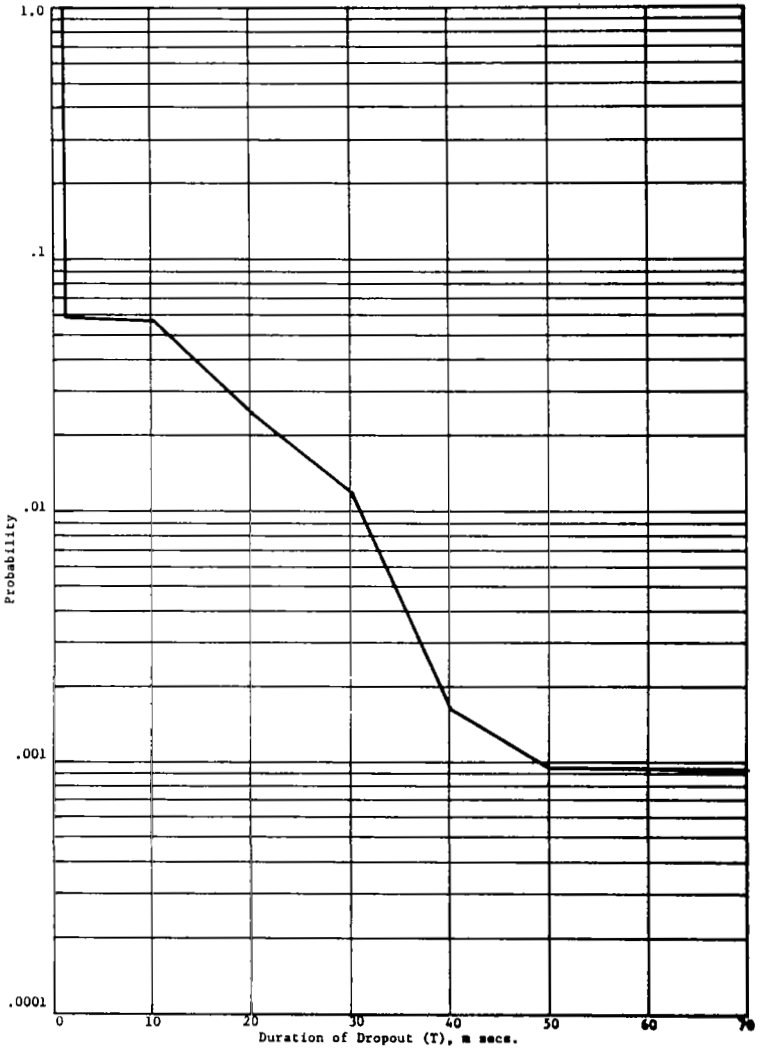


Fig. A-3b. 127 bit code (7,6,5,2).

Fig. A-3. Probability of a dropout of duration greater than T for the code as indicated. Code length = 1270 m secs, FM slope = 16.6 MHz/sec., notch width = 10 KHz.

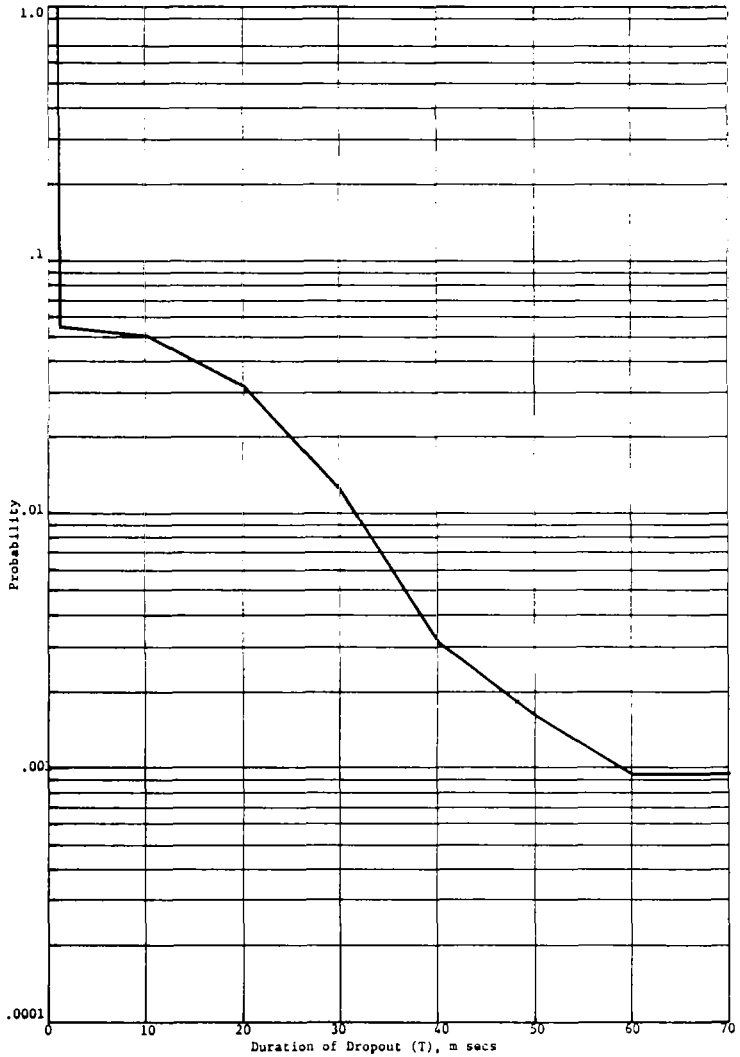


Fig. A-3c. 127 bit code (7,6,3,1).

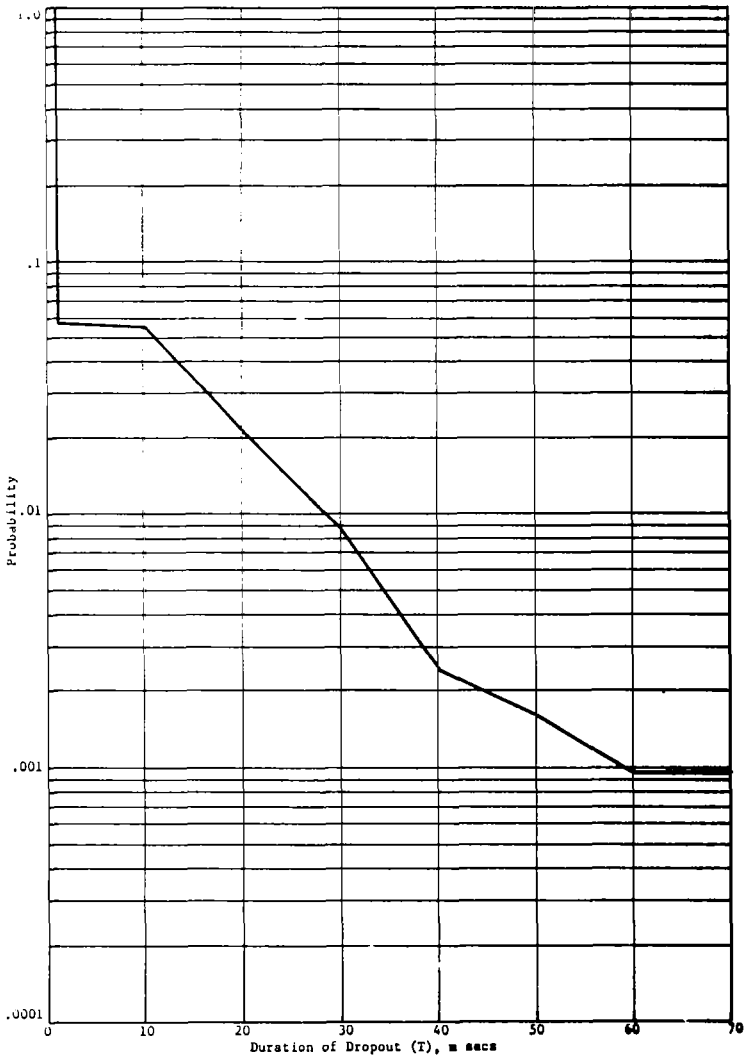


Fig. A-3d. 127 bit code (7,1).

Fig. A-3. Continued.

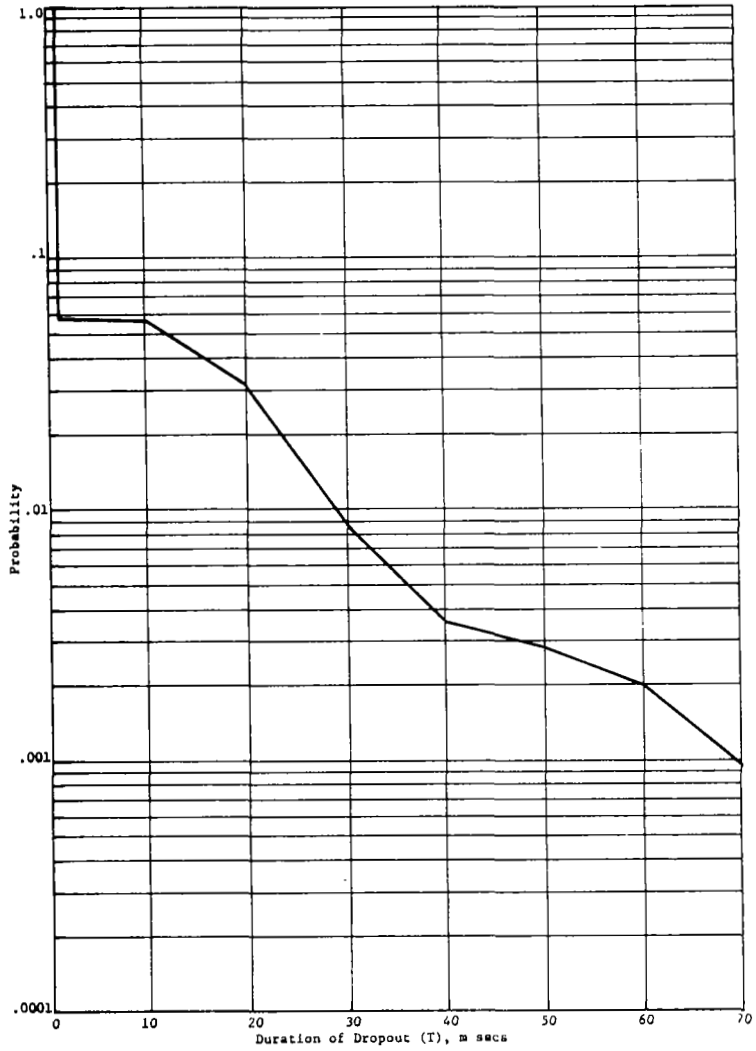


Fig. A-3e. 127 bit code (7,5,4,3,2,1).

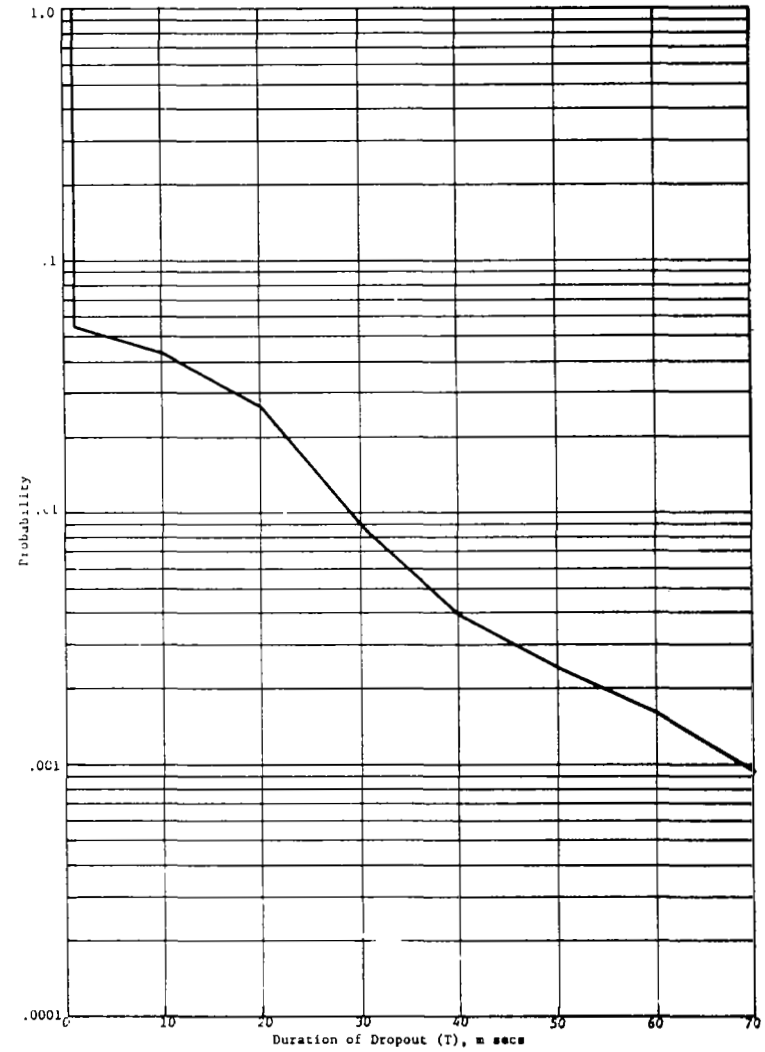


Fig. A-3f. 127 bit code (7,6,5,4,2,1).

Fig. A-3. Continued.

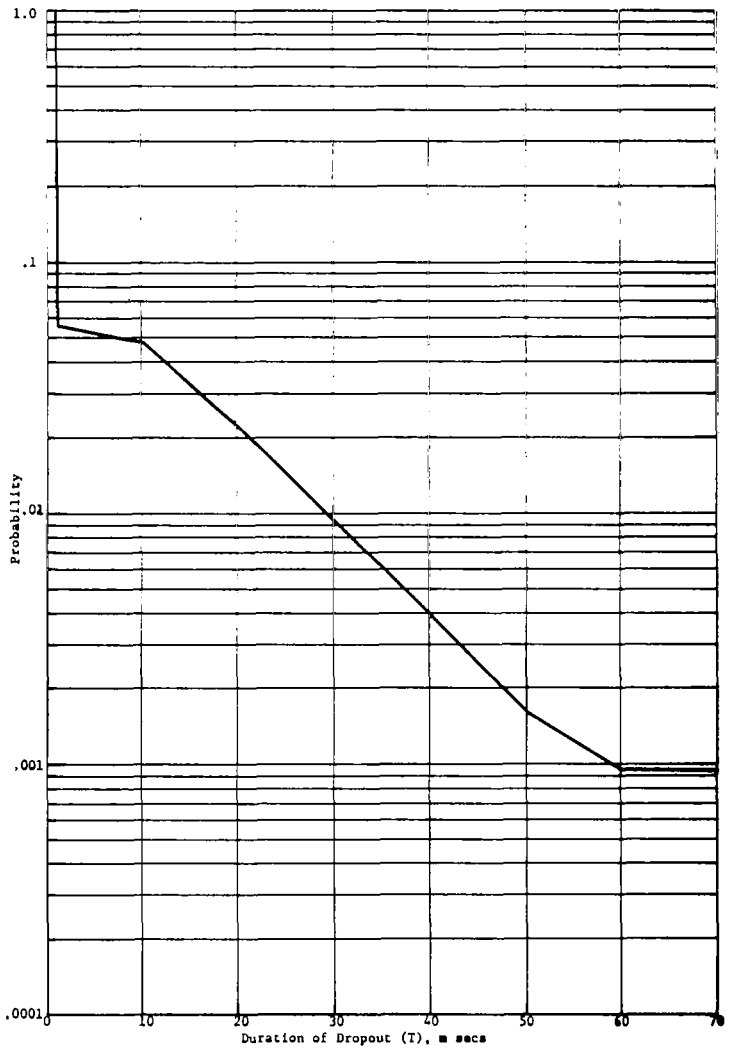


Fig. A-3g. 127 bit code (7,4,3,2).

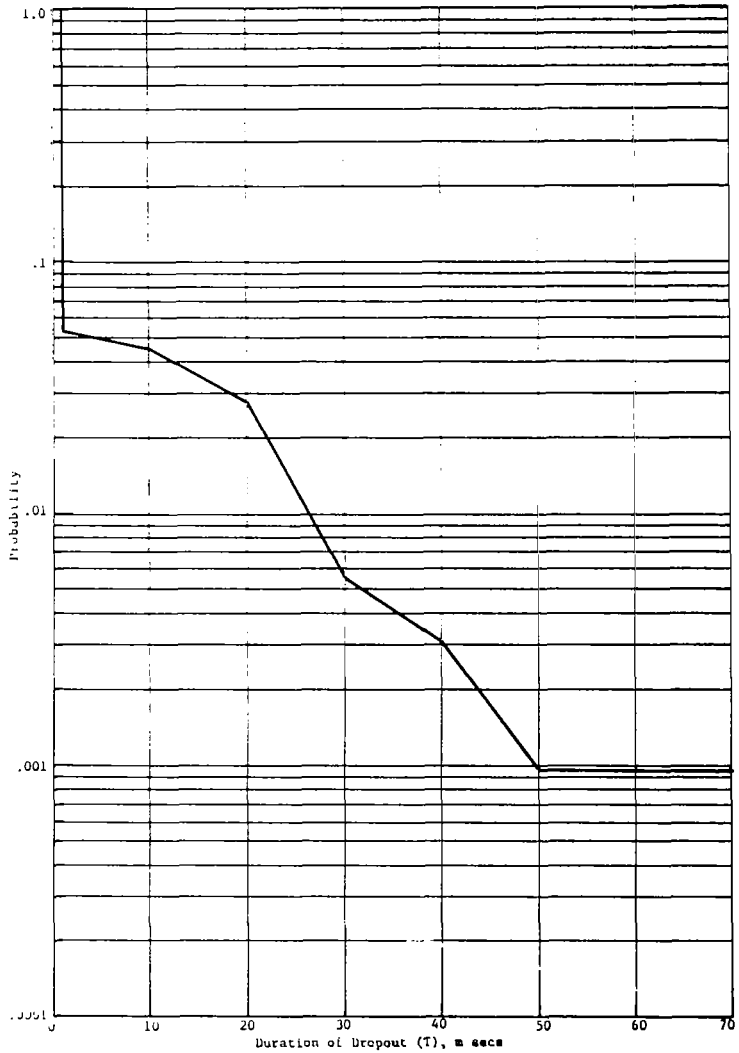


Fig. A-3h. 127 bit code (7,3,2,1).

Fig. A-3. Concluded.

## APPENDIX B

### Calculations for System Simulations

I. General

The saturation studies for the Phase III system are quite similar to those conducted during Phase II (see Ref. [3]). Initially, the system will be simulated using Hour 11 of the NAFEC radar data.

The initial calculations are the same as reported in [3] up to the point of the calculations of path losses, frequencies, and transponder and receiver outputs. The following gives the calculations for the system outputs assuming that the range, velocity, relative azimuth and relative elevation matrices have been calculated. The list of system parameters is given in Table B-1.

II. Calculations

A. Loss matrices and frequency matrix

1. Transmitter-transponder loss matrix (loss from i to j)

$$XL_{ij} = 10 \log_{10} \left[ \frac{1.83 \times 10^{-9} \lambda_T^2}{R_{ij}^2} \right] + G_T(\theta_{ij},\phi_{ij}) + G_{XR}(\theta_{ji},\phi_{ji}) \quad \text{db}$$

where $\lambda_T = \frac{300}{f_T}$ meters

$f_T$ = transmitted frequency (MHz) = P(2)

$G_T$ = transmitter ant. gain function

$G_{XR}$ = transponder receiver ant. gain function

$R_{ij}$ = relative range (n.mi.).

2. Transponder-receiver loss matrix (loss from j to i)

$$XLR_{ji} = 10 \log_{10} \left[ \frac{1.83 \times 10^{-9} \lambda_R^2}{R_{ji}^2} \right] + G_{XT}(\theta_{ji},\phi_{ji}) + G_R(\theta_{ij},\phi_{ij}) \quad \text{db}$$

where $\lambda_R = \frac{300}{f_R}$ meters

$f_R$ = received frequency (MHz) = P(17)

$G_{XT}$ = transponder transmitter ant. gain function

$G_R$ = receiver ant. gain function.

Table B-1. System Parameters.

| No. | Parameter | Units |
|---|---|---|
| 1. | Transmitted Power | dbm |
| 2. | Transmitted Frequency | MHz |
| 3. | FM Slope | MHz/sec |
| 4. | Peak Deviation | MHz |
| 5. | Code Length | bits |
| 6. | Bit Period | msec |
| 7. | Transmitter Ant. Peak Gain | db |
| 8. | Clock Oscillator Error Variance | $Hz^2$ |
| 9. | Transponder Gain Constant | db |
| 10. | Transponder Noise Bandwidth | MHz |
| 11. | Transponder Noise Figure | db |
| 12. | Notch Filter 6 db Bandwidth | KHz |
| 13. | Transponder Output Saturation Level | dbm |
| 14. | Transponder Receiver Ant. Peak Gain | db |
| 15. | Transponder-Transmitter Ant. Peak Gain | db |
| 16. | Transmitter-Transponder Isolation | db |
| 17. | Received Frequency | MHz |
| 18. | Receiver Noise Figure | db |
| 19. | Receiver 1st IF Noise Bandwidth | MHz |
| 20. | Doppler Filter Noise Bandwidth | KHz |
| 21. | Receiver Ant. Peak Gain | db |
| 22. | Receiver Gain to Limiter | db |
| 23. | Limiter-Disc. Conversion Constant | volts/KHz |
| 24. | Range Conversion Factor | nm/volt |
| 25. | Velocity Conversion Factor | Kts/volt |
| 26. | Alarm Threshold (Time) | secs |
| 27. | Alarm Threshold (Range) | nm |
| 28. | Alarm Threshold (Altitude) | ±ft. |
| 29. | Velocity Offset (Dsicriminator) | Kts |
| 30. | Range Acceleration Voltage Time Constant | secs |
| 31. | Velocity Voltage Time Constant | secs |
| 32. | Acceleration Constant u | g units |
| 33. | Power Threshold Variation | db |

3. Doppler frequency matrix

$$FREK_{ij} = \frac{VC_{ij}}{C} (f_T + f_R) \times 10^{-3} \quad KHz$$

where $VC_{ij}$ = relative closing velocity (knots)

C = velocity of light (knots)

$f_T, f_R$ as defined above.

B. Transponder outputs

1. Received power from transmitter i at transponder j.

$$PXD_{ij} = P_T + XL_{ij} \quad \text{dbm}$$

$P_T$ = transmitted power (dbm) = P(1).

2. Transponder noise power referred to input

$$PXNM = (1.38 \times 10^{-23})\, B_{XI}(10^{NFX/10} - 1)(290 \times 10^{9}) \quad \text{mw}$$

$$PXNMD = 10 \log_{10} (PXNM)$$

$B_{XI}$ = transponder bandwidth (MHz) = P(10)

NFX = transponder noise figure = P(11).

3. Total power input to transponder j

$$PXSM_j = \sum_{i=1}^{N} EXP_{10}(PXD_{ij}/10) + PXNM \quad \text{mw}$$

$$PXSD_j = 10 \log_{10}(PXSM_j) \quad \text{dbm}.$$

4. Transponder j saturation factor

$$SATF_j = 1 + PXSM_j/PSAT$$

PSAT = saturation power level (mw)

$$= EXP_{10}[\,(P(13) - FX)/10].$$

5. Signal power output at transponder j from transmitter i

$$PSD_{ij} = FX + PXD_{ij} - 10 \log_{10}(SATF_j)$$

FX = transponder gain constant (db) = P(9).

6. Transponder output noise power

$$POND_j = FX + 10 \log_{10} PXNM - 10 \log_{10}(SATF_j) \quad \text{dbm}.$$

7. Total transponder signal output power

$$PSTD_j = 10 \log_{10}(PXSM_j - PXNM) + FX - 10 \log_{10}(SATF_j) \quad \text{dbm}.$$

8. Total transponder output power

$$PTOD_j = PXSD_j + FX - 10 \log_{10}(SATF_j) \quad \text{dbm}.$$

C. Receiver outputs

1. Signal power received at receiver i from transponder j

$$PRSD_{ij} = PSD_{ij} + XLR_{ji} \quad \text{dbm.}$$

2. Noise power received at receiver i from all transponders in mw and dbm

$$PRNM_i = \sum_{j=1}^{N} EXP_{10}\left[(POND_j + XLR_{ji})/10\right] \quad \text{mw}$$

$$PRND_i = 10 \log_{10} PRNM_i \quad \text{dbm.}$$

3. Undesired signal power received at receiver i in mw and dbm

$$PRUM_i = \sum_{\substack{j=1 \\ j,k\neq i}}^{N} \sum_{k=1}^{N} EXP_{10}\left[(PSD_{kj} + XLR_{ki})/10\right] \quad \text{mw}$$

$$PRUD_i = 10 \log_{10} PRUM_i \quad \text{dbm.}$$

4. Internal receiver noise density at receiver i input

$$PHIR = 1.38 \times 10^{-23}(10^{NFR/10} - 1)(290 \times 10^3) \quad \text{mw/Hz}$$

NFR = receiver noise figure (db) = P(18).

5. Transponder noise density at receiver i input

$$PHIX_i = (PRNM_i/B_{XI})\ 10^{-6} \quad \text{mw/Hz.}$$

6. Undesired signal power density at output of receiver i 1st IF referred to input

$$PHIU_i = (PRUM_i/2\ DELF)\ 10^{-6} \quad \text{mw/Hz}$$

DELF = total deviation of transmitted signal (MHz) = P(4).

7. Internal noise power at doppler filter output

$$PND1 = 10 \log_{10}\left[(BD)(PHIR)\ 10^3\right] + KRD \quad \text{dbm}$$

BD = Doppler filter bandwidth (KHz) = P(20)

KRD = receiver gain to Doppler filter output (db) = P(22).

8. Noise power at Doppler filter output due to transponders

$$PND2_i = 10 \log_{10}\left[(BD)(PHIX_i)\ 10^3\right] + KRD \quad \text{dbm.}$$

9. Interference power at Doppler filter output

$$PUFKD_i = 10 \log_{10}\left[(BD)(PHIU_i)\ 10^3\right] + KRD \quad \text{dbm.}$$

10. Total noise power at Doppler filter output

$$PRNFD_i = 10 \log_{10}\left[(BD)(PHIX_i + PHIR)\ 10^3\right] + KRD \quad \text{dbm.}$$

11. Total noise and interference power at Doppler filter output

$$PPNI_i = 10 \log_{10}\left[(BD)(PHIR + PHIX_i + PHIU_i)\ 10^3\right] + KRD \quad \text{dbm.}$$

12. Signal levels at Doppler filter output

$$PRSDD_{ij} = KRD + PRSD_{ij} \quad \text{dbm} \quad \text{if } FREK_{ij} > -FREKC$$

$$= -200 \text{ if } FREK_{ij} \leq -FREKC$$

$$FREKC = \text{Doppler offset frequency (KHz)} = \frac{P(29)}{C}\ (f_T + f_R)\ 10^{-3}\ .$$

13. Signal levels at double differentiator output (differentiator gain = 5/16 at Doppler frequency of BD/2)

$$PRSD2_{ij} = PRSDD_{ij} + 40 \log_{10}\left\{\frac{FREK_{ij}+FREKC}{BD/2}\right\} - 10 \log_{10}\left(\frac{16}{5}\right) \text{ if } FREK_{ij} > -FREKC$$

$$= -200 \text{ if } FREK_{ij} \leq -FREKC.$$

14. Signal-to-noise plus interference ratio at d.d. output

$$SNIK_{ij} = PRSD2_{ij} - PPNI_i \quad \text{db.}$$

15. Signal-to-noise plus interference ratio at Doppler filter output

$$SNIDK_{ij} = PRSDD_{ij} - PPNI_i \quad \text{db.}$$

16. Signal-to-noise plus interference ratio of range voltage at discriminator output

Let $$SNIlL_i = \text{largest } \{SNIK_{ij}\}$$

---

Note: The gain of the double differentiator is selected so that the internal noise power, noise power due to transponders, interference power, and total noise plus interference power is the same at the d.d. output as at the Doppler filter output.

IF $SNI1L_i \geq 0$

Then $$SNI2M_i = 3D^2\left(\frac{BD}{2BB}\right) EXP_{10}\{SNI1L_i/10\} \quad \text{in mw,}$$

$$SNI2D_i = 10 \log_{10}(SNI2M_i) \quad \text{db}$$

where

$BB = 1/t_o$ KHz

$t_o$ = bit period (m sec) = P(6)

BD = Doppler bandwidth (KHz) = P(20)

D = Deviation ratio (MHz)

$$= \frac{\beta R_{ij}}{C(BB)} \times 10^{-3}$$

C = velocity of light (nm/sec)

$\beta$ = FM slope (MHz/sec) = P(3).

IF $SNI1L_i < 0$

then $$SNI2D_i = (SNI1L_i)(2) \quad \text{db.}$$

D. Alarm Logic

Let $R_{ij}$, $V_{ij}$ be the range and velocity associated with the signal $PRSD2_{ij}$ determining $SNI1L_i$. The system is in an alarm status if:

$$SNI1L_i \geq 3 \text{ db}$$

and if

$$R_{ij} - K \leq \tau_{mk} V_{ij} \quad (1/3600)$$

where $K = (U\tau_{mk}^2/2)(32.2/6080)$ n.mi.

U = acceleration protection (g units) = P(32)

$\tau_{mk}$ = alarm threshold (secs) = P(26)

$V_{ij}$ = closing velocity (knots).

E. Antenna patterns

Note that in the following, the ij subscripts are omitted.

1. Transmitter

$$G_{TA}(\theta) = 20 \log_{10}[1 + .316 \sin 1.64|\theta| - .45 \sin .5|\theta|] \quad \text{db}$$

for $180^{\circ} \leq \theta \leq 180^{\circ}$

$$G_{TE}(\phi) = 10 \log_{10}\left[\frac{\sin^2 6\phi}{(.103\phi)^2}\right] \quad \text{db}$$

for $-90^{\circ} \leq \phi \leq -3^{\circ}$; $\quad 3^{\circ} \leq \phi \leq 90^{\circ}$

$$G_{TE}(\phi) = 0$$

for $-3^{\circ} < \phi < 3^{\circ}$

$$G_T(\theta,\phi) = G_{TA}(\theta) + G_{TE}(\phi) + P(7).$$

2. Transponder receiver

$$G_{XR}(\theta,\phi) = 10 \log_{10}[(1 - .0104|\phi|)^2 \cos^2 2.57\phi] + P(14) \quad \text{db}$$

for $-90^{\circ} \leq \phi \leq 90^{\circ}$.

3. Transponder transmitter

$$G_{XT}(\theta,\phi) = G_{XR}(\theta,\phi) - P(14) + P(15) \quad \text{db}$$

for $-90^{\circ} \leq \phi \leq 90^{\circ}$.

4. Receiver

$$G_R(\theta,\phi) = G_T(\theta,\phi) - P(7) + P(21) \quad \text{db}.$$

Plots of the pattern fits are shown in Figs. B-1 through B-3.

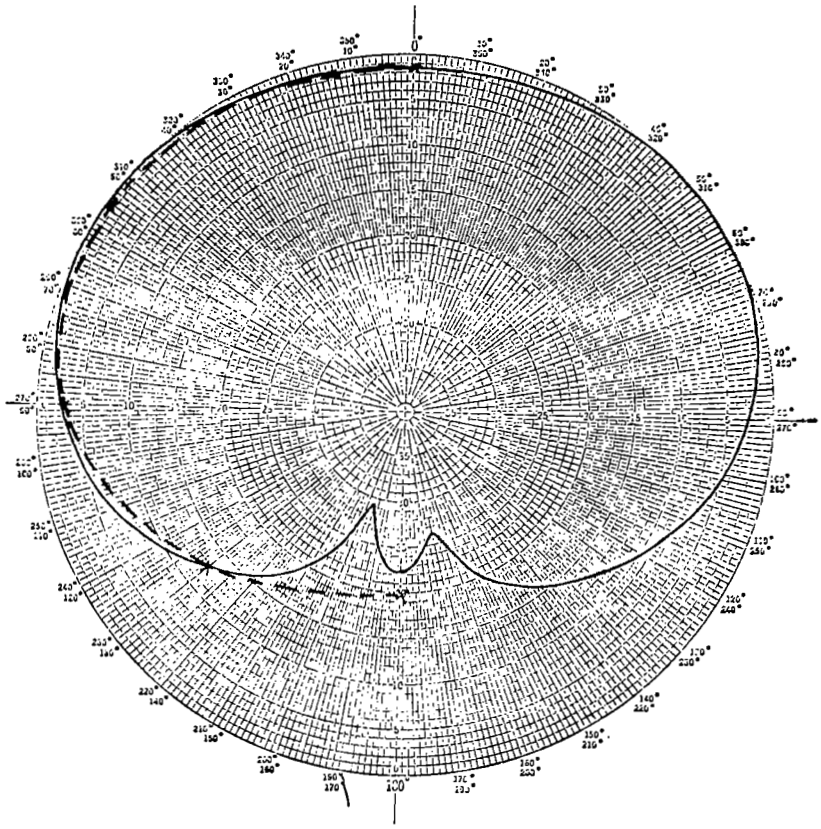

Fig. B-1. Receiver azimuth pattern.

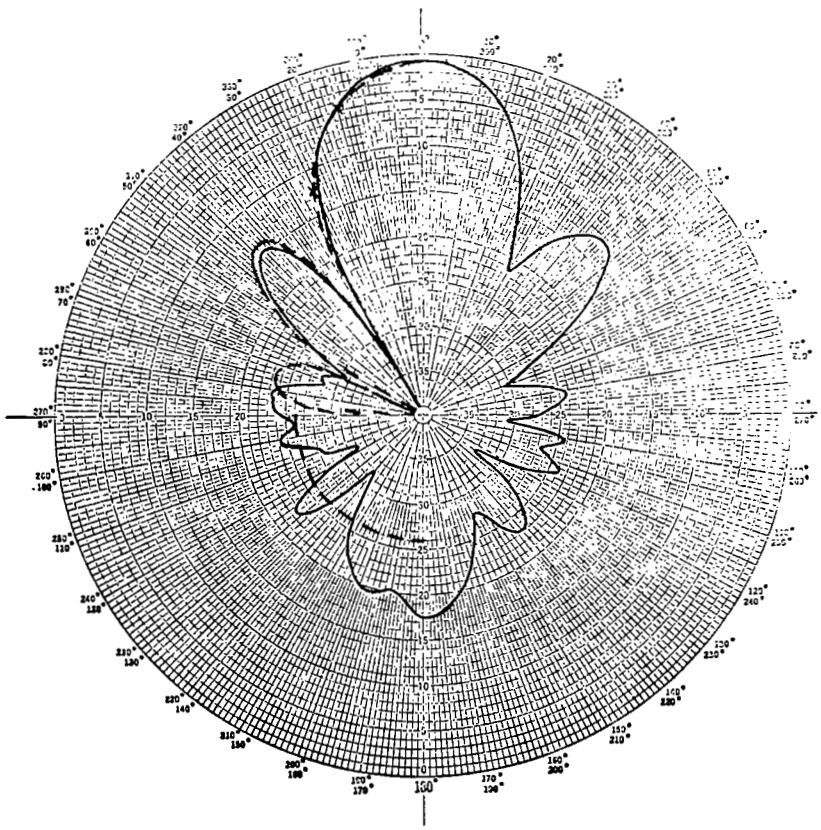

Fig. B-2. Receiver elevation pattern.

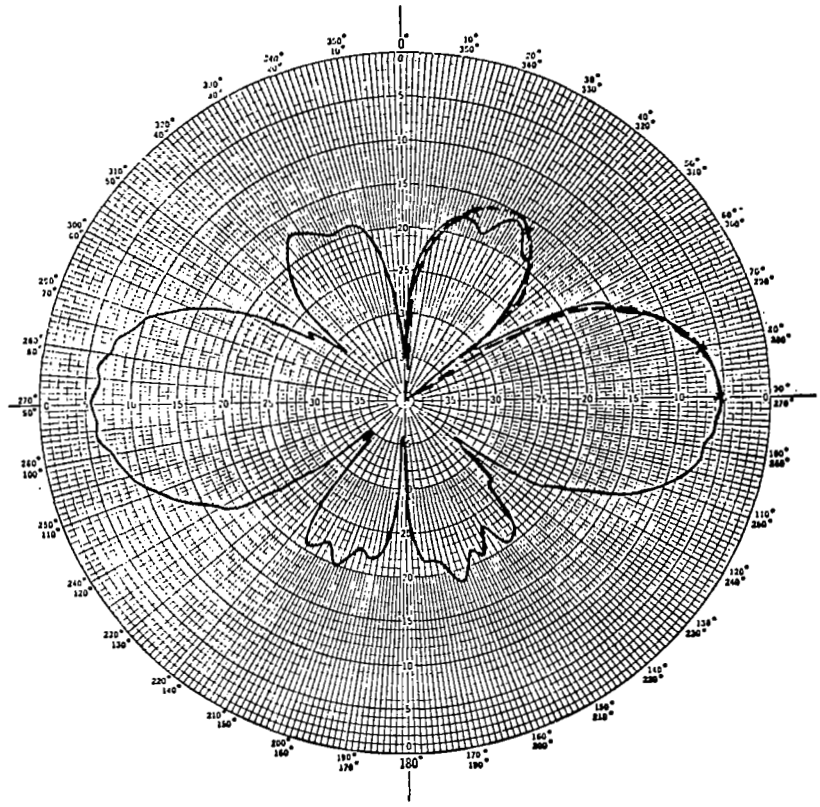

Fig. B-3. Transponder receiver elevation pattern.

## III. Outputs

For the evaluation of the severity of the saturation and interference problem, the main emphasis has been on "the percent of time that a certain power level exceeded a given level." Since the simulation itself provides the discrimination, no added discrimination (e.g., altitude difference discrimination) is necessary as was used in the Phase II Statistical Analysis Programs (see Ref. [1]).

"Percent of time" histograms have therefore been calculated for the following parameters:

Noise plus interference power at the transponder output,

Total transponder output power,

Saturation factor minus one,

The level of the five largest signals at the transponder output,

The level of the five largest signal-to-noise plus interference power levels at the transponder output,

The ratio of the largest signal to the next largest signal at the transponder output.

The following parameters have been measured for the receiver, with power levels referred to the output of the Doppler filter (or, the double differentiator):

Undesired signal power level,

Noise plus interference power level,

The five largest signals with frequency greater than offset,

The five largest signal-to-noise plus interference powers with frequency greater than offset,

The five largest signals while in an alarm status,

The five largest signal-to-noise plus interference ratios while in an alarm status.

## APPENDIX C

## REAL-TIME SIMULATIONS OF THE PWI SYSTEM IN A MULTIPLE AIRCRAFT ENVIRONMENT

### I. General

Simulations were conducted during which an intruding aircraft under control of a "pilot" was flown through a traffic environment represented by the Atlanta data base. The objective of this series of simulations was to show the feasibility of real-time simulations using the Atlanta data tapes to provide a realistic environment. The computations were performed on the LRC CDC 6600 real-time simulation console.

Figure C-1 shows a block diagram representing the major features of the simulation. Major inputs included the Atlanta radar traffic tape, the set of system parameters and antenna patterns, the dynamic characteristics of the intruder aircraft, and a set of computer instructions. The pilot commands were provided by means of a small control stick and potentiometers on the display console to simulate throttle commands. Output displays included simulated instruments for intruder heading, altitude, attitude, and a display which indicated a blip on the oscilloscope representing the position of the most hazardous target in the intruder coordinate system.

A controller display was simulated using a conventional oscilloscope to display the Atlanta traffic and the intruding aircraft positions. The PWI outputs were calculated at the intruding aircraft and placed on strip chart recorders to record values of relative range, closing velocity, projected miss distance, alarm status, and power levels at the intruding aircraft receiver. Specific calculations used for the simulation are given in Appendix D.

### II. Results

The simulation was found to be feasible and well within the capabilities of the LRC computers. A problem was encountered with program storage, however, this was due to the necessity of storing the Atlanta traffic data prior to use. Thus, it was only possible to store approximately 10 minutes

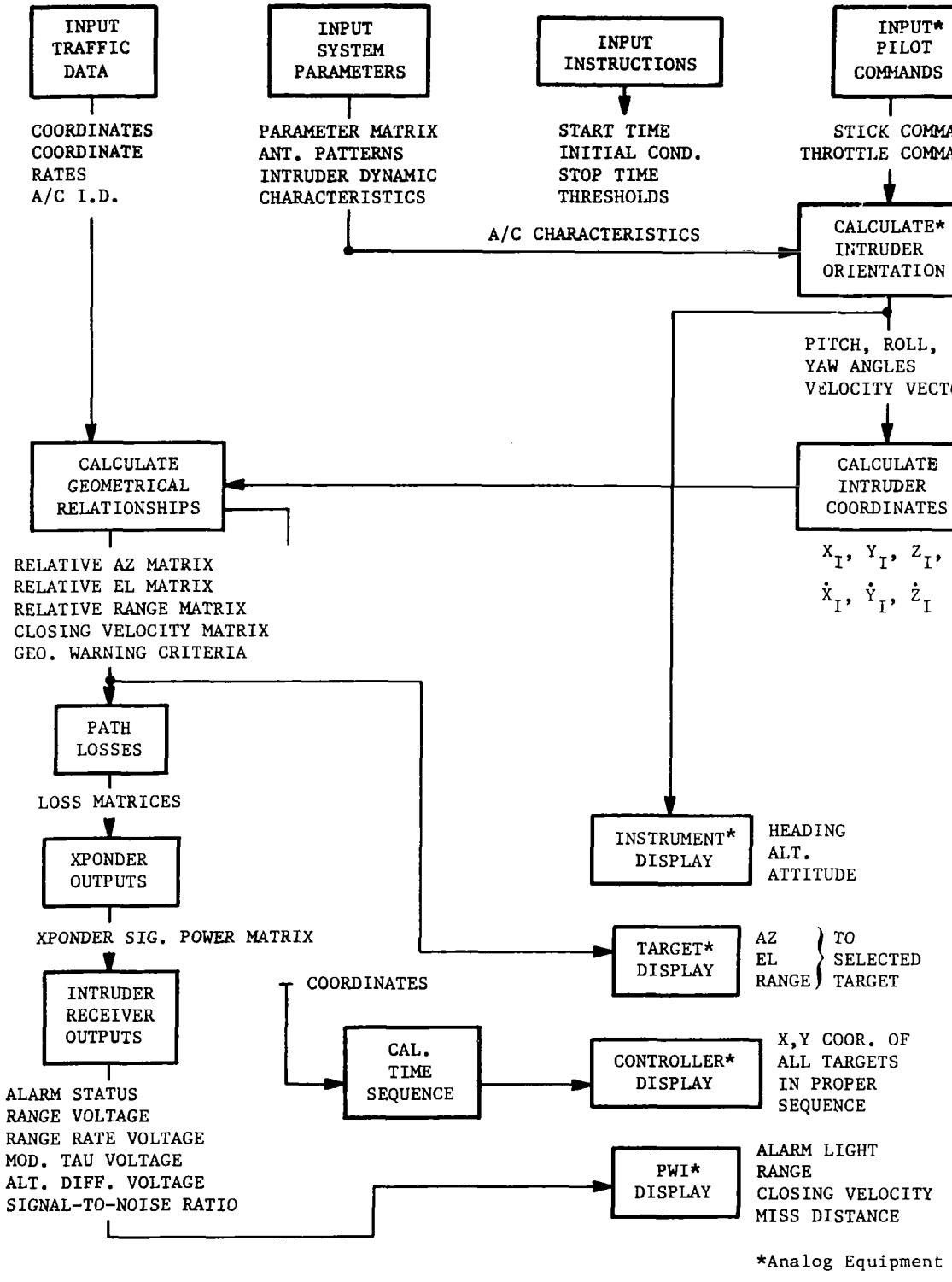


Fig. C-1. PWI real-time simulation block diagram.

of the Atlanta traffic data and this 10 minutes of data storage required approximately 20,000 words of memory. This storage problem was later overcome by the systems programmers at LRC by the development of system routines to read data tapes in real time.

Another problem area noted was that of displaying the Atlanta traffic data on the CRT in real time. The CRT update is a function of the amount of information displayed, hence, it is somewhat difficult to get a continuous-appearing display with large amounts of information. This display limitation is inherent in the present CRT control units, but is not a large effect. That is, the update rates with reasonable amounts of information are such that a real-time appearance is achieved.

Examples of the output of the real-time simulations are shown in Figs. C-2 through C-4. Figure C-2 shows the simulated controller radar display (on an oscilloscope) at scan 300 of Hour 11 of the Atlanta data base. In this photograph, the terminal is at the center of the picture at the location of the bright dot. The location of the intruder aircraft under "pilot" control is shown by the arrow in the photograph. Figure C-3 shows the tracks of the aircraft after a period of time has elapsed such that the intruder and an aircraft coming in from the North are in an encounter (alarm) situation.

Figure C-4 shows the strip chart recordings for the encounter situation shown in the photograph (Fig. C-3). This encounter is a near head-on situation with an approximate altitude separation of 1000 ft. Altitude discrimination was not used in the simulation, hence the strip chart recording indicates that an alarm was received at a range of approximately 5.3 miles from the target in the data base. At this time, the value of modified tau as read off the strip chart was 32 seconds. The closing velocity is relatively constant at 365 knots.

The miss-distance voltage has large variations which are primarily due to the four-second update rate in the Atlanta traffic data. Since the miss-distance calculation is based on the second derivative of relative range, it is expected to be somewhat noisy in actual practice, however, the excursions shown on the strip chart recorder should be attributed to the computer updating techniques rather than to system characteristics.

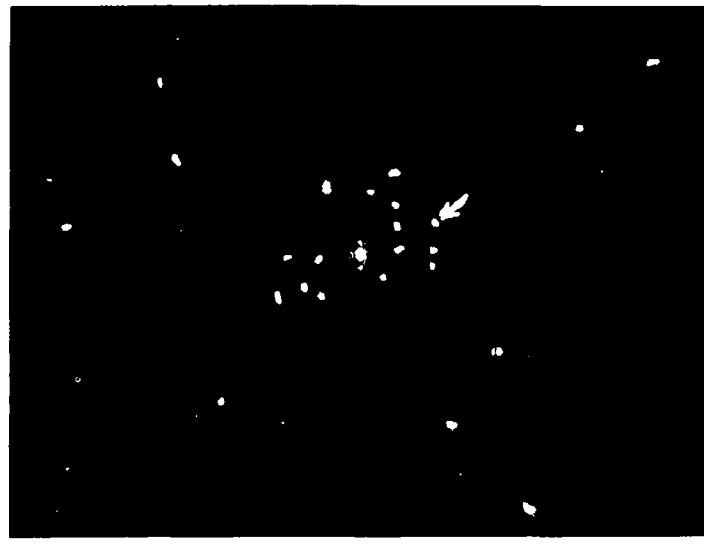

Fig. C-2. Simulated controller radar display (on an oscilloscope) at scan 300 of Hour 11 of the Atlanta data base.

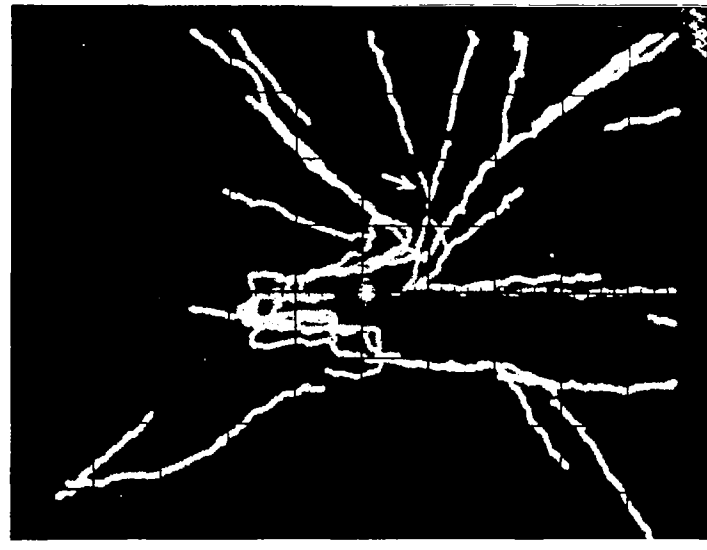

Fig. C-3. Aircraft tracks on oscilloscope display. The intruder aircraft track is indicated by the arrow.

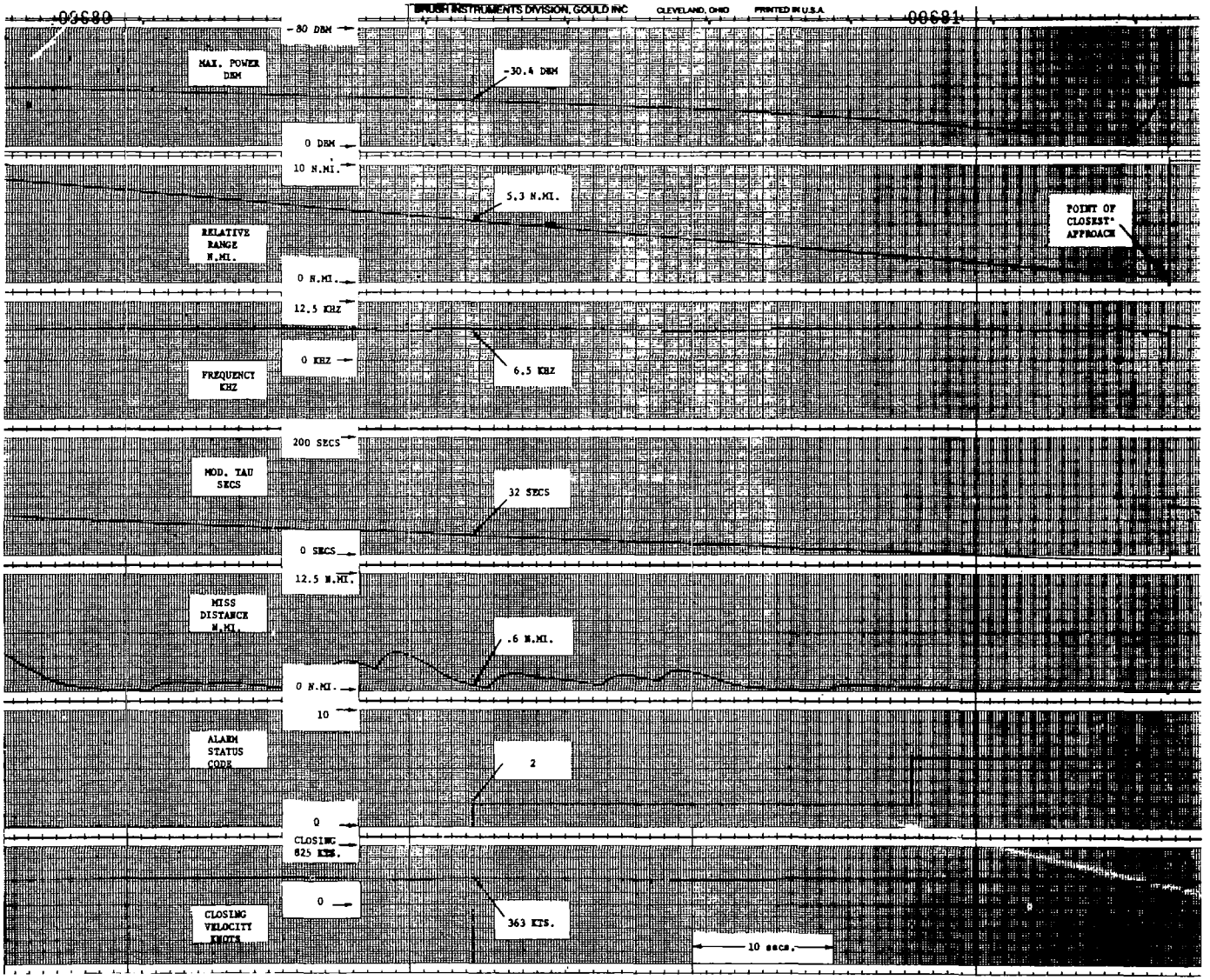


Fig. C-4. Strip chart recording of various receiver parameters from the real-time computer simulation.

# APPENDIX D
# REAL-TIME SIMULATION CALCULATIONS

## I. General

For the real-time simulation studies, no supplementary analog computing equipment was used. All inputs were provided at the operator console.

The objective of this simulation was to show the feasibility of real-time simulations using the Atlanta data tapes. Also, the feasibility of using a conventional oscilloscope as a radar display will be demonstrated. If desirable, the simulation could later be expanded by adding a cockpit and additional aircraft dynamic equations.

A flow chart of the real-time program is given in Fig. D-1.

## II. Inputs to the Program

1. Atlanta data tape (approximately 10 minutes of data)
   - A. X, Y, Z coordinates (nautical miles)
   - B. Scan number, track number
   - C. X and Y velocity components (nautical miles per second)
     These velocity components will be computed from the coordinate data if memory capacity becomes a problem.
2. System parameters.
   The system parameter values are given in Table 1, page 19.
3. Instructions and initial conditions (these will be entered on the display console keyboard)
   - A. Intruder initial position $X_o$, $Y_o$, $Z_o$
     Altitude will be in feet whereas the coordinates are in nautical miles.
   - B. Intruder initial heading (degrees)
   - C. The starting scan number
   - D. The final scan number
4. Input variables (on display panel potentiometers)
   - A. Aircraft bank angle, $\phi$ (degrees)
   - B. Rate of climb/descent (ft./sec.)

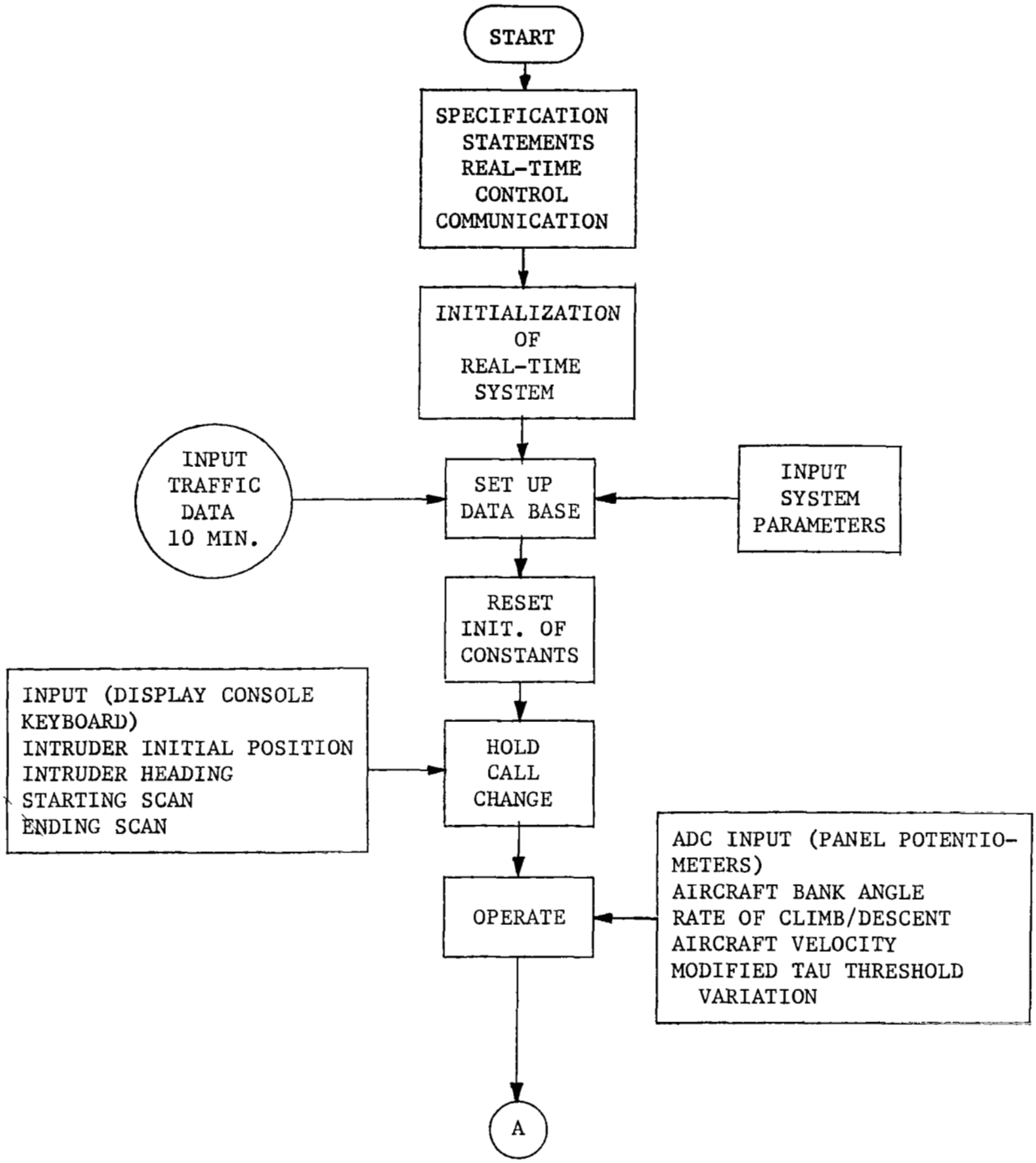


Fig. D-1. Computer flow chart of real-time simulation program.

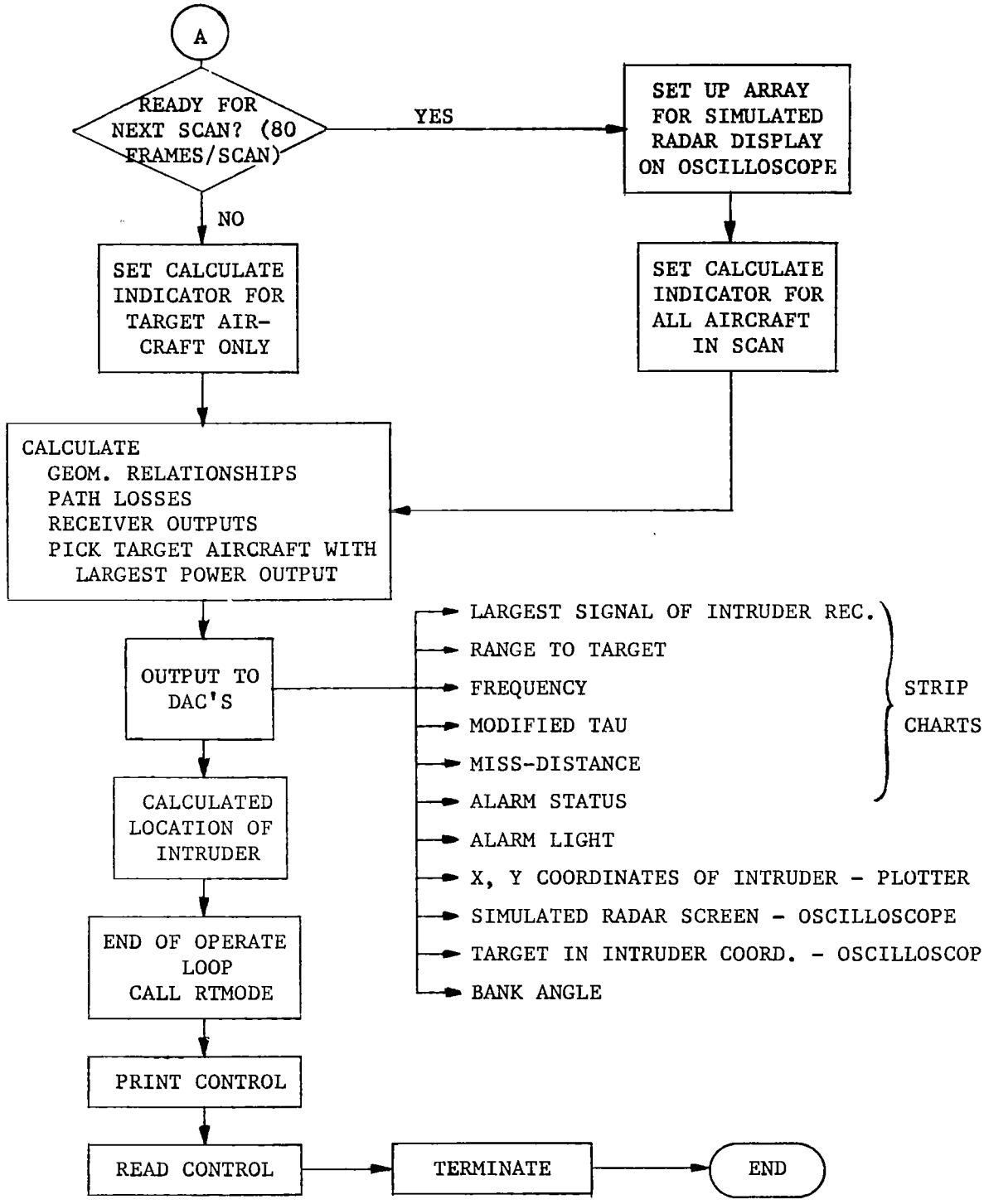


Fig. D-1. Concluded.

C. Aircraft velocity (knots)

D. Modified tau threshold variation (± db)

III. Program Outputs

1. X, Y, and intensity pulses to traffic display oscilloscope
2. Intruder X and Y coordinates to X, Y plotter
3. Target in intruder coordinates on oscilloscope
4. Outputs to strip chart recorders
   A. Largest signal of intruder receiver
   B. Range to target providing largest signal
   C. Frequency of the largest signal
   D. Calculated value of modified tau for target providing largest signal
   E. Projected miss-distance to target with largest signal
   F. Alarm status of receiver
5. Intruder roll angle on volt meter
6. Alarm light - red lights on console
7. Intruder altitude
8. Altitude differential between intruder and target with largest signal
9. Intruder heading
10. Intruder - target differential

IV. Calculations

1. Intruder path (calculated each frame time, or every 1/64 second)
   A. Intruder heading at $i^{th}$ time increment

$$\psi_i = (\Delta t)\ g/V \sin \phi + \psi_{i-1} \qquad \text{(deg)} \qquad \text{(D-1)}$$

where

$\Delta t$ = calculation increment (secs)

$g$ = 32.2 ft./sec.$^2$

$V$ = aircraft velocity in ft./sec. (input from pot.)

$\phi$ = roll angle in degrees (input from pot.)

$\psi_o$ = initial heading angle in degrees (input from keyboard)

b. Intruder coordinate velocities

$$VX_i = V \sin \psi_i \quad \text{(Kts)}$$
$$VY_i = V \cos \psi_i \quad \text{(Kts)} \qquad \text{(D-2)}$$
$$VZ_i = (RC) \quad \text{(ft./sec.)}$$

where V = aircraft velocity in Kts

RC = rate of climb (+) or descent (-) (input from pot.).

c. Intruder coordinates

$$X_i = (\Delta t)\ V \sin \psi_i + X_{i-1} \quad \text{(n.mi.)}$$
$$Y_i = (\Delta t)\ V \cos \psi_i + Y_{i-1} \quad \text{(n.mi.)} \qquad \text{(D-3)}$$
$$Z_i = (\Delta t)\ (RC) + Z_{i-1} \quad \text{(ft.)}$$

where V = velocity in n.mi./sec.

2. Geometry

a. For each aircraft j with respect to intruder i in the scan, the following are calculated:

(1) relative azimuth $AZ_{ij}$ and $AZ_{ji}$
(2) relative elevation $EL_{ij}$ and $EL_{ji}$
(3) relative range $R_{ij}$
(4) relative closing velocity $VC_{ij}$.

3. Intruder receiver outputs

a. Power outputs

$$PRSD2_{ij} = PRSDD_{ij} + 40 \log_{10} \left\{ \frac{FREK_{ij} + FREKC}{BD/2} \right\} - 10 \log_{10} (16/5) \qquad \text{(D-4)}$$

if $FREK_{ij} + FREKC > 0$

where: $= -200$ if $FREK_{ij} + FREKC \leq 0$

$$\text{FREKC} = \text{Doppler offset (KHz)} = \frac{P(29)^*}{C}\,(f_T + f_R)\,10^3$$

$$\text{FREK}_{ij} = \frac{VC_{ij}}{C}\,(f_T + f_R)\,10^3$$

$C$ = velocity of light, knots

$VC_{ij}$ = closing velocity, knots

$$\text{PRSDD}_{ij} = P(22) + XLR_{ji} + P(9) + P(1) + XL_{ij}. \qquad \text{(D-5)}$$

$$XL_{ij} = 10 \log_{10}\left[\frac{1.83 \times 10^{-9}\lambda_T^2}{R_{ij}^2}\right] + G_T(\theta_{ij},\phi_{ij}) + G_{XR}(\theta_{ji},\phi_{ji}) \quad \text{db} \qquad \text{(D-6)}$$

where

$\lambda_T = \frac{300}{f_T}$ meters

$f_T$ = transmitted frequency (MHz) = P(2)

$G_T$ = transmitter ant. gain function

$G_{XR}$ = transponder receiver ant. gain function

$R_{ij}$ = relative range (n.mi.)

$$XLR_{ji} = 10 \log_{10}\left[\frac{1.83 \times 10^{-9}\lambda_R^2}{R_{ji}^2}\right] + G_{XT}(\theta_{ji},\phi_{ji}) + G_R(\theta_{ij},\phi_{ij}) \quad \text{db} \qquad \text{(D-7)}$$

where

$\lambda_R = \frac{300}{f_R}$ meters

$f_R$ = received frequency (MHz) = P(17)

$G_{XT}$ = transponder transmitter ant. gain function

$G_R$ = receiver ant. gain function

---

*The P(·) array is given in Table B-1.

b. Antenna Patterns

Note that in the following, the ij subscripts are omitted.

1. Transmitter

$$G_{TA}(\theta) = 20 \log_{10}[1 + .316 \sin 1.64|\theta| - .45 \sin .5|\theta|] \quad \text{db} \qquad \text{(D-8)}$$

for $180° \leq \theta \leq 180°$

$$G_{TE}(\phi) = 10 \log_{10} \left[\frac{\sin^2 6\phi}{(.103\phi)^2}\right] \quad \text{db} \qquad \text{(D-9)}$$

for $-90° \leq \phi \leq -3°$; $3° \leq \phi \leq 90°$

$$G_{TE}(\phi) = 0 \qquad \text{for } -3° < \phi < 3°$$

$$G_T(\theta,\phi) = G_{TA}(\theta) + G_{TE}(\phi) + P(7). \qquad \text{(D-10)}$$

2. Transponder Receiver

$$G_{XR}(\theta,\phi) = 10 \log_{10}[(1 - .0104|\phi|)^2 \cos^2 2.57\phi] + P(14) \quad \text{db} \qquad \text{(D-11)}$$

for $-90° \leq \phi \leq 90°$

3. Transponder Transmitter

$$G_{XT}(\theta,\phi) = G_{XR}(\theta,\phi) - P(14) + P(15) \quad \text{db} \qquad \text{(D-12)}$$

for $-90° \leq \phi \leq 90°$

4. Receiver

$$G_R(\theta,\phi) = G_T(\theta,\phi) - P(7) + P(21) \quad \text{db} \qquad \text{(D-13)}$$

c. Alarm logic

An alarm may be sensed in two different ways: 1) a power level threshold (PT) may be used to provide an alarm, and 2) an alarm criterion may be calculated from the measured range and velocity. For this latter measurement to be possible, the signal-to-noise ratio of the measurements must be greater than a threshold value.

1. The various threshold values are:

(1) Power Threshold

$$PT = P(1) + P(9) + P(22) + XLX + XLRX + 40 \log_{10}(2(FREKC)/BD) \qquad \text{(D-14)}$$

$$- 10 \log_{10}(16/5) + (\text{modified tau threshold variation})$$

where

$$XLX = 10 \log_{10}\left[\frac{1.83 \times 10^{-9}\lambda_T^2}{R_o^2}\right]$$

$$XLRX = 10 \log_{10}\left[\frac{1.83 \times 10^{-9}\lambda_R^2}{R_o^2}\right]$$

$$R_o = \frac{U(25)^2}{2}\left(\frac{32.2}{6080}\right)$$

$$U = P(32).$$

(2) Signal-to-noise threshold

$$SNR_t = 5 + 5 \log_{10}(P(20)\ P(6)). \qquad \text{(D-15)}$$

(3) Modified tau threshold

$$\tau_{mk} = P(26). \qquad \text{(D-16)}$$

2. The parameters that are compared with the threshold values are

(1) Power level

$$P1 = \text{largest } (PRSD2_{ij}) \quad \text{dbm.} \tag{D-17}$$

(2) Signal-to-noise (real-time simulation only)

$$SNR = \text{largest } (PRSD2_{ij}) - PPRT \tag{D-18}$$

where $PPRT = 10 \log_{10} [(BD)(PHIR)] + 8.0 + P(22)$

$PHIR = 1.38 \times 10^{-23}(10^{NFR/10} - 1)(290 \times 10^{3})$

$NFR = P(18)$.

(3) Modified tau

$$\tau_m = \frac{R_{ij} - K}{V_{ij}} (3600) \qquad \text{(secs)} \tag{D-19}$$

where $R_{ij}$; $V_{ij}$ = range and closing velocity associated with largest signal in n.mi. and Kts.

$$K = \frac{U\tau_{mk}^{2}}{2} \frac{32.2}{6080} \qquad \text{(n.mi.)}$$

$U = P(32)$ (g units)

$\tau_{mk} = P(26)$ (secs).

The alarm status code is indicated in Fig. D-2.

4. Receiver voltage outputs (all outputs use geometrical values associated with largest signal)

a. Range voltage

$$V_i = K_1 R_{ij} \tag{D-20}$$

$K_1$ = constant scale factor (volts/n.mi.)

b. Range rate voltage

$$V_2 = K_2 VC_{ij} \tag{D-21}$$

$K_2$ = scale factor (volts/Kt)

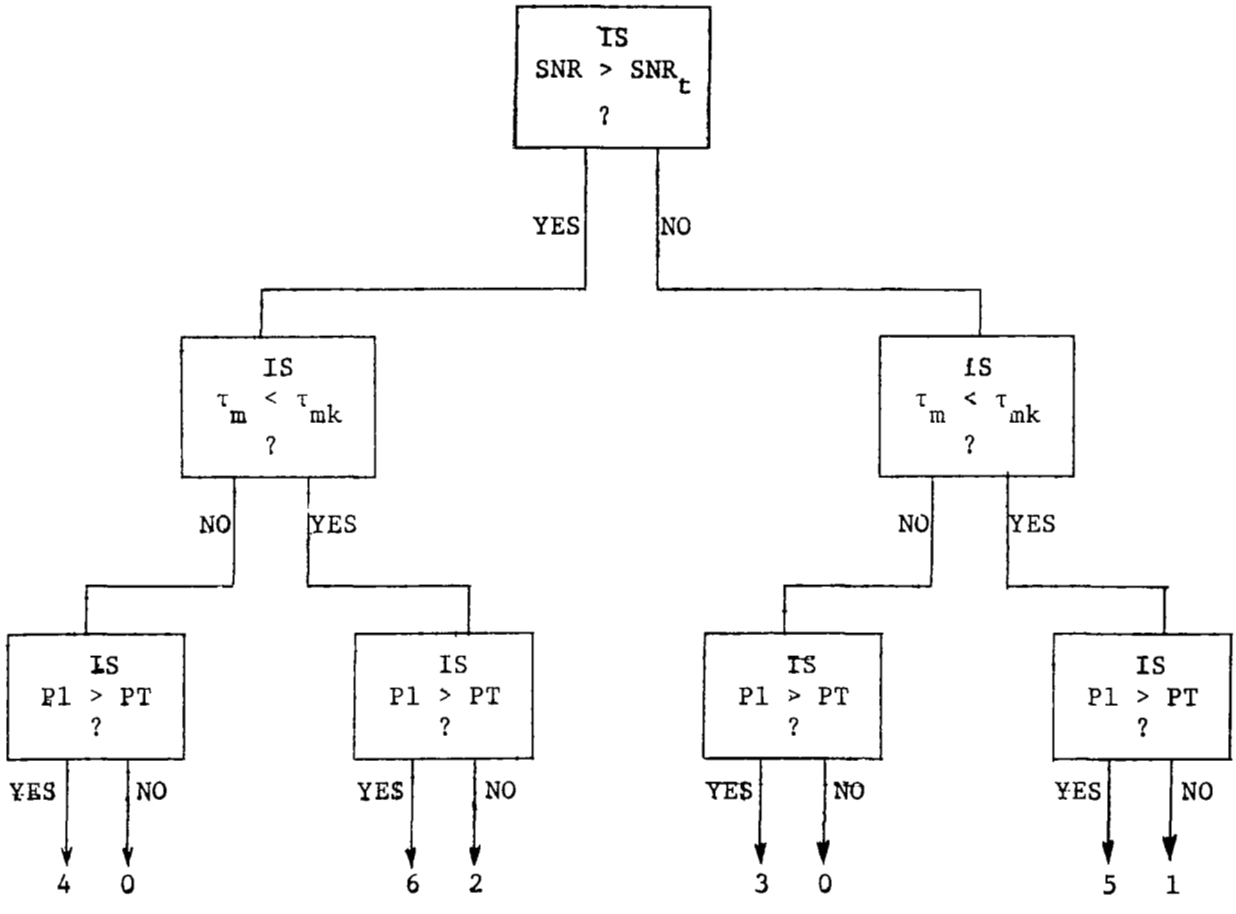


Alarm Status Designation

P1 = power output of the double differentiator

$\tau_{mk}$ = modified tau threshold, P(26)

$\tau_m$ = calculated value of modified tau

SNR = signal-to-noise ratio at double differentiator output

PT = power level threshold.

Fig. D-2. Alarm status code logic.

smoothed voltage (output)

$$V_{2s}^{n+1} = V_{2s}^{n} + \frac{(\Delta T)}{\tau_V}\left[V_2^{n} - V_{2s}^{n}\right] \qquad \text{(D-22)}$$

where

$(\Delta T)$ = time increment (secs)

$\tau_V$ = velocity voltage time constant = P(31)

c. Miss distance voltage

$$V_m = K_m d \qquad \text{(D-23)}$$

where

$K_m$ = scale factor (volts/nm)

d = miss distance (nm)

$$d = \left[\frac{R_{ij}^{3} A_{ij}}{VC_{ij}^{2}}\right]^{1/2} \quad \text{(nm)}$$

$$A_{ij} = \frac{VC^{n+1} - VC^{n}}{(\Delta t)} \quad \text{range acceleration (nm/sec}^2\text{)}$$

IF $A_{ij} < 0$ set $d = 0$

$VC_{ij}$ = closing velocity (n.mi./sec.)

$R_{ij}$ = relative range (n.mi.)

$(\Delta t)$ = calculation increment.

Smoothed miss distance voltage (output)

$$V_{ms}^{n+1} = V_{ms}^{n} + \frac{(\Delta t)}{\tau_a}\left[V_m^{n} - V_{ms}^{n}\right] \quad \text{volts.} \qquad \text{(D-24)}$$

$\tau_a$ = P(30)

d. Alarm status voltage

$$V_a = .1 \times (\text{status code}). \qquad \text{(D-25)}$$

5. Display Outputs

a. X,Y coordinates are ordered in each scan in accordance with

$$\Delta T_i = \frac{1}{\omega} \tan^{-1} \frac{y_i}{x_i} \quad \text{secs} \qquad \text{(D-26)}$$

where $\omega$ = scan rate (rad./sec.)

$T_i$ = output time increment after start of scan.

X voltage, Y voltage, and intensity voltage is output on DACs every other frame.

$$V_{xi} = K_x X_i$$
$$V_{yi} = K_y Y_i \qquad \text{(D-27)}$$
$$V_I = K_z \quad \text{(constant)}$$

where $K_x$ and $K_y$ are scale factors.

In alternate frames, all voltages are set = zero.

6. Input/output scale factors

| | | Voltage Scale Factor | |
|---|---|---|---|
| Variable | Max. Value | (100 Volts/Unit) | (Volts/Unit) |
| x, y | $\pm$ 40 n.mi. | .0025 | 2.5 |
| z | 10,000 ft. | .0001 | .01 |
| d | 5 n.mi. | .2 | 20 |
| $R_{ij}$ | 10 n.mi. | .1 | 10 |
| $\dot{R}_{ij}$ | 1000 kts | .001 | .1 |
| x (heading) | $360^o$ | .0025 | .25 |
| $\tau_m$ | 50 sec. | .02 | 2 |
| freq. | 10 KHz | .1 | 10 |
| $\phi$ (roll) | $\pm$ $50^o$ | .02 | 2 |
| V (velocity) | 333 kts | .003 | .3 |
| Rate of climb/descent | 25 fps | .04 | 4 |
| Mod tau threshold | $\pm$ 20 db | .05 | 5 |

## APPENDIX E

### Extended Aircraft Density Model

### I. General

This appendix describes the logic which develops simulated terminal area environments used in saturation studies of the PWI system. Output of the routine described in this appendix consists of positional information (x,y,z) and velocity information ($v_x$,$v_y$,$v_z$) for each of N aircraft. Statistics valid for pairs of aircraft in a terminal area environment have been used to position N-1 aircraft relative to an "ownship" at (x=0, y=0, z=0) with velocity ($v_x$=0, $v_y$=0, $v_z$=0). This information is then provided as input to the saturation studies program.

In generating the positional and velocity information, a pseudo-random number generator is used with a set of probability density functions. For each of the N-1 aircraft, a value of relative range R from the "ownship" is chosen randomly. Given R, a value of closing velocity is selected. Subsequently, a value $\theta$ is picked, conditioned on the selected value of $\dot{R}$. Once $\theta$ and $\dot{R}$ are determined, one of two possible values of heading $\alpha$ is randomly assigned. A coordinate transformation provides the output ($x,y,z,v_x,v_y,v_z$), where $(v_x^2 + v_y^2 + v_z^2)^{1/2}$ is assumed constant for all N aircraft.

Figure E-1 provides a flow chart of the logic used to provide this output. The variables included in the flow chart are defined as follows:

ALPHA(k) = vector of headings for each aircraft, $1 \leq K \leq N - 1$

CLOSV(k) = vector of ordered closing velocities, $1 \leq K \leq N - 1$

N = number of aircraft in the terminal area

RELR(k) = vector of ordered relative velocities, $1 \leq K \leq N - 1$

RR(I) = vector of 41 ordered relative ranges where RR(1) = 0.5 n.mi., RR(41) = 55.0 n.mi.

RX(I) = vector of probability weights representing discretized marginal probability density f(R)

THETA(k) = vector of azimuths from ownship, $1 \leq K \leq N - 1$

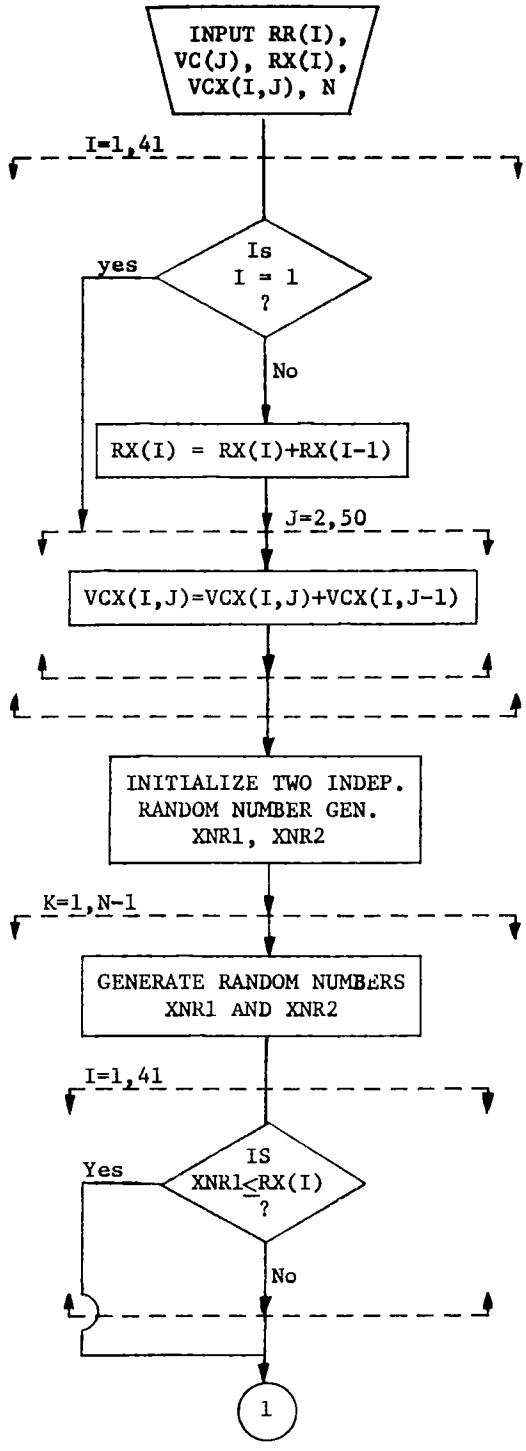


Fig. E-1. Flow chart for generation of extended density data.

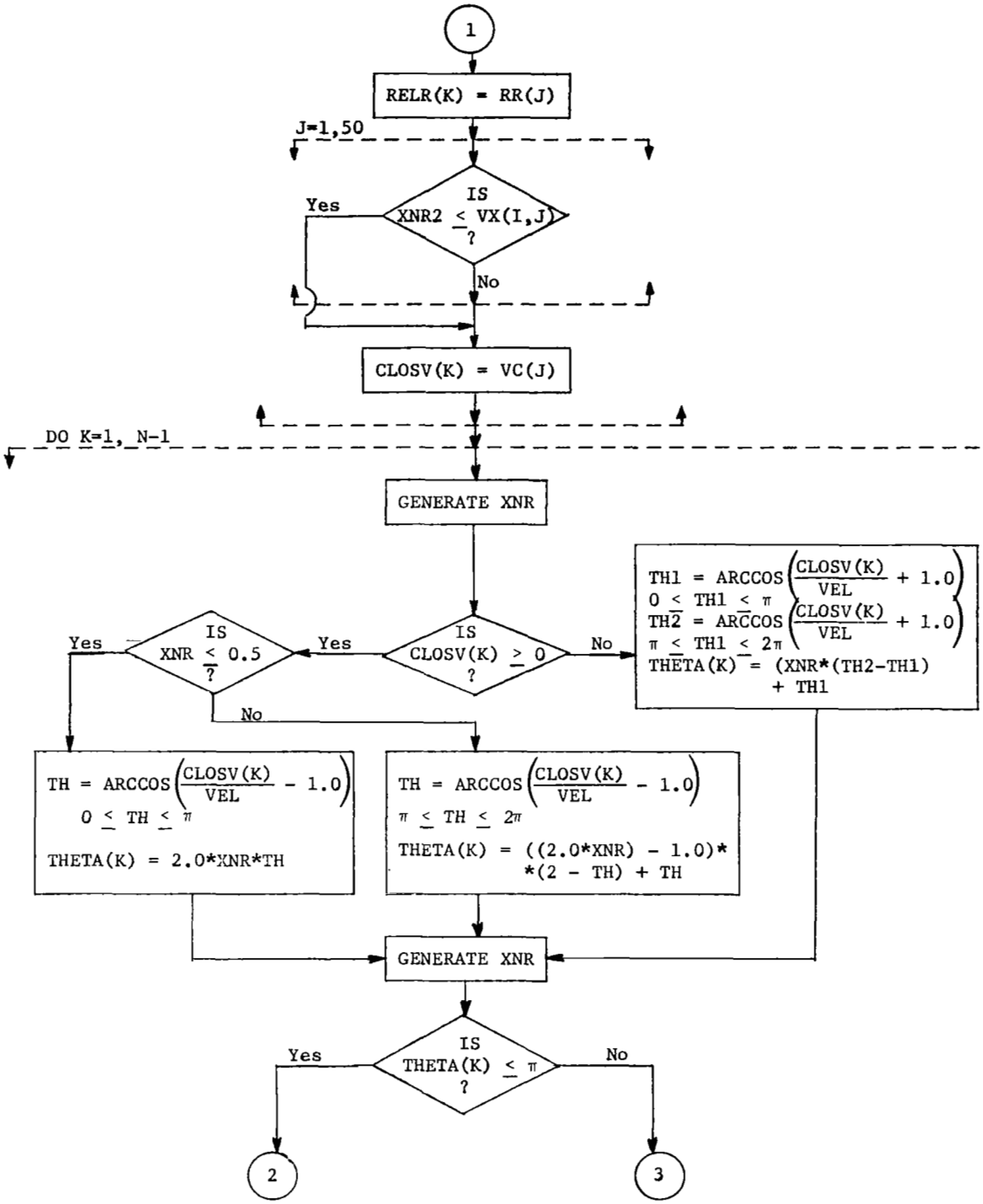


Fig. E-1. Continued.

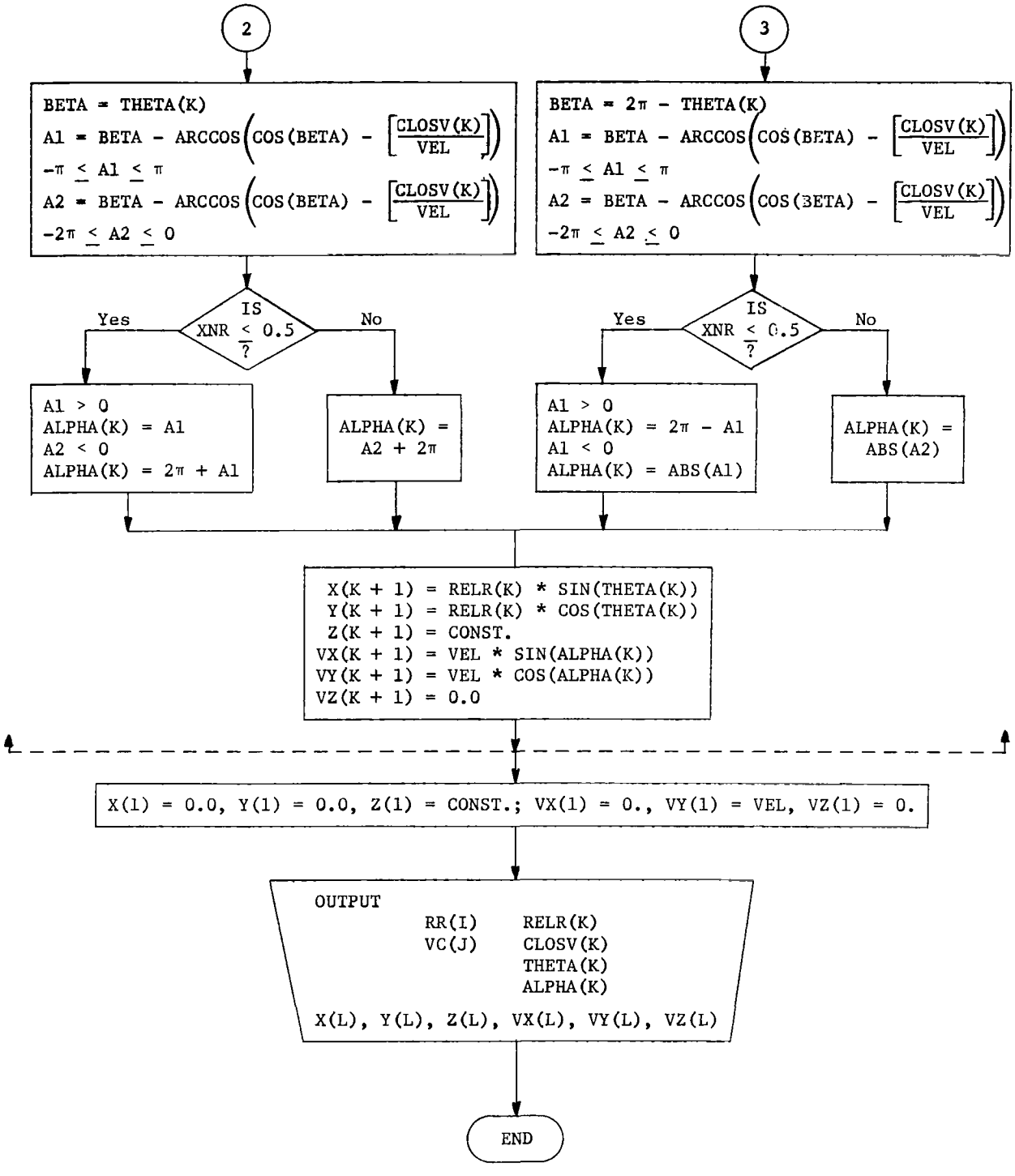


Fig. E-1. Concluded.

VC(J) = vector of 50 ordered closing velocities where VC(1) = -490 knots and VC(50) = +490 knots

VCX(I,J) = vector of probability weights representing discretized conditional probability density $f(\dot{R}|R)$

VX(L) = X direction velocity of aircraft, $1 \leq L \leq N$

VY(L) = Y direction velocity of aircraft, $1 \leq L \leq N$

VZ(L) = Z direction velocity of aircraft, $1 \leq L \leq N$

X(L) = X coordinate of aircraft, $1 \leq L \leq N$

Y(L) = Y coordinate of aircraft, $1 \leq L \leq N$

Z(L) = Z coordinate of aircraft, $1 \leq L \leq N$

## II. Probability Functions Relevant to the Data Base Extension

This model makes use of three probability density functions. The functions $f(R)$, density of relative ranges between pairs of aircraft, and $f(\dot{R}|R)$, density of closing velocity between pairs of aircraft conditioned on relative range between aircraft pairs, are taken from an heuristically determined joint density $f(\dot{R}|R)$. Under the assumption that all aircraft are flying at a constant velocity, a density function $f(\theta|\dot{R})$, where $\theta$ is bearing angle from one aircraft to the other of the pair, has been analytically determined. Given a closing velocity $\dot{R}$ and a bearing angle $\theta$, the heading of the second aircraft relative to the first in a given aircraft pair can have at most two possible values. The following paragraphs describe the statistics used in the simulation model.

Using procedures developed in analyzing the data which have been presented in the Phase I report [Ref. 3], the joint probability density function of relative range and closing velocity between randomly selected pairs of aircraft $f(R,\dot{R})$ has been obtained. A normalized version of this density function, where

$$\int_R \int_{\dot{R}} f(R,\dot{R})\, dR d\dot{R} = 1 \qquad \text{(E-1)}$$

is determined. This joint density $f(R,\dot{R})$ can then be factored into the marginal density $f(R)$ and the conditional density $f(\dot{R}|R)$ according to Bayes theorem.

Under the constraint that all aircraft are at constant velocity V with

constant altitude A, there are only certain values that azimuth from ownship to any aircraft , $\theta$, can assume. This is illustrated in Fig. E-2. Note that in Fig. E-2b, for any given value of $\theta$, $\dot{R}_{min} \leq \dot{R} \leq \dot{R}_{max}$. For $\dot{R} \geq 0$, $0 \leq \theta \leq \theta_2$ or $\theta_3 \leq \theta \leq 360$ where $\theta_2$ and $\theta_3$ are determined from the $\dot{R}_{max}(\theta)$ curve. Note

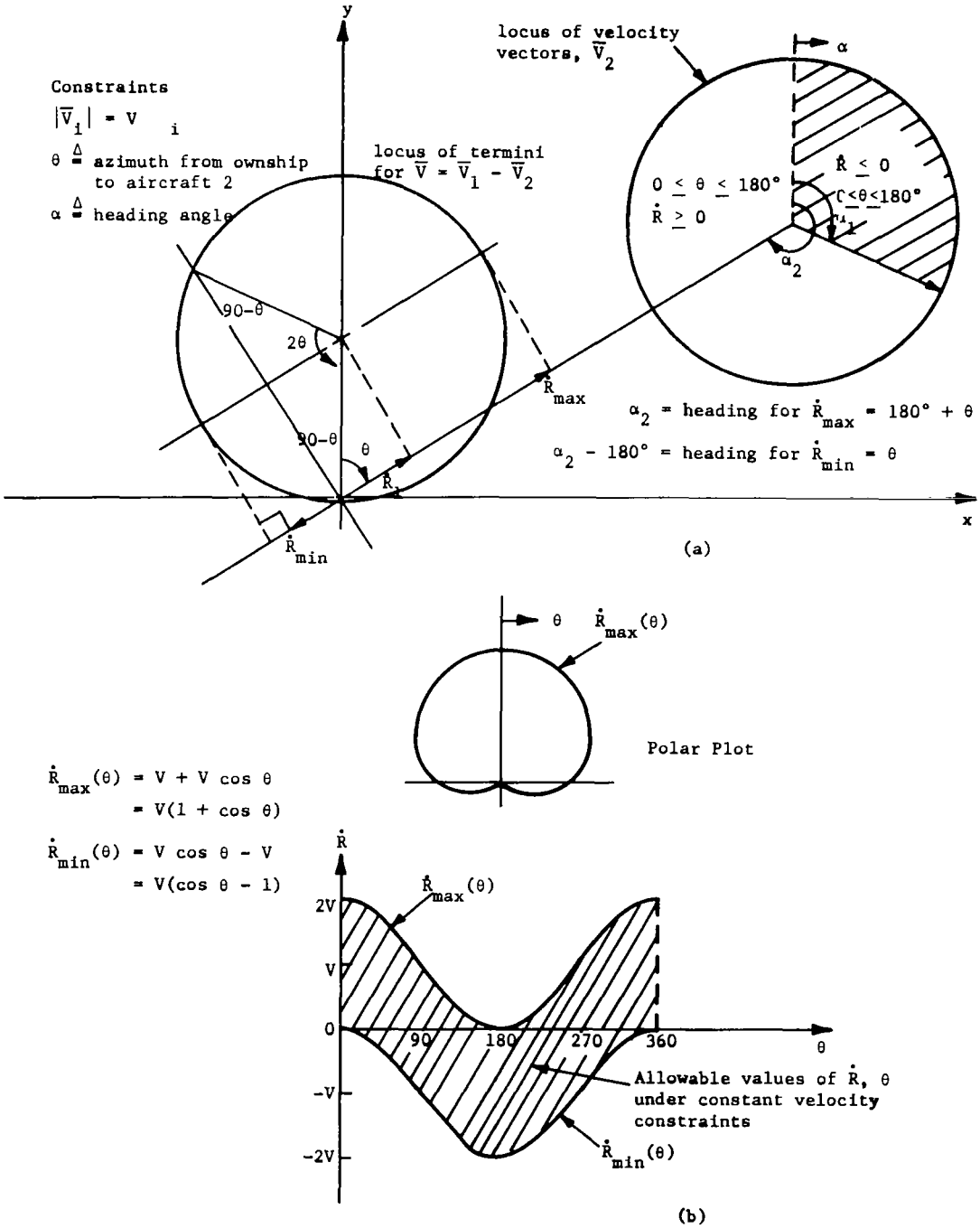


Fig. E-2. Relationship between range rate and azimuth under constant velocity constraint.

that $\theta_1 = \theta_4 = 180^\circ$ for $\dot{R} = -2V$. It is assumed that conditional to a particular value of $\dot{R}$ the probability density function of $\theta$ is evenly distributed over the range of possible values.

$$f(\theta|\dot{R}) = \left\{ \begin{array}{l} \frac{1}{2(\theta_2)} \quad ; 0 \quad \theta \quad \theta_2; \dot{R} \quad 0 \\ \frac{1}{2(2\pi - \theta_3)} \quad ; \theta_3 \quad \theta \quad 2\pi; \dot{R} \quad 0 \\ \frac{1}{(\theta_4 - \theta_1)} \quad ; \theta_1 \quad \theta \quad \theta_4; \dot{R} \quad 0 \end{array} \right\}$$

and is plotted in Fig. E-3.

For each set of values $(\dot{R},\theta)$ there are two possible values that the heading angle $\alpha$ can assume. Consider Fig. E-4 for $0 \leq \theta \leq 180^\circ$. It can be seen that

$$\dot{R} = \dot{R}_1 + \dot{R}_2 \quad \text{or} \quad \dot{R}_2 = \dot{R} - V \cos \theta$$

under the constant velocity constraint. Also from Fig. E-4,

$$\dot{R}_2 = V \cos \beta \quad \text{where} \quad \beta = \theta + (180^\circ - \alpha) = 180^\circ - (\alpha - \theta)$$

or

$$R_2 = -V \cos (\alpha - \theta).$$

Then,

$$\alpha = \theta + \cos^{-1} \left\{ \cos \theta - \frac{\dot{R}}{V} \right\} . \qquad \text{(E-2)}$$

Equation (E-2) has two solutions, $\alpha = \alpha_1$ or $\alpha = \alpha_2$.

Similarly, for $\pi \leq \theta \leq 2\pi$ from Fig. E-5, where $\theta' = 2\pi - \theta$,

$$\dot{R} = \dot{R}_1 + \dot{R}_2 \quad \text{or} \quad \dot{R}_2 = \dot{R} - V \cos \theta'$$

and

$$\dot{R}_2 = V \cos (\theta' + (180^\circ - \alpha'))$$

and

$$\alpha' = \theta' + \cos^{-1} \left\{ \cos \theta' - \frac{\dot{R}}{V} \right\} . \qquad \text{(E-3)}$$

Equation (E-3) has two solutions also:

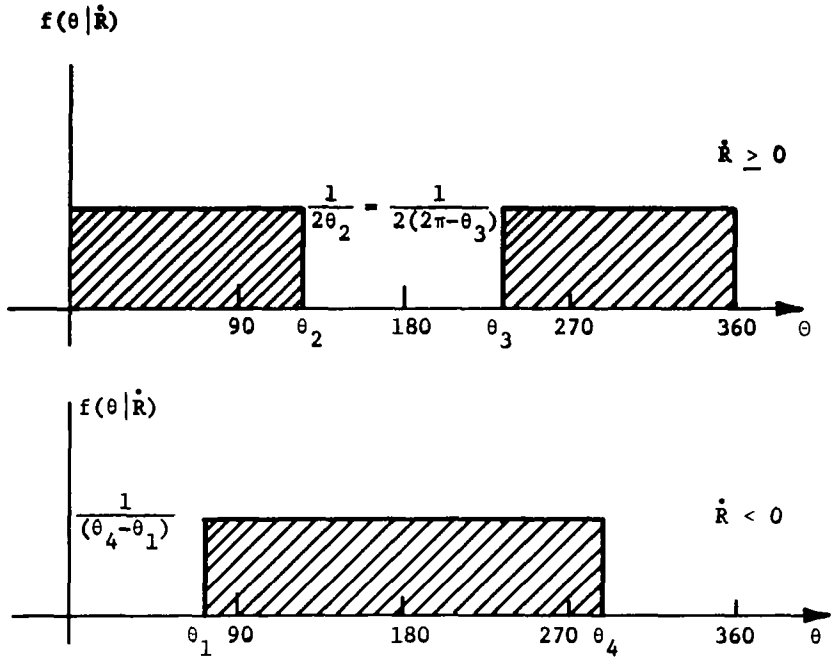


Fig. E-3. Conditional probability of observing an azimuth angle within the ranges shown.

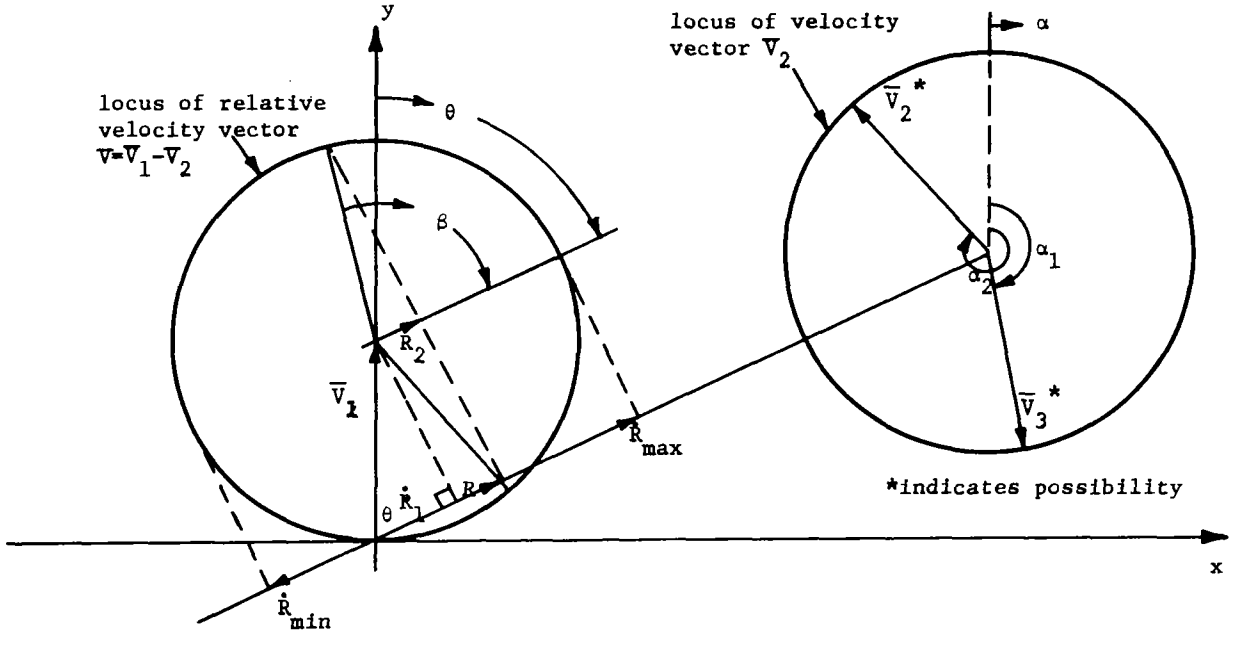


Fig. E-4. Relationship between closing velocity, $\dot{R}$, azimuth, $\theta$, and heading, $\alpha$, for $0 \leq \theta \leq \pi$.

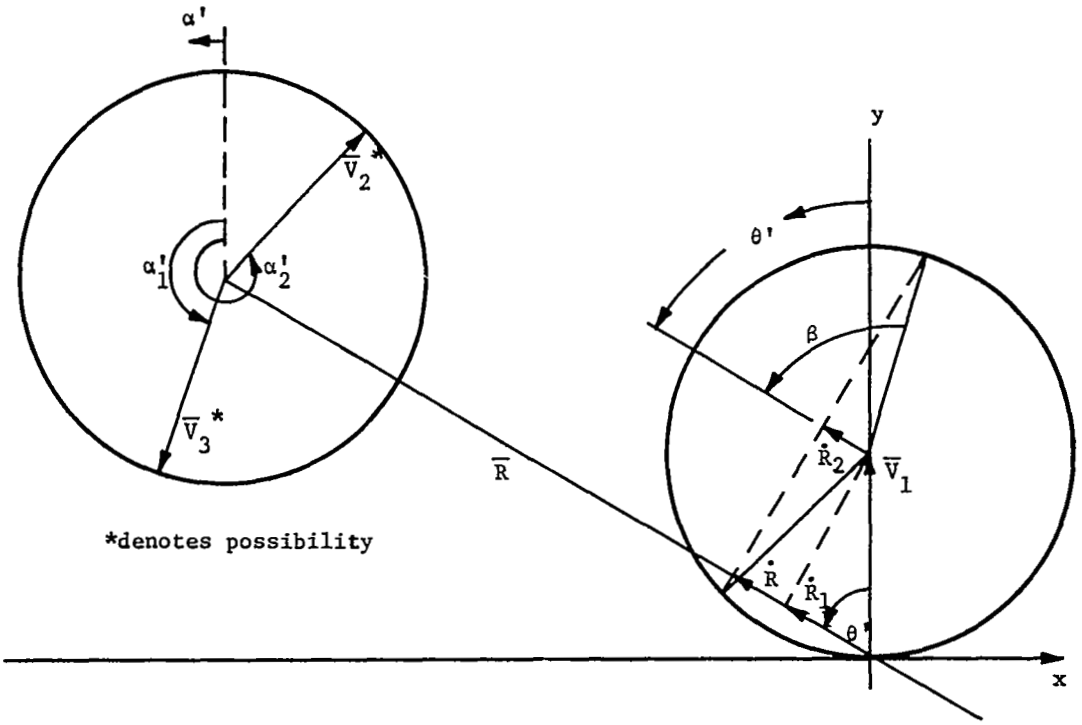


Fig. E-5. Relationship between closing velocity, $\dot{R}$, azimuth, $\theta$, and heading, $\alpha$, for $\pi \leq \theta \leq 2\pi$.

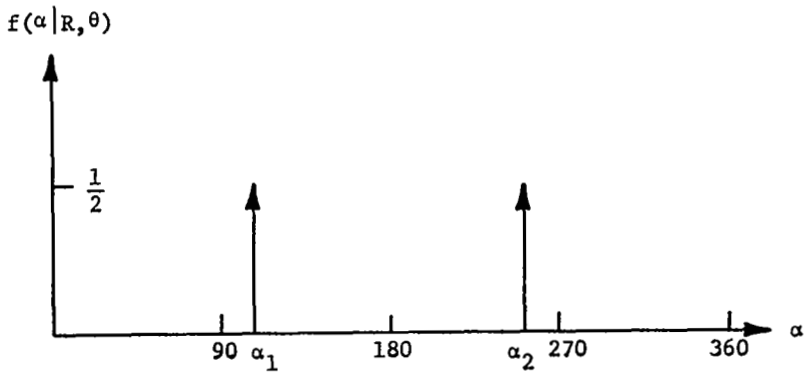


Fig. E-6. Conditional probability of heading angle, $\alpha$.

$$\alpha = [360^{\circ} - \alpha_1'], \; [360^{\circ} - \alpha_2'].$$

Thus, each of the two values for $\alpha$ for a given pair $(R,\theta)$ will be considered equally likely, such that

$$f(\alpha|\dot{R},\theta) = \left\{ \begin{array}{ll} \frac{1}{2}\,\delta(\alpha - \alpha_1) + \frac{1}{2}\,\delta(\alpha - \alpha_2) & ;\; 0 \leq \theta \leq \pi \\ \frac{1}{2}\,\delta(\alpha - (2\pi - \alpha_1^1)) + \frac{1}{2}(\alpha - (2\pi - \alpha_2^1)); & \pi \leq \theta \leq 2\pi \end{array} \right\}$$

where $f(\alpha|\dot{R},\theta)$ is shown in Fig. E-6.

## APPENDIX F

## Two-Dimensional Probability Distributions from the Atlanta Data Base

### I. Two-Dimensional Distributions of the Percent of Time in an Encounter Status

For the approximate determination of the percent of time in an encounter status for an arbitrary protection region (such as a range-tau system) in the R, $\dot{R}$ plane, the two-dimensional distribution of Fig. F-1 has been calculated. The figure indicates the distribution of measurements of range and range rate to the closest closing aircraft from an arbitrary aircraft I, for all I, and for Hour 11 data. Thus, the histogram data, when divided by the total count, represents an estimate of the conditional probability

$$\text{Prob.}(R_k \leq R < R_{k+1} \text{ and } \dot{R}_k \leq \dot{R} < \dot{R}_{k+1} / \dot{R} > 0) \qquad \text{(F-1)}$$

where k = 0,1,2, . . . ,11, R is the relative range measurement, and $\dot{R}$ is the closing velocity measurement to the closest closing aircraft.

For estimation of an encounter probability, an approximate integration can be performed over the protection region defined by the system warning logic. For example, for a system operating on the threshold R < 2 n.mi. and $\dot{R} > 0$, we would not expect the fraction of flying time in an alarm status to exceed 1.9 percent under Hour 11 conditions. This number is the sum of the columns to the left of the R = 2 n.mi. line, converted into a percentage (see Fig. F-2).

Note that no other discrimination has been used in obtaining the data.

### II. Probability Density Functions of Relative Range and Closing Velocity Between Pairs of Aircraft.

As discussed in Section V.D., the Atlanta data base was extended using the techniques outlined in that section. The probability density

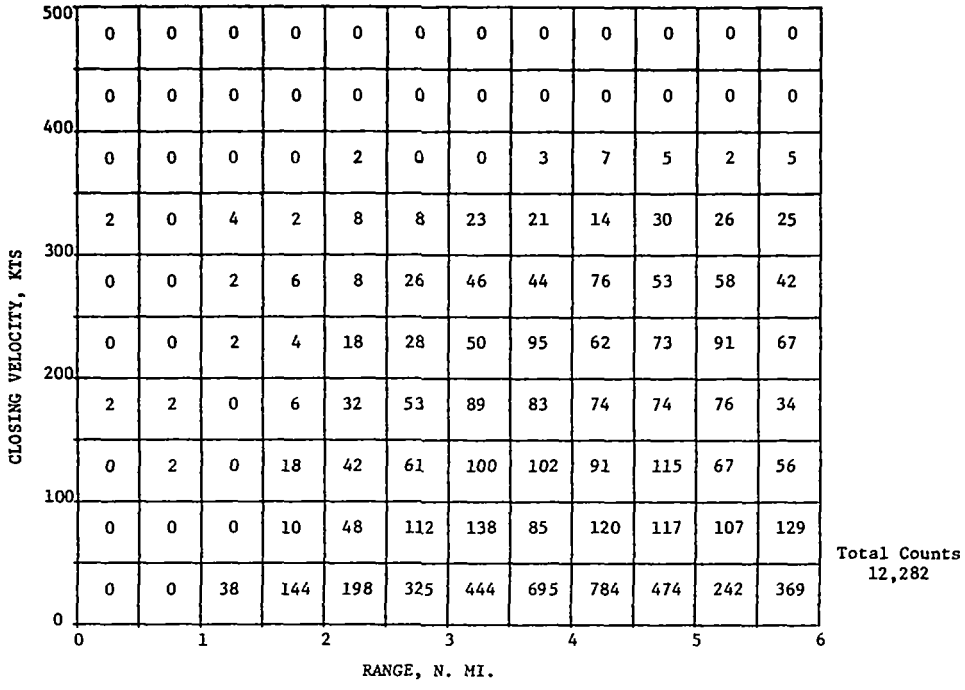


Fig. F-1. Two-dimensional distribution of counts of encounters with closest closing aircraft defined by $R_k \leq R < R_{k+1}$ and $\dot{R}_k \leq \dot{R} < \dot{R}_{k+1}$. (Hour 11 data) Additional discrimination: none.

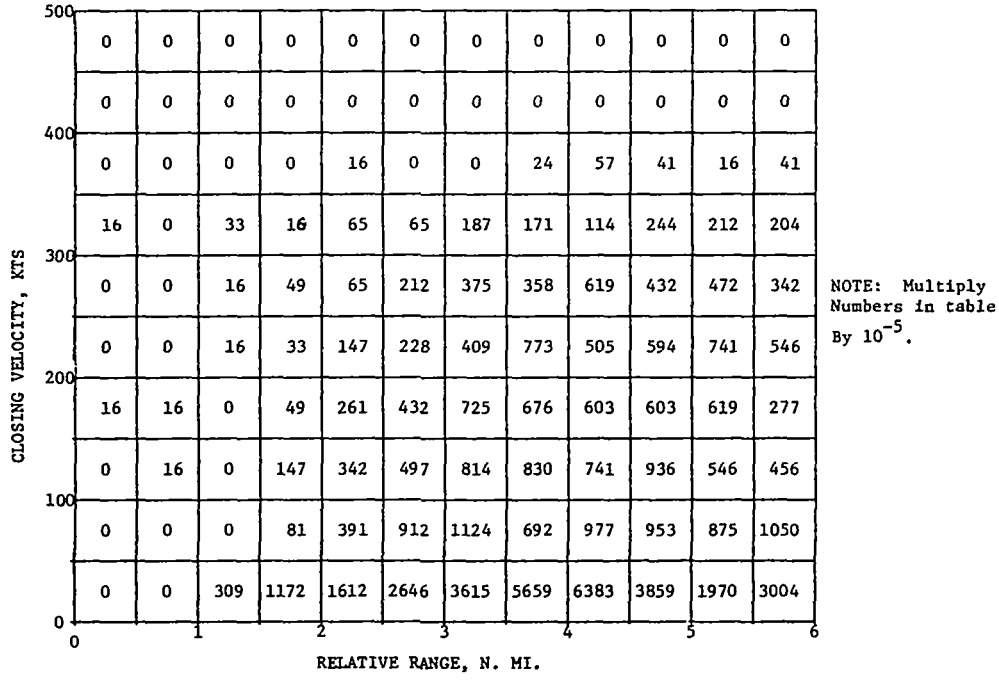


Fig. F-2. Joint probability of observing a value of range, $R_k \leq R < R_{k+1}$ and a value of closing velocity, $\dot{R}_k \leq \dot{R} < \dot{R}_{k+1}$ (to the closest closing aircraft) under Hour 11 conditions. Additional discrimination: none.

function used to extend the data was the joint distribution of relative range and closing velocity between pairs of aircraft in Hour 11 of the data base.

Figure F-3 shows a sketch of portions of this two-dimensional distribution. Figure F-4 plots the marginal probability density of relative range between pairs of aircraft, and Figure F-5 plots the marginal density function of closing velocity. The closing velocity curve is skewed towards positive values of closing velocity because arrivals outnumbered departures in the data base. Thus, most of the aircraft in the data were converging rather than diverging.

The relative range distribution reflects the separation standards used in the terminal area as well as the total area covered by the data base.

Computer printouts of the joint density function of range and velocity between pairs of aircraft are given in Fig. F-6.

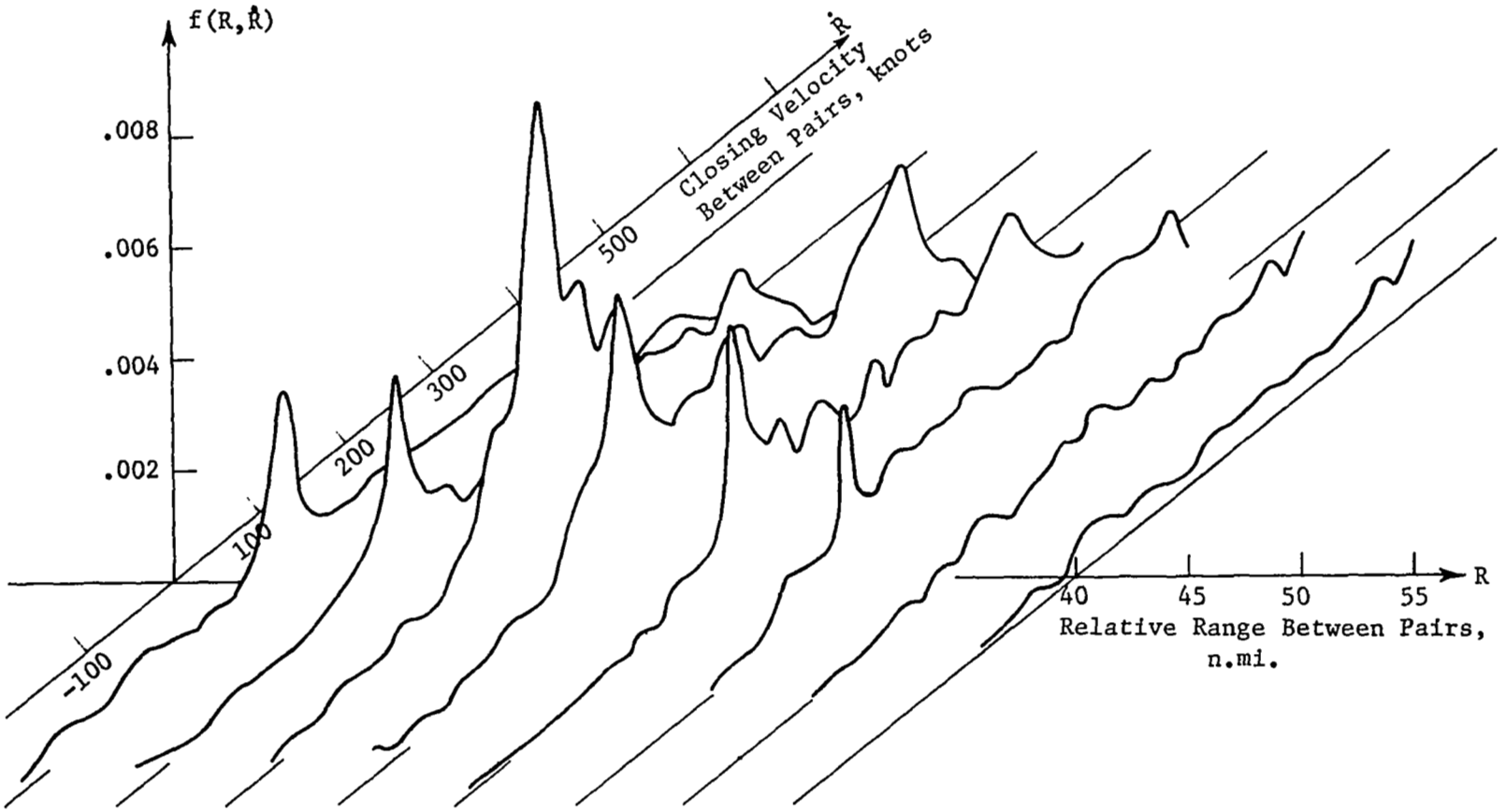


Fig. F-3. Sketch of various cross-sections of the joint probability density of relative range and closing velocity between pairs of aircraft.

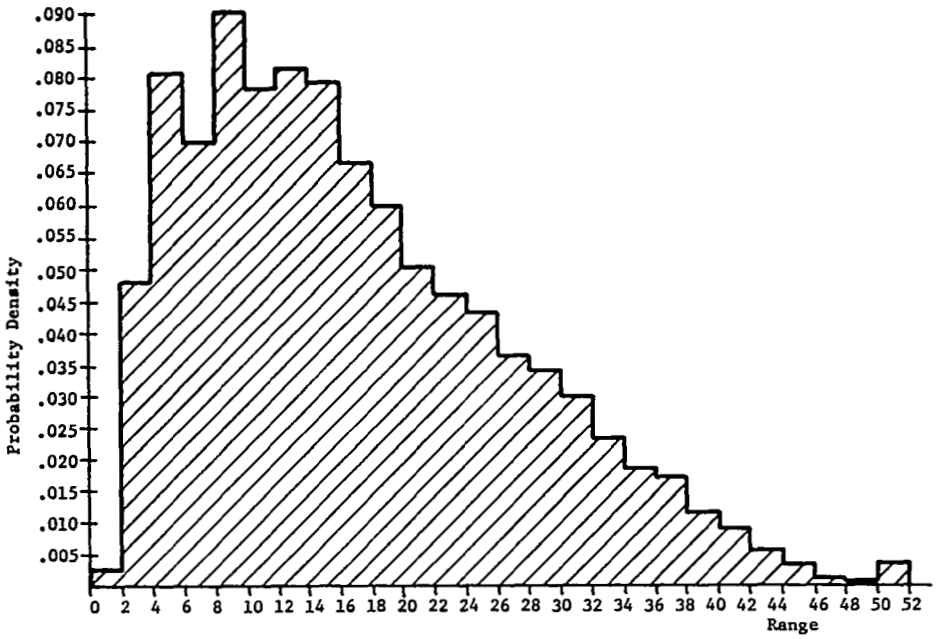


Fig. F-4. Marginal probability density function of relative range between pairs of aircraft.

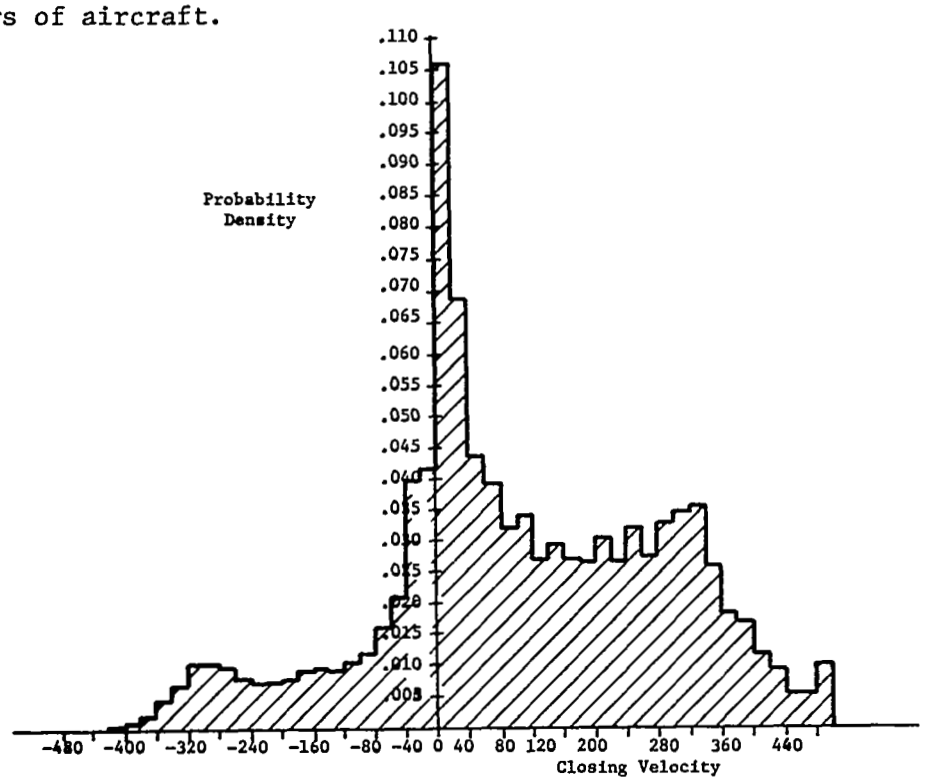


Fig. F-5. Marginal probability density function of closing velocity between pairs of aircraft.

JOINT DISTRIBUTION OF RANGE AND CLOSING VELOCITY FOR HOUR479

RANGE (NM)

| VC (KNTS) | .5 | 1.0 | 1.5 | 2.0 | 2.5 | 3.0 | 3.5 | 4.0 | 4.5 | 5.0 |
|---|---|---|---|---|---|---|---|---|---|---|
| -500 - -480 | 0 | 0 | 0 | 0 | 0 | 0 | 0 | 0 | 0 | 0 |
| -480 - -460 | 0 | 0 | 0 | 0 | 0 | 0 | 0 | 0 | 0 | 0 |
| -460 - -440 | 0 | 0 | 0 | 0 | 0 | 0 | 0 | 0 | 0 | 0 |
| -440 - -420 | 0 | 0 | 0 | 0 | 0 | 0 | 0 | 0 | 0 | 0 |
| -420 - -400 | 0 | 0 | 0 | 0 | 0 | 0 | 0 | 0 | 0 | 0 |
| -400 - -380 | 0 | 0 | 0 | 0 | 0 | 0 | 0 | 0 | 0 | 2 |
| -380 - -360 | 0 | 0 | 0 | 0 | 0 | 0 | 0 | 0 | 2 | 0 |
| -360 - -340 | 0 | 0 | 0 | 2 | 2 | 2 | 0 | 0 | 2 | 2 |
| -340 - -320 | 0 | 0 | 2 | 0 | 0 | 4 | 2 | 2 | 6 | 8 |
| -320 - -300 | 0 | 0 | 0 | 0 | 0 | 0 | 4 | 10 | 18 | 26 |
| -300 - -280 | 0 | 0 | 2 | 0 | 2 | 2 | 4 | 30 | 24 | 36 |
| -280 - -260 | 0 | 0 | 0 | 0 | 2 | 4 | 26 | 24 | 54 | 60 |
| -260 - -240 | 0 | 0 | 0 | 0 | 2 | 8 | 22 | 26 | 52 | 80 |
| -240 - -220 | 0 | 0 | 0 | 0 | 2 | 18 | 16 | 52 | 62 | 72 |
| 220 - -200 | 0 | 2 | 0 | 2 | 2 | 28 | 34 | 66 | 58 | 52 |
| -200 - -180 | 0 | 0 | 0 | 0 | 10 | 12 | 36 | 74 | 84 | 48 |
| -180 - -160 | 0 | 0 | 0 | 0 | 20 | 34 | 82 | 90 | 62 | 82 |
| -160 - -140 | 0 | 0 | 2 | 4 | 16 | 36 | 62 | 100 | 64 | 118 |
| -140 - -120 | 0 | 0 | 0 | 2 | 22 | 44 | 80 | 78 | 90 | 94 |
| 120 - -100 | 0 | 0 | 0 | 4 | 26 | 50 | 96 | 108 | 64 | 74 |
| -100 - -80 | 0 | 0 | 0 | 6 | 18 | 46 | 66 | 118 | 80 | 60 |
| -80 - -60 | 0 | 2 | 0 | 10 | 26 | 72 | 64 | 92 | 88 | 82 |
| -60 - -40 | 0 | 0 | 2 | 10 | 36 | 80 | 60 | 80 | 110 | 60 |
| -40 - -20 | 0 | 0 | 2 | 24 | 66 | 110 | 176 | 130 | 230 | 98 |
| -20 - 0 | 0 | 0 | 2 | 32 | 56 | 92 | 86 | 208 | 300 | 252 |
| 0 - 20 | 0 | 0 | 10 | 96 | 172 | 312 | 366 | 322 | 994 | 540 |
| 20 - 40 | 0 | 0 | 30 | 60 | 78 | 116 | 172 | 374 | 302 | 200 |
| 40 - 60 | 0 | 0 | 0 | 10 | 38 | 72 | 100 | 92 | 86 | 104 |
| 60 - 80 | 0 | 0 | 0 | 2 | 20 | 64 | 58 | 46 | 108 | 86 |
| 80 - 100 | 0 | 0 | 0 | 10 | 20 | 44 | 68 | 54 | 70 | 72 |
| 100 - 120 | 0 | 2 | 0 | 2 | 22 | 28 | 54 | 58 | 78 | 98 |
| 120 - 140 | 0 | 0 | 0 | 0 | 10 | 30 | 46 | 72 | 66 | 90 |
| 140 - 160 | 0 | 2 | 0 | 4 | 22 | 26 | 46 | 52 | 68 | 92 |
| 160 - 180 | 0 | 0 | 0 | 0 | 6 | 26 | 54 | 52 | 60 | 72 |
| 180 - 200 | 0 | 0 | 0 | 4 | 12 | 24 | 54 | 54 | 42 | 70 |
| 200 - 220 | 0 | 0 | 0 | 0 | 10 | 14 | 26 | 82 | 70 | 70 |
| 220 - 240 | 0 | 0 | 0 | 2 | 2 | 12 | 36 | 60 | 60 | 82 |
| 240 - 260 | 0 | 0 | 4 | 2 | 0 | 8 | 20 | 64 | 76 | 80 |
| 260 - 280 | 0 | 0 | 0 | 0 | 6 | 12 | 16 | 28 | 74 | 76 |
| 280 - 300 | 0 | 0 | 0 | 2 | 4 | 14 | 22 | 12 | 34 | 74 |
| 300 - 320 | 0 | 0 | 2 | 2 | 4 | 8 | 14 | 16 | 30 | 52 |
| 320 - 340 | 0 | 0 | 2 | 0 | 0 | 0 | 4 | 14 | 18 | 22 |
| 340 - 360 | 0 | 0 | 0 | 2 | 0 | 0 | 2 | 2 | 12 | 12 |
| 360 - 380 | 0 | 0 | 0 | 0 | 4 | 0 | 2 | 4 | 0 | 10 |
| 380 - 400 | 0 | 0 | 0 | 0 | 0 | 2 | 0 | 0 | 2 | 2 |
| 400 - 420 | 0 | 0 | 0 | 0 | 0 | 0 | 0 | 0 | 0 | 0 |
| 420 - 440 | 0 | 0 | 0 | 0 | 0 | 0 | 0 | 0 | 0 | 0 |
| 440 - 460 | 0 | 0 | 0 | 0 | 0 | 0 | 0 | 0 | 0 | 0 |
| 460 - 480 | 0 | 0 | 0 | 0 | 0 | 0 | 0 | 0 | 0 | 0 |
| 480 - 500 | 0 | 0 | 0 | 0 | 0 | 0 | 0 | 0 | 0 | 0 |

Fig. F-6. Joint density function of range and velocity.

JOINT DISTRIBUTION OF RANGE AND CLOSING VELOCITY FOR HOUR479

| | RANGE (NM) | | | | | | | | | |
|---|---|---|---|---|---|---|---|---|---|---|
| | 5.5 | 6.0 | 6.5 | 7.0 | 7.5 | 8.0 | 8.5 | 9.0 | 9.5 | 10.0 |
| VC (KNTS) | | | | | | | | | | |
| -500 - -480 | 0 | 0 | 0 | 0 | 0 | 0 | 0 | 0 | 0 | 0 |
| -480 - -460 | 0 | 0 | 0 | 0 | 0 | 0 | 0 | 0 | 0 | 0 |
| -460 - -440 | 0 | 0 | 0 | 0 | 0 | 0 | 0 | 0 | 0 | 0 |
| -440 - -420 | 0 | 0 | 0 | 0 | 0 | 0 | 0 | 0 | 0 | 0 |
| -420 - -400 | 0 | 0 | 0 | 0 | 0 | 0 | 0 | 2 | 0 | 2 |
| -400 - -380 | 2 | 2 | 2 | 4 | 0 | 2 | 0 | 0 | 4 | 0 |
| -380 - -360 | 4 | 0 | 0 | 2 | 6 | 4 | 8 | 4 | 6 | 8 |
| -360 - -340 | 10 | 8 | 4 | 8 | 8 | 16 | 20 | 20 | 20 | 36 |
| -340 - -320 | 20 | 24 | 24 | 40 | 36 | 48 | 36 | 42 | 42 | 52 |
| -320 - -300 | 30 | 36 | 68 | 62 | 76 | 80 | 98 | 112 | 94 | 66 |
| -300 - -280 | 58 | 88 | 102 | 90 | 122 | 116 | 86 | 86 | 72 | 68 |
| -280 - -260 | 90 | 72 | 84 | 102 | 76 | 88 | 94 | 50 | 44 | 46 |
| -260 - -240 | 76 | 72 | 54 | 92 | 78 | 40 | 38 | 54 | 30 | 28 |
| -240 - -220 | 58 | 70 | 92 | 44 | 38 | 52 | 36 | 30 | 20 | 24 |
| -220 - -200 | 56 | 110 | 60 | 50 | 38 | 28 | 26 | 36 | 28 | 10 |
| -200 - -180 | 92 | 44 | 54 | 54 | 38 | 28 | 22 | 18 | 18 | 34 |
| -180 - -160 | 70 | 68 | 38 | 20 | 8 | 24 | 26 | 26 | 32 | 52 |
| -160 - -140 | 50 | 36 | 44 | 40 | 34 | 26 | 30 | 34 | 46 | 20 |
| -140 - -120 | 50 | 28 | 30 | 42 | 44 | 24 | 12 | 20 | 42 | 50 |
| 120 - -100 | 54 | 38 | 40 | 32 | 22 | 26 | 34 | 48 | 44 | 38 |
| -100 - -80 | 64 | 26 | 34 | 22 | 28 | 12 | 20 | 78 | 58 | 52 |
| -80 - -60 | 74 | 52 | 28 | 30 | 42 | 24 | 64 | 84 | 60 | 72 |
| -60 - -40 | 90 | 100 | 44 | 46 | 46 | 56 | 64 | 86 | 96 | 100 |
| -40 - -20 | 144 | 224 | 134 | 198 | 82 | 112 | 162 | 276 | 236 | 132 |
| -20 - 0 | 154 | 124 | 74 | 104 | 134 | 152 | 144 | 206 | 140 | 202 |
| 0 - 20 | 272 | 362 | 280 | 342 | 330 | 404 | 340 | 598 | 926 | 574 |
| 20 - 40 | 126 | 158 | 202 | 222 | 128 | 252 | 308 | 414 | 322 | 276 |
| 40 - 60 | 128 | 114 | 82 | 76 | 82 | 108 | 176 | 202 | 216 | 172 |
| 60 - 80 | 98 | 92 | 104 | 88 | 62 | 58 | 118 | 118 | 120 | 156 |
| 80 - 100 | 48 | 58 | 72 | 58 | 74 | 70 | 86 | 72 | 94 | 66 |
| 100 - 120 | 72 | 80 | 66 | 70 | 70 | 56 | 92 | 108 | 84 | 96 |
| 120 - 140 | 58 | 42 | 42 | 54 | 74 | 64 | 46 | 48 | 66 | 58 |
| 140 - 160 | 70 | 60 | 40 | 34 | 52 | 60 | 64 | 56 | 44 | 60 |
| 160 - 180 | 52 | 56 | 50 | 46 | 54 | 62 | 72 | 64 | 52 | 60 |
| 180 - 200 | 84 | 84 | 66 | 46 | 42 | 52 | 48 | 74 | 70 | 48 |
| 200 - 220 | 96 | 96 | 82 | 60 | 30 | 36 | 44 | 72 | 92 | 108 |
| 220 - 240 | 84 | 94 | 102 | 96 | 84 | 70 | 80 | 82 | 90 | 104 |
| 240 - 260 | 102 | 124 | 138 | 124 | 110 | 90 | 84 | 74 | 88 | 98 |
| 260 - 280 | 76 | 78 | 86 | 128 | 132 | 92 | 100 | 88 | 94 | 92 |
| 280 - 300 | 94 | 92 | 96 | 82 | 100 | 124 | 102 | 98 | 102 | 86 |
| 300 - 320 | 68 | 64 | 80 | 82 | 90 | 118 | 120 | 124 | 112 | 114 |
| 320 - 340 | 40 | 64 | 62 | 82 | 104 | 100 | 92 | 78 | 80 | 110 |
| 340 - 360 | 12 | 16 | 30 | 34 | 32 | 22 | 52 | 68 | 66 | 70 |
| 360 - 380 | 4 | 4 | 4 | 9 | 20 | 20 | 22 | 20 | 24 | 30 |
| 380 - 400 | 2 | 8 | 4 | 12 | 8 | 10 | 8 | 16 | 18 | 8 |
| 400 - 420 | 0 | 2 | 2 | 3 | 0 | 2 | 2 | 4 | 6 | 4 |
| 420 - 440 | 0 | 0 | 0 | 0 | 0 | 0 | 2 | 2 | 2 | 4 |
| 440 - 460 | 0 | 0 | 0 | 0 | 0 | 0 | 0 | 0 | 0 | 0 |
| 460 - 480 | 0 | 0 | 0 | 3 | 0 | 0 | 0 | 0 | 2 | 2 |
| 480 - 500 | 0 | 0 | 0 | 0 | 0 | 0 | 0 | 0 | 0 | 0 |

Fig. F-6. Continued.

JOINT DISTRIBUTION OF RANGE AND CLOSING VELOCITY FOR HOUR479

RANGE (NM)

| VC (KNTS) | 12.0 | 14.0 | 16.0 | 18.0 | 20.0 | 22.0 | 24.0 | 26.0 | 28.0 | 30.0 |
|---|---|---|---|---|---|---|---|---|---|---|
| -500 - -480 | 0 | 0 | 0 | 0 | 0 | 0 | 0 | 0 | 0 | 0 |
| -480 - -460 | 0 | 0 | 0 | 0 | 0 | 0 | 0 | 0 | 0 | 0 |
| -460 - -440 | 0 | 0 | 2 | 0 | 2 | 0 | 0 | 0 | 0 | 0 |
| -440 - -420 | 0 | 0 | 8 | 6 | 4 | 2 | 0 | 0 | 0 | 0 |
| -420 - -400 | 4 | 4 | 12 | 16 | 12 | 2 | 0 | 0 | 0 | 0 |
| -400 - -380 | 22 | 18 | 42 | 14 | 14 | 4 | 6 | 0 | 2 | 0 |
| -380 - -360 | 38 | 60 | 32 | 30 | 14 | 10 | 8 | 12 | 0 | 0 |
| -360 - -340 | 96 | 96 | 124 | 92 | 30 | 34 | 30 | 10 | 0 | 2 |
| -340 - -320 | 206 | 182 | 90 | 62 | 28 | 46 | 26 | 20 | 14 | 8 |
| -320 - -300 | 290 | 168 | 112 | 104 | 88 | 38 | 18 | 10 | 6 | 2 |
| -300 - -280 | 220 | 100 | 70 | 88 | 70 | 26 | 24 | 4 | 2 | 0 |
| -280 - -260 | 116 | 136 | 98 | 62 | 68 | 40 | 4 | 8 | 8 | 0 |
| -260 - -240 | 110 | 118 | 92 | 52 | 36 | 26 | 8 | 6 | 6 | 2 |
| -240 - -220 | 82 | 110 | 82 | 64 | 38 | 26 | 14 | 14 | 2 | 0 |
| -220 - -200 | 78 | 82 | 116 | 52 | 46 | 48 | 38 | 8 | 4 | 4 |
| -200 - -180 | 102 | 136 | 124 | 68 | 32 | 52 | 10 | 4 | 4 | 0 |
| -180 - -160 | 134 | 160 | 104 | 74 | 72 | 50 | 24 | 12 | 6 | 4 |
| -160 - -140 | 144 | 140 | 114 | 88 | 74 | 56 | 34 | 26 | 2 | 0 |
| -140 - -120 | 98 | 126 | 162 | 80 | 82 | 54 | 24 | 16 | 6 | 16 |
| -120 - -100 | 126 | 168 | 136 | 92 | 122 | 66 | 52 | 42 | 4 | 8 |
| -100 - -80 | 194 | 210 | 142 | 138 | 106 | 104 | 44 | 42 | 54 | 22 |
| -80 - -60 | 228 | 298 | 216 | 310 | 116 | 100 | 58 | 40 | 68 | 72 |
| -60 - -40 | 302 | 288 | 276 | 228 | 208 | 160 | 176 | 106 | 70 | 128 |
| -40 - -20 | 596 | 498 | 506 | 404 | 332 | 286 | 294 | 114 | 116 | 112 |
| -20 - 0 | 586 | 586 | 520 | 474 | 406 | 322 | 302 | 138 | 152 | 132 |
| 0 - 20 | 1352 | 1272 | 1134 | 864 | 800 | 490 | 432 | 716 | 314 | 492 |
| 20 - 40 | 948 | 1148 | 1276 | 742 | 568 | 360 | 496 | 408 | 240 | 194 |
| 40 - 60 | 770 | 848 | 706 | 414 | 388 | 308 | 352 | 308 | 190 | 182 |
| 60 - 80 | 538 | 680 | 730 | 414 | 314 | 364 | 252 | 324 | 246 | 234 |
| 80 - 100 | 406 | 434 | 490 | 432 | 350 | 326 | 290 | 192 | 312 | 206 |
| 100 - 120 | 348 | 466 | 582 | 392 | 342 | 314 | 300 | 300 | 266 | 216 |
| 120 - 140 | 244 | 288 | 358 | 366 | 412 | 222 | 214 | 224 | 162 | 210 |
| 140 - 160 | 274 | 360 | 344 | 400 | 438 | 284 | 170 | 180 | 254 | 242 |
| 160 - 180 | 224 | 306 | 354 | 248 | 298 | 234 | 254 | 290 | 276 | 220 |
| 180 - 200 | 340 | 292 | 304 | 302 | 316 | 264 | 230 | 184 | 222 | 172 |
| 200 - 220 | 326 | 362 | 382 | 430 | 314 | 372 | 262 | 260 | 192 | 182 |
| 220 - 240 | 350 | 400 | 286 | 258 | 244 | 212 | 200 | 250 | 186 | 162 |
| 240 - 260 | 356 | 376 | 354 | 392 | 234 | 248 | 296 | 298 | 312 | 188 |
| 260 - 280 | 374 | 256 | 304 | 320 | 324 | 252 | 194 | 220 | 218 | 156 |
| 280 - 300 | 408 | 408 | 336 | 398 | 408 | 318 | 314 | 278 | 270 | 224 |
| 300 - 320 | 390 | 380 | 398 | 370 | 436 | 420 | 418 | 342 | 242 | 252 |
| 320 - 340 | 388 | 368 | 302 | 456 | 520 | 506 | 392 | 380 | 284 | 260 |
| 340 - 360 | 258 | 214 | 240 | 264 | 298 | 302 | 322 | 278 | 256 | 226 |
| 360 - 380 | 136 | 146 | 180 | 196 | 166 | 212 | 230 | 192 | 230 | 222 |
| 380 - 400 | 50 | 88 | 80 | 88 | 148 | 154 | 120 | 150 | 236 | 272 |
| 400 - 420 | 22 | 48 | 72 | 40 | 50 | 92 | 136 | 148 | 144 | 128 |
| 420 - 440 | 20 | 16 | 42 | 28 | 44 | 54 | 90 | 118 | 100 | 94 |
| 440 - 460 | 6 | 16 | 4 | 36 | 24 | 8 | 34 | 56 | 58 | 90 |
| 460 - 480 | 6 | 6 | 24 | 20 | 8 | 34 | 30 | 46 | 44 | 40 |
| 480 - 500 | 2 | 16 | 22 | 10 | 24 | 36 | 54 | 64 | 56 | 86 |

Fig. F-6. Continued.

JOINT DISTRIBUTION OF RANGE AND CLOSING VELOCITY FOR HOUR479

| | RANGE (NM) | | | | | | | | | |
|---|---|---|---|---|---|---|---|---|---|---|
| VC (KNTS) | 32.0 | 34.0 | 36.0 | 38.0 | 40.0 | 42.0 | 44.0 | 46.0 | 48.0 | 50.0 | UP |
| -500 - -480 | 0 | 0 | 0 | 0 | 0 | 0 | 0 | 0 | 0 | 0 | 0 |
| -480 - -460 | 0 | 0 | 0 | 0 | 0 | 0 | 0 | 0 | 0 | 0 | 0 |
| -460 - -440 | 0 | 0 | 0 | 0 | 0 | 0 | 0 | 0 | 0 | 0 | 0 |
| -440 - -420 | 0 | 0 | 0 | 4 | 0 | 0 | 0 | 0 | 0 | 0 | 0 |
| -420 - -400 | 0 | 0 | 0 | 0 | 0 | 0 | 0 | 0 | 0 | 0 | 0 |
| -400 - -380 | 0 | 0 | 4 | 6 | 6 | 0 | 0 | 0 | 0 | 0 | 0 |
| -380 - -360 | 2 | 2 | 0 | 0 | 0 | 0 | 0 | 0 | 0 | 0 | 0 |
| 360 - -340 | 10 | 10 | 12 | 2 | 4 | 0 | 0 | 0 | 0 | 0 | 0 |
| -340 - -320 | 4 | 8 | 8 | 6 | 0 | 0 | 0 | 0 | 0 | 0 | 0 |
| -320 - -300 | 4 | 2 | 2 | 4 | 4 | 0 | 0 | 0 | 0 | 0 | 0 |
| -300 - -280 | 2 | 2 | 2 | 0 | 4 | 0 | 0 | 0 | 0 | 0 | 0 |
| -280 - -260 | 2 | 2 | 4 | 0 | 0 | 2 | 0 | 0 | 0 | 0 | 0 |
| -260 - -240 | 2 | 2 | 0 | 0 | 2 | 4 | 0 | 0 | 0 | 0 | 0 |
| -240 - -220 | 2 | 2 | 2 | 2 | 2 | 0 | 0 | 0 | 0 | 0 | 0 |
| -220 - -200 | 0 | 0 | 2 | 0 | 2 | 4 | 0 | 0 | 0 | 0 | 0 |
| -200 - -180 | 0 | 6 | 2 | 2 | 0 | 0 | 0 | 0 | 0 | 0 | 0 |
| -180 - -160 | 0 | 8 | 4 | 8 | 4 | 12 | 0 | 0 | 0 | 0 | 0 |
| -160 - -140 | 0 | 6 | 2 | 0 | 2 | 0 | 0 | 0 | 0 | 0 | 0 |
| -140 - -120 | 2 | 12 | 6 | 4 | 0 | 2 | 0 | 0 | 0 | 0 | 0 |
| -120 - -100 | 0 | 2 | 16 | 2 | 8 | 20 | 0 | 0 | 0 | 0 | 0 |
| -100 - -80 | 8 | 2 | 36 | 24 | 8 | 10 | 0 | 0 | 0 | 0 | 0 |
| -80 - -60 | 20 | 8 | 16 | 8 | 20 | 36 | 18 | 0 | 0 | 0 | 0 |
| -60 - -40 | 104 | 20 | 16 | 60 | 42 | 20 | 0 | 2 | 0 | 0 | 0 |
| -40 - -20 | 118 | 56 | 72 | 88 | 2 | 8 | 30 | 12 | 0 | 0 | 0 |
| -20 - 0 | 130 | 102 | 40 | 126 | 22 | 16 | 2 | 2 | 0 | 0 | 14 |
| 0 - 20 | 238 | 244 | 114 | 220 | 98 | 74 | 20 | 8 | 0 | 0 | 0 |
| 20 - 40 | 152 | 114 | 100 | 122 | 102 | 56 | 40 | 12 | 0 | 2 | 6 |
| 40 - 60 | 194 | 82 | 42 | 74 | 50 | 56 | 18 | 24 | 0 | 6 | 0 |
| 60 - 80 | 252 | 90 | 84 | 100 | 50 | 20 | 4 | 10 | 2 | 10 | 0 |
| 80 - 100 | 240 | 142 | 94 | 72 | 52 | 46 | 10 | 26 | 0 | 2 | 0 |
| 100 - 120 | 256 | 140 | 136 | 74 | 24 | 38 | 10 | 8 | 4 | 4 | 0 |
| 120 - 140 | 226 | 194 | 102 | 78 | 12 | 38 | 14 | 2 | 12 | 0 | 0 |
| 140 - 160 | 178 | 146 | 164 | 70 | 68 | 70 | 32 | 8 | 12 | 0 | 0 |
| 160 - 180 | 148 | 182 | 116 | 58 | 58 | 58 | 48 | 22 | 4 | 0 | 0 |
| 180 - 200 | 166 | 102 | 80 | 58 | 52 | 28 | 52 | 36 | 2 | 0 | 0 |
| 200 - 220 | 160 | 162 | 116 | 72 | 60 | 68 | 36 | 14 | 4 | 0 | 0 |
| 220 - 240 | 132 | 100 | 72 | 70 | 68 | 30 | 14 | 20 | 4 | 0 | 2 |
| 240 - 260 | 124 | 180 | 104 | 92 | 50 | 42 | 46 | 22 | 4 | 0 | 8 |
| 260 - 280 | 158 | 74 | 88 | 80 | 56 | 10 | 10 | 36 | 8 | 2 | 2 |
| 280 - 300 | 234 | 150 | 128 | 108 | 38 | 12 | 20 | 22 | 0 | 2 | 6 |
| 300 - 320 | 196 | 104 | 110 | 94 | 60 | 42 | 28 | 28 | 38 | 20 | 2 |
| 320 - 340 | 210 | 180 | 116 | 98 | 66 | 44 | 26 | 24 | 16 | 20 | 2 |
| 340 - 360 | 164 | 156 | 170 | 146 | 118 | 94 | 74 | 32 | 8 | 28 | 22 |
| 360 - 380 | 198 | 188 | 96 | 88 | 62 | 60 | 54 | 18 | 6 | 14 | 52 |
| 380 - 400 | 264 | 214 | 172 | 148 | 138 | 92 | 42 | 34 | 40 | 8 | 54 |
| 400 - 420 | 172 | 162 | 198 | 124 | 86 | 114 | 46 | 24 | 16 | 28 | 58 |
| 420 - 440 | 84 | 134 | 138 | 104 | 124 | 62 | 66 | 50 | 36 | 14 | 66 |
| 440 - 460 | 50 | 50 | 36 | 60 | 50 | 34 | 36 | 42 | 22 | 18 | 74 |
| 460 - 480 | 58 | 64 | 64 | 68 | 90 | 44 | 18 | 26 | 32 | 14 | 68 |
| 480 - 500 | 104 | 96 | 108 | 118 | 94 | 128 | 142 | 100 | 72 | 68 | 264 |

Fig. F-6. Concluded.

## REFERENCES


[1] Britt, C. L., et al.: Statistical Evaluation of Aircraft Collision-Hazard Warning System Techniques in the Terminal Area - Phase II. NASA CR-1470, Contract NAS1-7537, Research Triangle Institute, Research Triangle Park, NC, December 1969.

[2] Britt, C. L., et al.: Investigation of the Performance Characteristics of a Doppler Radar Technique for Aircraft Collision Hazard Warning. Contract NAS1-7537, Research Triangle Institute, Research Triangle Park, NC, Phase II Report, November 18, 1969. (Available as NASA CR-66894.)

[3] Britt, C. L. and J. H. Schrader: A Statistical Evaluation of Aircraft Collision-Hazard Warning System Techniques in the Terminal Area. IEEE Trans. on Aerospace and Electronic Systems, Vol. AES-6, No. 1, January 1970.

[4] Britt, C. L.: An Evaluation of Aircraft Collision-Hazard Warning Radar Techniques in the Terminal Area. Ph.D. Thesis, North Carolina State University, Department of Electrical Engineering, Raleigh, NC, 1970.

[5] Holt, J.; L. Belden; and W. Jameson: Computer Simulation Study of Air-Derived Separation Assurance Systems in Multiple Aircraft Environments. Third Interim Report, Contract FA-WA-4598, Collins Radio Company, Cedar Rapids, Iowa, 1968.

[6] Golomb, S. W.: Digital Communications. Prentice-Hall, Inc., Englewood Cliffs, NJ, 1964.